MIT Joint Program on the Science and Policy of Global Change

A Global Land System Framework for Integrated Climate-Change Assessments

C. Adam Schlosser, David Kicklighter and Andrei Sokolov

Report No. 147
May 2007

The MIT Joint Program on the Science and Policy of Global Change is an organization for research, independent policy analysis, and public education in global environmental change. It seeks to provide leadership in understanding scientific, economic, and ecological aspects of this difficult issue, and combining them into policy assessments that serve the needs of ongoing national and international discussions. To this end, the Program brings together an interdisciplinary group from two established research centers at MIT: the Center for Global Change Science (CGCS) and the Center for Energy and Environmental Policy Research (CEEPR). These two centers bridge many key areas of the needed intellectual work, and additional essential areas are covered by other MIT departments, by collaboration with the Ecosystems Center of the Marine Biology Laboratory (MBL) at Woods Hole, and by short- and long-term visitors to the Program. The Program involves sponsorship and active participation by industry, government, and non-profit organizations.

To inform processes of policy development and implementation, climate change research needs to focus on improving the prediction of those variables that are most relevant to economic, social, and environmental effects. In turn, the greenhouse gas and atmospheric aerosol assumptions underlying climate analysis need to be related to the economic, technological, and political forces that drive emissions, and to the results of international agreements and mitigation. Further, assessments of possible societal and ecosystem impacts, and analysis of mitigation strategies, need to be based on realistic evaluation of the uncertainties of climate science.

This report is one of a series intended to communicate research results and improve public understanding of climate issues, thereby contributing to informed debate about the climate issue, the uncertainties, and the economic and social implications of policy alternatives. Titles in the Report Series to date are listed on the inside back cover.

Henry D. Jacoby and Ronald G. Prinn,
Program Co-Directors

For more information, please contact the Joint Program Office

Postal Address: Joint Program on the Science and Policy of Global Change
77 Massachusetts Avenue
MIT E40-428
Cambridge MA 02139-4307 (USA)

Location: One Amherst Street, Cambridge
Building E40, Room 428
Massachusetts Institute of Technology

Access: Phone: (617) 253-7492
Fax: (617) 253-9845
E-mail: globalchange@mit.edu
Web site: http://MIT.EDU/globalchange/

Printed on recycled paper

A Global Land System Framework for Integrated Climate-Change Assessments

C. Adam Schlosser[†], David Kicklighter[*] and Andrei Sokolov[†]

Abstract

Land ecosystems play a major role in the global cycles of energy, water, carbon and nutrients. A Global Land System (GLS) framework has been developed for the Integrated Global Systems Model Version 2 (IGSM2) to simulate the coupled biogeophysics and biogeochemistry of these ecosystems, as well as the interactions of these terrestrial processes with the climate system. The GLS framework has resolved a number of water and energy cycling deficiencies and inconsistencies introduced in IGSM1. In addition, a new representation of global land cover and classification as well as soil characteristics has been employed that ensures a consistent description of the global land surface amongst all the land components of the IGSM2. Under this new land cover classification system, GLS is run for a mosaic of land cover types within a latitudinal band defined by the IGSM2 atmosphere dynamics and chemistry sub-model. The GLS shows notable improvements in the representation of land fluxes and states of water and energy over the previous treatment of land processes in the IGSM1. In addition, the zonal features of simulated carbon fluxes as well as key trace gas emissions of methane and nitrous oxide are comparable to estimates based on higher resolution models constrained by observed climate forcing. Given this, the GLS framework represents a key advance in the ability of the IGSM to faithfully represent coupled terrestrial processes to the climate system, and is well poised to support more robust two-way feedbacks of natural and managed hydrologic and ecologic systems with the climate and socio-economic components of the IGSM2.

Contents

1. INTRODUCTION

Living organisms (plants, microbes, fungi, animals, people) on the land surface have a large influence on the terrestrial storage of energy, water, carbon, nitrogen, and other elements and the fluxes of these entities among the atmosphere, hydrosphere and lithosphere. While the importance of terrestrial organisms in providing food, water and shelter to society has long been recognized, other ecosystem services such as regulation of atmospheric chemistry and climate, resistance and resilience to disturbances, or formation of soil (Costanza *et al.*, 1997) have only

[†] Joint Program on the Science and Policy of Global Change, Massachusetts Institute of Technology
[*] The Ecosystems Center, Marine Biological Laboratory, Woods Hole, MA

been appreciated recently. These latter ecosystem services result from the evolution of feedbacks from previous activities of living organisms. Furthermore, different characteristics of the landscape may have different effects on a variable of interest. For example, changes in land surface albedo may have compensatory effects on radiative forcing as concurrent changes in net carbon exchange of terrestrial ecosystems with the atmosphere (Brovkin *et al.*, 2006). To better understand the role of these terrestrial dynamics on current and future energy exchange and element cycling on earth, several "earth system models" (*e.g.*, Prinn *et al.*, 1999; Cox *et al.*, 2000; Friedlingstein *et al.*, 2001; Claussen *et al.,* 2002; Thompson *et al.*, 2004) have been developed that attempt to account for the heterogeneity in ecosystem structure across the earth's surface and the feedback between changing environmental conditions and the activities of terrestrial organisms.

One such earth system model is the MIT Integrated Global System Model (IGSM). In Version 1 of the IGSM (IGSM1, Prinn *et al.*, 1999), extant models that describe atmospheric chemistry, climate dynamics, terrestrial carbon dynamics, trace gas dynamics and economic activities have been adapted as sub-models in the IGSM such that outputs from one sub-model are used as inputs to other sub-models (**Figure 1**). In this approach, each of the sub-models calculates its own water and energy balances at various spatial and temporal scales based on different assumptions about the structure of vegetation (*e.g.,* land cover) and the underlying soil profile. This approach incorporates the expertise in various disciplines and has been useful for producing preliminary estimates of carbon, water and energy fluxes among the atmosphere, oceans and land. However, the use of disparate and inconsistent water assumptions among the various sub-models has led to questions about how well the IGSM faithfully represents the global land system.

In developing Version 2 of the IGSM (IGSM2, Sokolov *et al.*, 2005), we have developed a new Global Land System (GLS) framework (**Figure 2**) to ensure consistency and robust biogeophysical and biogeochemical coupling among the sub-models. In this new framework, soil moisture and thermal dynamics are simulated by a single model, which then provides estimates to the other models in the framework at the appropriate spatial and temporal scales. A new common representation of land cover has also been developed for use by all the models in the framework to eliminate this inconsistency. However, the characterization of vegetation and soil properties within a land cover type still varies among the models. Finally, the GLS has been designed such that the new framework could be run with either zonal or gridded interactions between land ecosystems and the atmosphere.

In this report, we first describe the new GLS framework, including the new common representation of land cover, and how the model couplings in this framework differ from those found in IGSM1. We then examine how these changes along with changes in the representation of land precipitation have influenced the estimates of contemporary evapotranspiration, snow cover and carbon sequestration by land ecosystems between the first and second versions of the IGSM. In addition, we examine how these GLS estimates along with corresponding estimates of soil temperature, and methane and nitrous oxide emissions compare to those based on or the

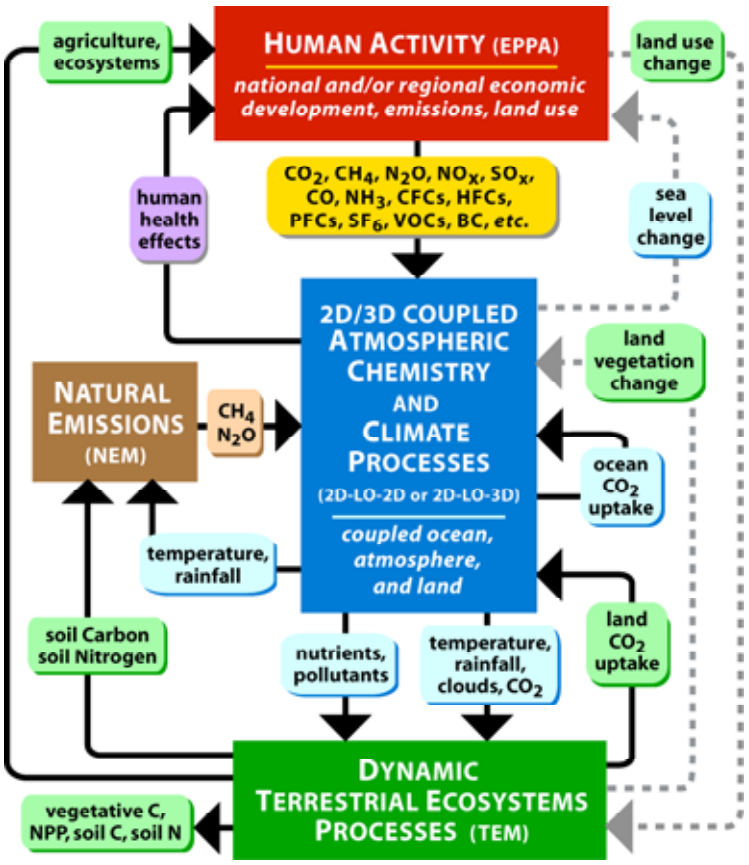

Figure 1. A schematic of the framework and processes in the MIT Integrated Global System Model (IGSM) Version 1. Existing feedbacks among the component models (*i.e.* EPPA, the 2D/3D coupled atmospheric dynamics and chemistry/ocean model, TEM, NEM) are shown as solid lines. Dashed lines represent proposed additional feedbacks to the IGSM Version 1 framework.

results of models using a finer spatial resolution. Finally, we examine various features of historical and potential future changes in water, energy and trace gas emissions from the land surface as simulated by the GLS. The coupling of the zonal GLS framework to the rest of the IGSM2 has been described previously (Sokolov *et al.,* 2005).

2. DEVELOPMENT OF GLOBAL LAND SYSTEM FRAMEWORK

In the Global Land System framework (GLS, Fig. 2), the land system is designed around the integration of three main modules: The Community Land Model (CLM), the Terrestrial Ecosystems Model (TEM), and the Natural Emissions Model (NEM). For the coupling of the key biogeophysical characteristics and fluxes between the atmosphere and land (*e.g.*, evapotranspiration, surface temperatures, albedo, surface roughness, maximum snow depth), CLM is well poised and is used alone. This interfacing allows the land and the atmosphere to interact in the same way that more sophisticated general circulation models (GCMs) do and replaces the land-atmosphere algorithms and parameters formerly used by the two-dimensional (2D) atmospheric/ chemistry model in IGSM1. In addition, CLM now provides all of the hydrothermal states and fluxes (*e.g.*, soil moisture, soil temperatures, evaporation, and

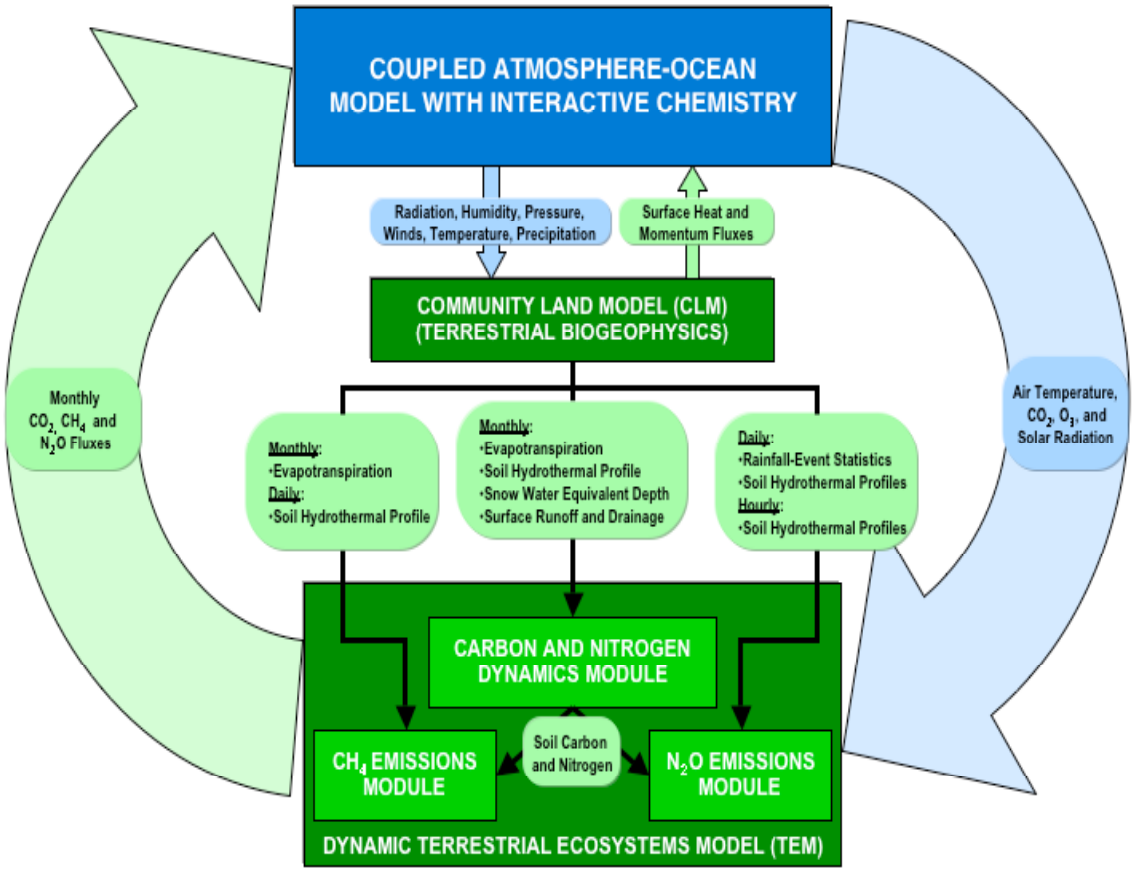

Figure 2. Schematic of the Global Land System (GLS), highlighting the linkages between the biogeophysical and biogeochemical land modules as well as interactions with the atmosphere-ocean-chemistry sub-models in the IGSM Version 2.

precipitation events), at the appropriate spatial and temporal scales, required by TEM and NEM. The atmospheric/chemistry model, however, still provides monthly estimates of solar radiation, air temperature and atmospheric chemistry (carbon dioxide and ozone) directly to TEM. The TEM is then used to estimate changes in terrestrial carbon storage and the net flux of carbon dioxide between land and the atmosphere as a result of ecosystem metabolism. The NEM (Liu, 1996) estimates the net flux of methane from global wetlands and tundra ecosystems and the net flux of nitrous oxide from all natural terrestrial ecosystems to the atmosphere. The module in NEM describing processes leading to nitrous oxide emissions is a globalization of the Denitrification Decomposition (DNDC) model of Li *et al.* (1992). As in IGSM1, all land areas across the globe are assumed by TEM and NEM to be covered by natural vegetation in the GLS framework. The influence of land-use change on global carbon dynamics is still simulated by the Emissions Prediction and Policy Analysis (EPPA) model of the IGSM2.

In addition to the use of a single model for describing hydrothermal dynamics in terrestrial ecosystems within the IGSM2, a new land cover classification scheme along with an associated spatially explicit land-cover data set have been developed to serve the needs of all of the models in the GLS framework. The new classification scheme attempts to incorporate all of the features

used in the different land cover classification schemes formerly used by the various models in the IGSM1 and CLM or attempts to improve upon these features. This new classification scheme has been used to develop a new land cover data set based on the spatially-explicit data sets of potential vegetation (Melillo *et al.*, 1993) and global wetlands (Matthews & Fung, 1987) used by TEM and/or NEM in IGSM1 and on the spatially explicit land cover data set used by CLM (Bonan, 2002). The new data set now represents land cover within each 4º latitudinal band across the globe as a mosaic of land cover types. All modules of the GLS framework use this new land cover data set to develop flux estimates between land and the atmosphere at the same horizontal spatial resolution. The modules are applied to each land cover type within a latitudinal band and the resulting flux estimates of water, heat, carbon and nitrogen are then weighted by the area of the appropriate land cover type found within that latitudinal band. The use of the new common land cover data set ensures more consistency among the fluxes estimated by the various models of the GLS framework.

Both TEM and NEM simulate carbon and nitrogen dynamics in terrestrial ecosystems, but use different assumptions to describe these dynamics. Similar to the use of different water balance algorithms, the different assumptions used for carbon and nitrogen dynamics can lead to inconsistencies in the fluxes estimated by these two models. As a first step towards resolving these inconsistencies, the algorithms in the Natural Ecosystems Model (NEM) that describe methane (CH_4) and nitrous oxide (N_2O) dynamics have been incorporated into TEM so that it now describes the hourly and daily dynamics of these trace gases in addition to the monthly dynamics of carbon dioxide and organic matter in terrestrial ecosystems (**Figure 3**). Because our development of the GLS framework has focused primarily on water and energy dynamics, the NEM algorithms have not yet been modified as they were incorporated into TEM so that the two models still describe somewhat different carbon and nitrogen dynamics. However, the more direct coupling between the two models now allow us to use monthly TEM estimates of reactive soil organic carbon to estimate nitrous oxide fluxes instead of the mean annual TEM estimates as in IGSM1. In addition, we can now explore how soil organic carbon pools estimated by TEM can be influenced by the estimated losses of carbon due to methane fluxes to the atmosphere estimated by NEM.

Besides the incorporation of NEM into TEM, the version of TEM used in the GLS contains some other enhancements. First, the effects of ozone pollution on terrestrial carbon and nitrogen dynamics have been added by including the algorithms of Felzer *et al.* (2004). The new version of TEM also includes algorithms describing the effects of row crop agriculture on terrestrial carbon and nitrogen dynamics (Felzer *et al.*, 2004), including those dynamics associated with land conversion and cropland abandonment (McGuire *et al.*, 2001). While the effects of human activities and land-use change on terrestrial carbon dynamics is still addressed in the IGSM2, work is currently underway to improve our ability to simulate the ecological consequences of policy decisions by linking the area associated with a particular land use, as simulated by EPPA, to the biogeophysical and biogeochemical processes occurring in that land cover type as simulated by the land models in the GLS.

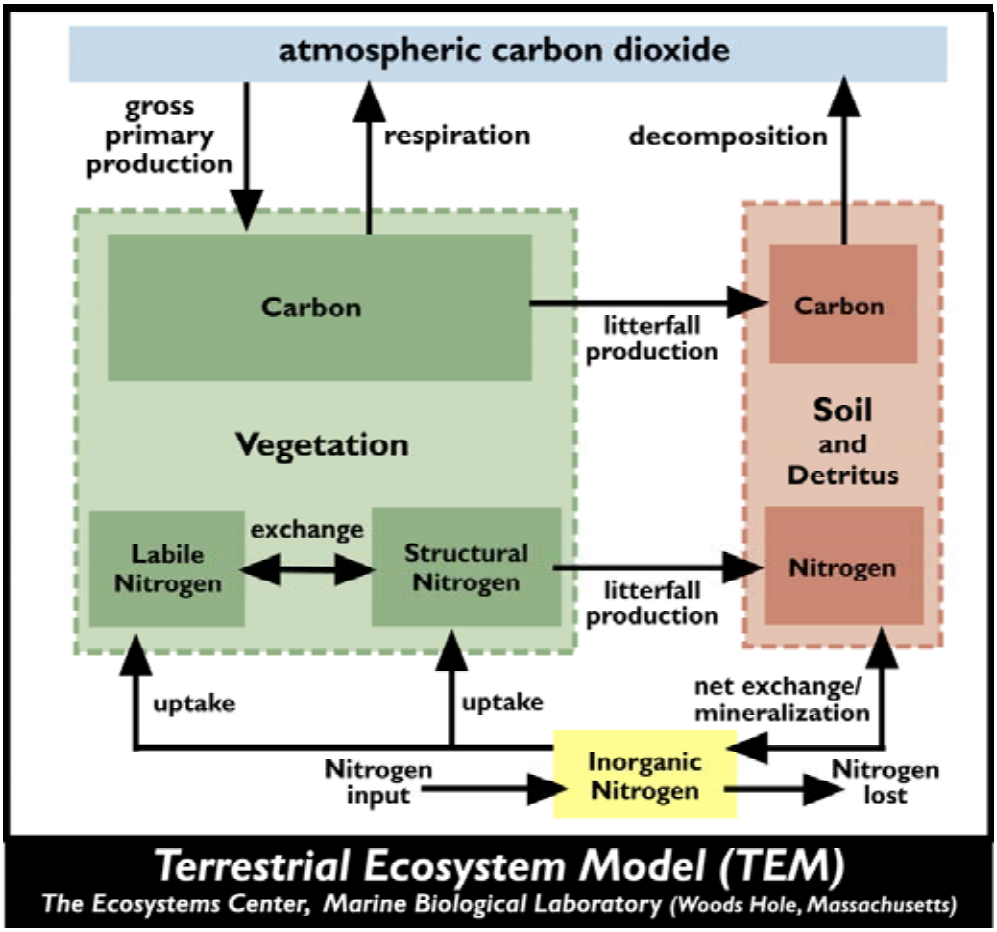

Figure 3. Schematic of the Terrestrial Ecosystems Model (TEM) indicating the key storages and exchanges of carbon and nitrogen considered among vegetation, soil and the atmosphere.

Below, we describe in more detail: 1) the structure and performance of the Community Land Model (CLM) used to simulate hydrothermal dynamics of terrestrial ecosystems in the IGSM2; 2) the development of the new land cover classification scheme including its relationship to the land cover classification schemes formerly used by the various models in the IGSM1; 3) the development of the new spatially explicit land cover data set associated with the new classification scheme and the development of two common soil characteristics data sets; 4) changes in the linkages of the atmospheric dynamics and chemistry model with TEM and with NEM as a result of incorporating CLM into the GLS framework; 5) issues related to the linkage of CLM estimates of precipitation, soil moisture and soil temperatures as inputs to TEM and NEM; and 6) issues related to the incorporation of NEM into TEM.

2.1 The biogeophysical model: CLM

The Community Land Model (CLM, Bonan, 2002) represents the terrestrial biogeophysical processes that govern surface energy and water fluxes. CLM is partially based upon the Common Land Model (Zeng *et al.*, 2002) that was derived from a multi-institutional collaboration of land models, and carefully tested (Dai *et al.*, 2003). CLM is used in global-scale land data

assimilation research (*e.g*. Rodell *et al.*, 2004) as well as coupled climate prediction studies (*e.g.,* Dai *et al.*, 2004, and Holland, 2003), and as such, it is well suited for interfacing with the atmospheric model of the IGSM2, as well as providing the necessary inputs of hydro-thermal state variables and fluxes for the TEM and NEM ecosystem models. Under the auspice of the land model working-group of the National Center for Atmospheric Research, Community Climate System Model (NCAR CCSM) effort, CLM is under constant development by the community-at-large. As such, future implementations of CLM in the IGSM will include these developments. For our initial efforts, we use the publicly available Version 2.1 of CLM. Further GLS development will likely leverage off of Version 3.0 of CLM (*e.g.*, Dickinson *et al.*, 2006).

The implementation of CLM as the biogeophysical model represents a substantial advance in the IGSM's capability to represent the processes that regulate terrestrial water and energy budgets (*c.f*. Bonan, 2002). Not only does CLM include more comprehensive and explicit controls on evapotranspiration, but CLM also provides a more detailed representation of the snowpack and soil-column profile (with up to 5 snow layers and 10 soil layers) as well as an explicit treatment of soil-layer frozen and liquid storages and the processes that govern them. Further, the numerical framework of the CLM allows for a mosaic representation of the various vegetation types with a given grid-cell, in which water and energy budgets are explicitly calculated and then area-weighted for grid-cell aggregation of the various water/energy fluxes and storages. The notable distinction here is that CLM is implemented in a *zonal* configuration for the IGSM2, such that the land mosaic now represents, in a lumped statistical sense, the distribution of vegetation/land-cover types across a given latitude band, according to the IGSM land classification (Section 2.3). Given this zonal implementation, additional statistically based modifications are made with regard to the episodic nature and spatial distribution of land precipitation (Section 2.4). In addition, further modifications to the IGSM precipitation convection and large-scale precipitation parameterization are made (Section 3.1) to improve the performance of zonal land precipitation.

2.2 Development of land classification scheme

Many parameter values in TEM, NEM, and CLM as well as the atmospheric dynamics and chemistry model are dependent upon major land cover types. Although TEM and NEM have used a similar vegetation classification scheme (TEMVEG, see **Table 1**) to stratify their parameters, this scheme is different from that used by the atmospheric dynamics and chemistry model (**Table 2**) and CLM (CLMVEG, see **Table 3**). In addition to the TEMVEG classification scheme, NEM has used a further stratification of wetland types (**Table 4**) based on Matthews & Fung (1987) to develop estimates of methane fluxes. To couple the models together in the new IGSM framework, a new vegetation classification (IGSMVEG) has been developed that relates the land cover categories of CLM to the land cover categories in TEM and NEM (**Table 5**). The new IGSMVEG classification scheme basically mimics the CLMVEG classification scheme. However, the single CLM wetlands category has been disaggregated into nine categories based on the general temperature regime (tropical, temperate, or boreal) experienced by the vegetation;

Table 1. Land cover classification scheme (TEMVEG) used by the Terrestrial Ecosystem Model (TEM) and the Natural Emissions Model (NEM) for natural vegetation.

TEMVEG	Description of Vegetation
1	Ice
2	Alpine Tundra and Polar Desert
3	Moist and Wet Tundra
4	Boreal Forest
5	Forested Boreal Wetlands
6	Boreal Woodlands
7	Non-forested Boreal Wetlands
8	Mixed Temperate Forests
9	Temperate Coniferous Forests
10	Temperate Deciduous Forests
11	Temperate Forested Wetlands
12	Tall Grasslands
13	Short Grasslands
14	Tropical Savanna
15	Arid Shrublands
16	Tropical Evergreen Forests
17	Tropical Forested Wetlands
18	Tropical Deciduous Forests
19	Xeromorphic Forests and Woodlands
20	Tropical Forested Floodplains
21	Deserts
22	Tropical Non-forested Wetlands
23	Tropical Non-forested Floodplains
24	Temperate Non-forested Wetlands
25	Temperate Forested Floodplains
26	Temperate Non-forested Floodplains
27	Wet Savannas
28	Salt Marsh
29	Mangroves
30	Tidal Freshwater Marshes
31	Temperate Savannas
32	(Reserved)
33	Temperate Broadleaved Evergreen
34	(Reserved)
35	Mediterranean Shrublands

Table 2. Land cover classification scheme used by the atmospheric dynamics and chemistry model (based on Matthews, 1984).

Category	Description of Vegetation
1	Desert
2	Tundra
3	Grass
4	Shrub
5	Trees
6	Deciduous forest
7	Evergreen forest
8	Rainforest

the presence of a tree cover; whether the wetland is covered by fresh or salt water; and the proximity of the wetland to the sea coast. In addition, four categories of floodplains have also been added to IGSMVEG along with categories for rice paddies and pastures. The wetland and floodplain categories have been added to support NEM estimates of methane emissions from natural ecosystems. The rice paddies and pasture categories have been added to allow consideration of these land cover types in future IGSM2 simulations. More land cover categories could be added as needed to the IGSMVEG classification scheme in the future as the IGSM becomes able to simulate the dynamics of managed ecosystems in more detail (*e.g.*, forestry, C3 versus C4 crops, and biofuels).

In the IGSM2 simulations, the modules of the GLS obtain an IGSMVEG value from a spatially explicit land cover data set and translate this value into the appropriate values of the land cover schemes normally used by the model to assign parameter values as depicted in Table 5.

Table 3. Land cover classification scheme (CLMVEG) used by the Community Land Model (CLM) of Bonan *et al.*, 2002.

CLMVEG	Description of Vegetation
0	Bare Ground
1	Needle-leaf Evergreen Tree (NET) temperate
2	Needle-leaf Evergreen Tree (NET) boreal
3	Needle-leaf Deciduous Tree (NDT) boreal
4	Broadleaved Evergreen Tree (BET) tropical
5	Broadleaved Evergreen Tree (BET) temperate
6	Broadleaved Deciduous Tree (BDT) tropical
7	Broadleaved Deciduous Tree (BDT) temperate
8	Broadleaved Deciduous Tree (BDT) boreal
9	Broadleaved Evergreen Shrub (BES) temperate
10	Broadleaved Deciduous Shrub (BDS) temperate
11	Broadleaved Deciduous Shrub (BDS) boreal
12	C3 grass arctic
13	C3 grass
14	C4 grass
15	Crop 1
16	Crop 2
17	Wetlands
18	Glaciers
19	Lakes
20	Urban

Table 4. Wetland classification scheme used by NEM for estimating methane (based on Matthews & Fung, 1987).

Wetland Category	Description of Vegetation
0	Upland (*i.e.* no wetlands), lakes or wetlands inundated with salt water
1	Forested bog
2	Non-forested bog
3	Forested swamp
4	Non-forested swamp
5	Alluvial formations

Table 5. Translation of former land cover classification schemes used in the IGSM1 (see Tables 1 to 4) to the IGSMVEG land cover classification scheme developed for use in the IGSM2. The last column represents the translation used to aggregate or disaggregate data from Melillo *et al.* (1993), which uses the TEMVEG classification, to develop the new land cover data set for the IGSM2 based on the IGSMVEG classification.

Description of Vegetation	IGSM VEG	CLMVEG	NEM Wetlands	TEMVEG Parameters	TEMVEG Map
Bare Ground	0	0	0	1	2, 21
Needle-leaf Evergreen Tree (NET) temperate	1	1	0	9	9, 8(50%)
Needle-leaf Evergreen Tree (NET) boreal	2	2	0	4	4, 6(30%)
Needle-leaf Deciduous Tree (NDT) boreal	3	3	0	4	N/A
Broadleaved Evergreen Tree (BET) tropical	4	4	0	16	16,18
Broadleaved Evergreen Tree (BET) temperate	5	5	0	33	33
Broadleaved Deciduous Tree (BDT) tropical	6	6	0	19	19, 14(30%)
Broadleaved Deciduous Tree (BDT) temperate	7	7	0	10	10, 8(50%), 31(30%)
Broadleaved Deciduous Tree (BDT) boreal	8	8	0	4	N/A
Broadleaved Evergreen Shrub (BES) temperate	9	9	0	35	35
Broadleaved Deciduous Shrub (BDS) temperate	10	10	0	15	15
Broadleaved Deciduous Shrub (BDS) boreal	11	11	0	3	N/A
C3 grass arctic	12	12	0	3	3, 6(70%)
C3 grass	13	13	0	13	13
C4 grass	14	14	0	13	12, 14(70%), 31(70%)
Crop 1	15	15	0	50	N/A
Crop 2	16	16	0	50	N/A
Wetlands (Tree tropical)	17	17	3	17	17, 27(30%)
Wetlands (No-tree tropical)	18	17	4	22	22, 27(70%)
Wetlands (Tree temperate)	19	17	3	11	11
Wetlands (No-tree temperate)	20	17	4	24	24
Wetlands (Tree boreal)	21	17	1	5	5
Wetlands (No-tree boreal)	22	17	2	7	7
Mangroves	23	17	0	29	29
Coastal salt marsh	24	17	0	28	28
Inland salt marsh	25	17	0	28	28
Floodplains (Tree tropical)	26	4	5	20	20
Floodplains (No-tree tropical)	27	14	5	23	23
Floodplains (Tree temperate)	28	7	5	25	25
Floodplains (No-tree temperate)	29	13	5	26	26
Glaciers	30	18	0	1	1
Lakes	31	19	0	-36	-36
Rice Paddies	32	15	4	52	---
Pastures	33	15	0	51	---
Urban	34	20	0	40	---

The atmospheric dynamics and chemistry sub-model now obtains values for its land parameters from CLM. As the TEMVEG classification scheme was originally intended only for natural vegetation, new categories have been added to the TEMVEG land cover scheme (**Table 6**) to allow for the eventual inclusion of managed ecosystems in future IGSM simulations.

Table 6. Vegetation classification scheme (TEMVEG) used by the Terrestrial Ecosystem Model (TEM) and the Natural Emissions Model (NEM) for managed ecosystems.

TEMVEG	Description of Vegetation
40	Urban
50	Generic Crop
51	Pasture
52	Rice

2.3 Development of the new land cover and soil characteristics data sets

In the IGSM1, multiple data sets of global land cover have been used simultaneously to represent terrestrial ecosystems. Global land cover for TEM has been prescribed by a data set of potential natural vegetation (Melillo *et al.*, 1993), gridded at a spatial resolution of 0.5º latitude x 0.5º longitude (**Figure 4**). Information in this spatially explicit land cover data set has also been aggregated to a spatial resolution of 2.5º latitude x 2.5º longitude for use in NEM. In both data sets, the land cover of each grid cell is represented with the dominant type found within that grid cell (*i.e.* no multiple land cover types or mosaic structure considered). In addition to potential vegetation, NEM has also used a 1.0º x 1.0º gridded data set that describes the global distribution of wetlands (Matthews & Fung, 1987) to develop its estimates of methane emissions from wetlands. Although land cover has not been used directly by the atmospheric dynamic and chemistry sub-model, a 7.83º latitude x 10.0º longitude land cover data set (Matthews, 1984) has been used to develop mean zonal estimates of seasonal ground albedo, seasonal ratios of near infrared albedo to visible albedo, masking depth and water field capacity based on the dominant vegetation type found in each of the grid cells within a particular 7.83º latitudinal band.

To provide a common representation of global land cover for all of the models in the IGSM2, the new IGSMVEG classification scheme described in the previous subsection is used to develop a new land cover data set. The new data set is based on spatially explicit information from a modified version of the TEMVEG potential vegetation data set (Melillo *et al.*, 1993) and the Matthews & Fung (1987) wetland distribution data set used in the IGSM1, along with the CLMVEG land cover data set used by CLM (Bonan, 2002). Unlike the other land cover data sets, the CLMVEG data set is designed to represent land cover as a mosaic of plant functional types (PFTs) at a variety of spatial resolutions. Because we would eventually like to discern the effects of human activities from natural variability on ecosystem structure and services across the globe, we first developed a baseline data set of potential natural vegetation. As the CLMVEG data set represents contemporary land cover (*i.e.* includes a "snapshot" of the distribution of agriculture in the early 1990s), we use the modified TEMVEG potential vegetation data set as the basis for developing the new IGSMVEG data set.

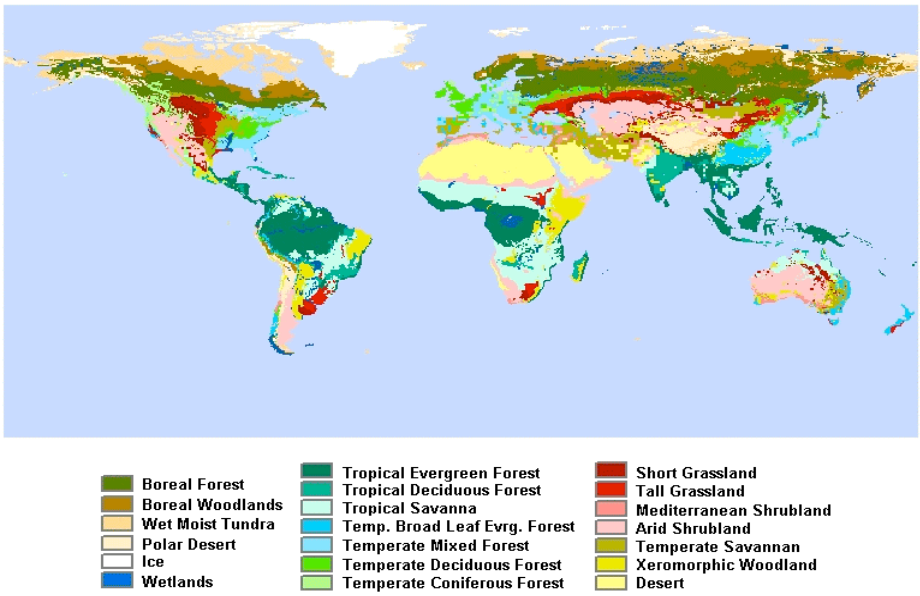

Figure 4. Distribution of potential vegetation across the globe as represented in the TEMVEG data set (Melillo *et al.,* 1993) used to represent land cover in the IGSM1.

In the IGSM1, the global land area has been represented in the TEMVEG data set by 62,483 grid cells with a spatial resolution of 0.5º latitude x 0.5º longitude. This distribution of grid cells matches the land distribution used by the Cramer & Leemans (2001) data sets of mean long-term climate. Land has been assumed to cover the entire area of each grid cell. In the modified TEMVEG potential vegetation data set, the global land area has been extended and is now represented by 67,420 grid cells with a spatial resolution of 0.5º latitude x 0.5º longitude. This distribution of grid cells matches the land distribution used by the New *et al.* (2000) data sets of historical climate for the twentieth century (also known as the Climate Research Unit of the University of East Anglia or CRU climate data sets). In the modified TEMVEG data set, land is no longer assumed to cover the entire area of the grid cell. Instead, the land area of each grid cell has been determined as the sum of 1 km^2 areas within the 0.5º latitude x 0.5º longitude grid cell that has an elevation greater than or equal to sea level as described by the Terrain Base elevation data set (GLOBE Task Team *et al.,* 1998).

To develop the IGSMVEG data set, the area of wetlands and lakes within each 0.5º x 0.5º grid cell used in the modified TEMVEG data set is first determined. A comparison of the Matthews & Fung (1987) wetlands data set used by NEM to the TEMVEG and CLMVEG data sets indicates that these latter data sets substantially underestimate the global area of wetlands (**Table 7**). Thus, the area of wetlands as described by the Matthews & Fung (1987) data set has been incorporated into the IGSMVEG land cover data set to better account for the effects of wetlands on global methane emissions. To include this information, the 1º latitude x 1º longitude wetlands data are first co-registered with the 0.5º latitude x 0.5º longitude data in the modified TEMVEG data set. The area of wetlands for each grid cell is determined from the land area associated with the grid cell multiplied by the proportion of the grid cell assumed to be wetlands in the Matthews & Fung (1987) inundation data set. Wetlands are assumed to be distributed

Table 7. Comparison of wetland area (km^2) among different land cover data sets used by CLM and the IGSM1.

Region	CLM	Matthews & Fung (1987)	TEMVEG*
Bogs	**1,982,348**	**2,974,000**	**1,067,365**
Boreal		2,607,000+	1,067,365
Temperate		250,000&	
Tropical		117,000#	
Forested		**2,077,000**	**232,424**
Boreal		1,723,000	
Temperate		249,000	
Tropical		105,000	
Non-forested		**897,000**	**834,941**
Boreal		884,000	
Temperate		1,000	
Tropical		12,000	
Swamps	**349,556**	**2,095,000**	**1,257,175**
Boreal		96,000+	
Temperate	102,554	288,000&	491,990
Tropical	247,002	1,709,000#	765,185
Forested		**1,087,000**	**783,360**
Boreal		30,000	
Temperate		115,000	154,163
Tropical		941,000	629,197
Non-forested		**1,008,000**	**473,815**
Boreal		66,000	
Temperate		173,000	337,827
Tropical		768,000	135,988
Total Bogs and Swamps	**2,331,904**	**5,069,000**	**2,324,540**
Mangroves and other coastal areas			209,205
Floodplains		**194,000**	**713,216**
Temperate		42,000&	203,055
Tropical		153,000#	510,161
Forested			**257,705**
Temperate			104,134
Tropical			153,571
Non-forested			**455,511**
Temperate			98,921
Tropical			356,590
Total Natural Wetlands and Floodplains	2,331,904	5,263,000	3,037,756

* Based on 62,483 grid cells defined by Cramer and Leemans (personal communication)

\+ Boreal assumed to be south of 50° S and north of 50° N

& Temperate assumed to be 50° – 30° S and 30° – 50° N

Tropical assumed to be 30° S – 30° N

uniformly across the four 0.5° potential vegetation grid cells comprising each 1° wetland grid cell. This wetland area is then assigned to an IGSMVEG wetland or floodplain category (Table 5) based on the wetland categories (Table 4) used by Matthews & Fung (1987). The forested swamps and non-forested swamps categories of Matthews & Fung (1987) have been disaggregated into the IGSMVEG tropical and temperate swamps categories based on latitude (between 30°S and 30°N are tropical; otherwise temperate). The alluvial category has been

disaggregated into the IGSMVEG tropical and temperate forested (tree) or non-forested (no tree) floodplains categories based on corresponding information in the modified TEMVEG data set. The area of lakes within each grid cell is determined from the CLMVEG data set organized at a spatial resolution of 0.5º latitude x 0.5º longitude.

After identifying the types and areas of wetlands, floodplains and lakes in each of the grid cells, the remaining "dryland" area of each grid cell is then determined by subtracting the area of wetlands, floodplains and lakes from the total land area of the 0.5º latitude x 0.5º longitude grid cell. The land cover of the dryland areas is then determined with the following protocol. First, the TEMVEG values (see last column of Table 5) in the modified Melillo *et al.* (1993) potential vegetation data set are translated into the appropriate IGSMVEG categories. To avoid inconsistencies with the Matthews & Fung (1987) wetland distribution, TEMVEG wetland and floodplain categories (except mangroves and salt marshes) are re-categorized as their upland counterparts. As some TEMVEG categories contain a mixture of vegetation types (*e.g.,* mixed temperate forests, savannas, boreal woodlands), we disaggregated these mixed vegetation types into two IGSMVEG types per grid cell. For example, mixed temperate forests (TEMVEG = 8) are assumed to be 50% temperate deciduous trees (TEMVEG = 10) and 50% temperate coniferous trees (TEMVEG = 9). If the area of land in a grid cell is 1000 km^2, then 500 km^2 is assigned to the IGSMVEG category "Broadleaved Deciduous Tree (BDT) temperate" (IGSMVEG = 7), and 500 km^2 is assigned to the IGSMVEG category "Needle-leaf Evergreen Tree (NET) temperate" (IGSMVEG = 1). Thus, a grid cell with mixed vegetation is represented by more than one dryland cover type in the IGSMVEG data set. For savannas, grasses are assumed to cover more area than trees so for a grid cell containing 1000 km^2 of tropical savannas (TEMVEG = 14), only 300 km^2 would be assigned to the IGSMVEG category "Broadleaved Deciduous Tree (BDT) tropical" (IGSMVEG = 6) and 700 km^2 would be assigned to the IGSMVEG category "C4 grass" (IGSMVEG = 14).

In some cases, a single TEMVEG category covers several IGSMVEG categories. For example, the TEMVEG boreal forest category (TEMVEG = 4) includes forests of needle-leaf evergreen trees (IGSMVEG = 2), needle-leaf deciduous trees (IGSMVEG = 3) and broadleaved deciduous trees (IGSMVEG = 8). To disaggregate a TEMVEG category into the component IGSMVEG categories, information from the CLMVEG data set, organized at a 0.5º latitude x 0.5º longitude spatial resolution, is used in conjunction with the gridded TEMVEG data set. Following up on our example, all of the land area of a grid cell considered as boreal forests by the TEMVEG data set is first assigned to the needle-leaf evergreen tree (NET) boreal category (IGSMVEG = 2). Next, the grid cell is compared to corresponding information in the CLMVEG data set. If the CLMVEG data set indicates that the grid cell contains some area of needle-leaf deciduous (NDT) boreal trees, then this area is assigned to a new IGSMVEG land cover type and subtracted from the area originally assigned to the needle-leaf evergreen tree (NET) boreal category. If the estimated area is greater than that assigned to the IGSMVEG needle-leaf evergreen tree (NET) boreal category, then the area of the needle-leaf deciduous trees (NDT) boreal category is set equal to the area of the IGSMVEG needle-leaf evergreen tree (NET) boreal

category, which in turn, is set to zero. Similarly, if the CLMVEG data set indicates that the grid cell contains some area of the broadleaved deciduous tree (BDT) boreal category, then this area is assigned to another new IGSMVEG land cover type and subtracted from the area remaining in the needle-leaf evergreen tree (NET) boreal category after the subtraction of the area associated with needle-leaf deciduous (NDT) boreal trees. Again, if the estimated area is greater than that assigned to the IGSMVEG needle-leaf evergreen tree (NET) boreal category, then the area of the broadleaved deciduous trees (BDT) boreal category is set equal to the area of the IGSMVEG needle-leaf evergreen tree (NET) boreal category, which in turn, is set to zero. Thus, a 0.5º latitude x 0.5º longitude grid cell may be represented by up to three dryland cover types in the IGSMVEG data set instead of a single land cover type as found in the TEMVEG data set. A similar procedure is used to disaggregate the TEMVEG moist and wet tundra category into the C3 grass arctic and broadleaved deciduous shrub (BDS) boreal categories of the IGSMVEG.

For grasslands, a slightly different procedure is used to convert the TEMVEG categories (*i.e.* short and tall) into the IGSMVEG categories (*i.e.* C3 grass and C4 grass). For each 0.5º latitude x 0.5º longitude grid cell, the ratio of the area of C4 grasses to the area of C3 grasses plus C4 grasses as determined in the CLMVEG data set is calculated. This ratio is then multiplied by the land area of the "short grasslands" or "tall grasslands" grid cell in the TEMVEG data set to determine the area of C4 grasses in the IGSMVEG data set. The area of C3 grasses in the IGSMVEG data set is then determined as the difference of the total land area of the grid cell and the area assigned to C4 grasses. In addition, area in grid cells originally designated as salt marsh in the modified TEMVEG data set is now assigned as either coastal salt marsh (IGSMVEG = 24) or inland salt marsh (IGSMVEG = 25) based on the connection or lack of a connection of the particular grid cell to an ocean.

Antarctica is not represented in the modified TEMVEG data set. As most of the continent is covered by ice, this exclusion has a minor effect on estimates of global biogeochemistry, but may bias estimates of biogeophysical interactions between land and atmosphere. To avoid this bias in the GLS framework, 0.5º latitude x 0.5º longitude grid cells that represent Antarctica have been added to the IGSMVEG data set. The distribution, area and land cover of these grid cells are based on information from the CLMVEG data set.

As indicated above, land cover within each 0.5º latitude x 0.5º longitude grid cell is no longer represented by the dominant vegetation type, but by a mosaic of vegetation types per grid cell in the IGSMVEG data set. This approach allows us to better incorporate the influence of vegetation types that may be limited in areal extent within a grid cell, but may be important sources of trace gas emissions to the atmosphere. It also eliminates the potential inconsistencies associated with using multiple land cover data sets at different spatial resolutions as area is conserved within the new single land cover data set.

The atmospheric dynamics and chemistry sub-model in the IGSM2, however, provides the GLS framework with zonal climate data (4º latitudinal bands) and requires terrestrial fluxes of water, carbon dioxide, methane and nitrous oxide from the GLS at the same zonal resolution. To match this spatial resolution, the areas for each land cover type in each 0.5º latitude x 0.5º

longitude grid cell of the IGSMVEG data set have been aggregated within each 4º latitudinal band used by the atmospheric dynamics and chemistry model. Thus, each latitudinal band represents a 4º latitude x 360º longitude grid cell in the GLS framework. The GLS is run for all land cover types found in these coarser grid cells (**Figure 5**) and the area covered by each land

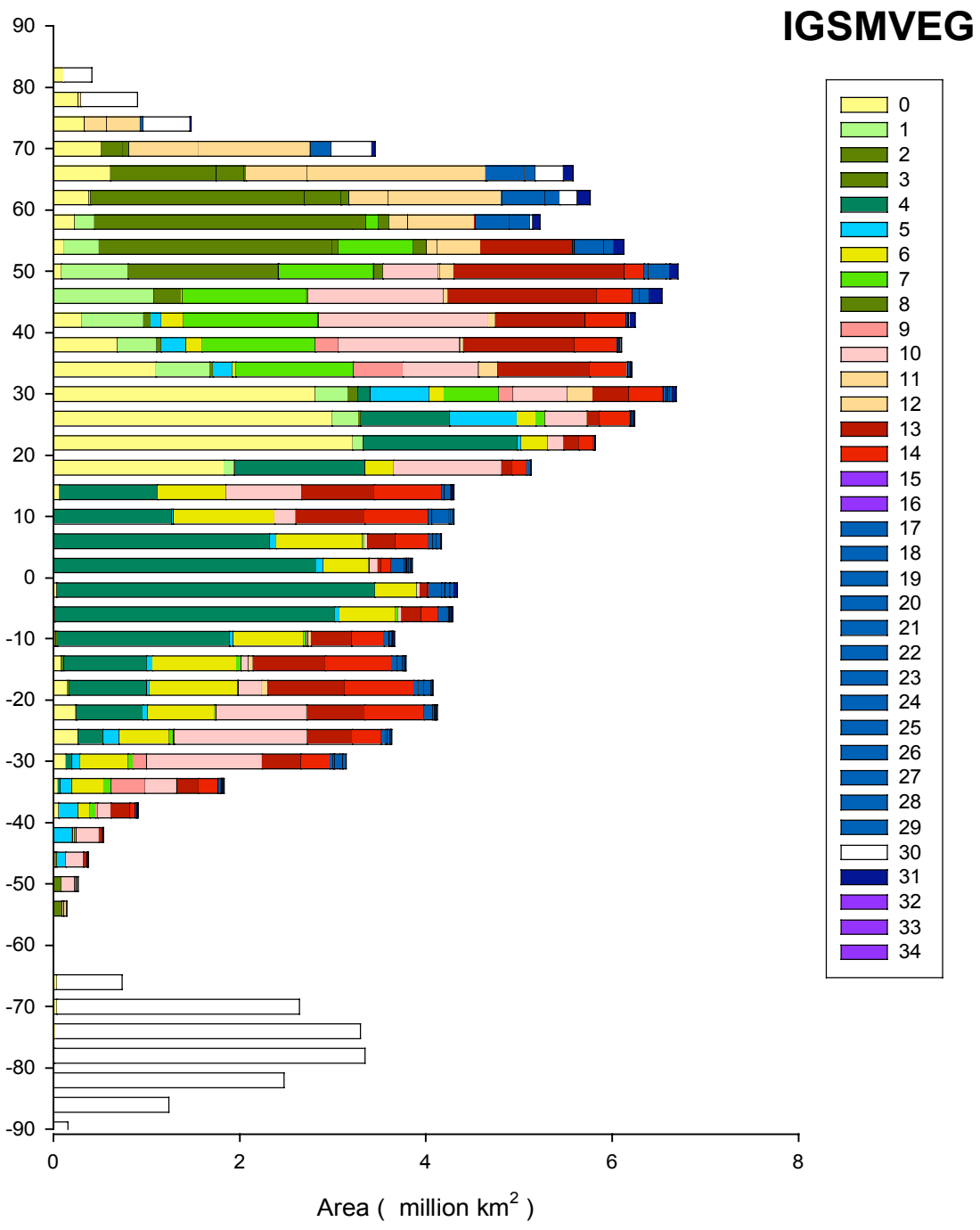

Figure 5. Distribution of potential vegetation across 4º latitudinal bands as represented by the new IGSMVEG data set. Color shading key follows the land cover categories of IGSMVEG, which are defined in Table 5. Color scheme has been chosen to relate similar land cover types between the new IGSMVEG classification and the TEMVEG classification (see Figure 4) used in the IGSM1.

cover type within a grid cell is used to determine the relative contribution of that land cover type to the overall carbon and nitrogen fluxes from terrestrial ecosystems in that grid cell. If future development of the IGSM requires land cover at finer zonal resolutions or even gridded land cover data, the relatively fine spatial resolution (0.5º latitude x 0.5º longitude) of the base information of the new IGSMVEG data set allows such needs to be met quickly with minimal additional efforts.

In addition to land cover, CLM, TEM and NEM also require spatially explicit information on soil characteristics. For the GLS framework, a common soil texture data set and a common soil profile characteristics data set have been developed for use by all of the models to eliminate the inconsistencies associated with using different data sets (Figs. 6 and 8). In the IGSM1, TEM and NEM need information on soil characteristics (Figs. 6a and 8a) to simulate water dynamics, which is now determined by CLM in the GLS. However, TEM also needs soil texture information (*i.e.* silt plus clay content) to set texture-dependent parameters that describe the uptake and release of carbon and nitrogen by plants and microbes for each grid cell; and NEM uses clay content to determine the decomposition rate of soil organic matter and the adsorption rate of inorganic compounds to soil particles. In addition, NEM needs information on soil porosity and saturated hydraulic conductivity to determine diffusion rates of nitrous oxide through the soil profile. To obtain this information, both TEM and NEM have used a spatially explicit soil texture data set (0.5º latitude x 0.5º longitude for TEM; 2.5º latitude x 2.5º longitude for NEM) derived from FAO soil maps (FAO-UNESCO, 1971) to develop their estimates in the IGSM1. In these data sets, the percentage of sand, silt and clay for a grid cell is based on one of the eight ordinal FAO soil texture classes (Pan *et al.*, 1996). In NEM, the clay content in the soil texture data set has been used to estimate the characteristics of the soil profile (Liu, 1996), including soil porosity and saturated hydraulic conductivity, based on empirical equations for twelve soil types (DeVries, 1975; Clapp & Hornberger, 1978). These characteristics have been assumed to be uniform across all soil layers in the profile. In contrast, the soil characteristics used by CLM are based on a spatially explicit data set of soil type (*c.f.* Bonan *et al.*, 2002) and vary among soil layers in the profile.

For the GLS, information regarding the percent sand, percent silt, and percent clay for the top 1 meter of the soil profile has been obtained from the IGBP Global Soil Data Task Group (2000) data set and aggregated to the 4º latitudinal band resolution used by the IGSM2 to develop a common soil texture data set for use by TEM and NEM. Unlike the FAO data set, in which soil texture is stratified among only eight classes, the IGBP data set has a more continuous representation of soil textures across the earth's surface. In addition, the native resolution (0.5º latitude x 0.5º longitude) information on the porosity and saturated hydraulic conductivity of each of the 10 soil layers used by CLM has been aggregated to the 4º latitudinal band resolution as a common soil profile characteristics data set for use by CLM and NEM. For NEM, a mean soil porosity and saturated hydraulic conductivity for the entire soil profile are determined from the weighted-average (based on soil layer thickness) of these characteristics in the top five soil layers used by CLM.

2.4 Land-Atmosphere linkages

The IGSM2's linkages between the land system and the atmospheric dynamics and chemistry model have changed considerably from its predecessor. In the IGSM1, TEM and NEM would obtain information on zonal (7.826º latitudinal bands) changes in climate and atmospheric chemistry estimated by the atmospheric dynamics and chemistry model and apply these changes to a baseline climate gridded at a finer spatial resolution to represent year-to-year climate inputs into these models. The baseline climate has been the climate database of Cramer & Leemans (2001) organized at a spatial resolution of 0.5º latitude x 0.5º longitude for TEM and organized at a spatial resolution of 2.5º x 2.5º and 4º x 5º for the nitrous oxide and methane modules of NEM, respectively. Details of the interpolation process used to create historical and future climate inputs for TEM have been described previously in Xiao *et al.* (1997). A somewhat similar approach has been used to develop historical and future climate data for NEM, but NEM interpolates the 7.826º latitudinal band climate estimates from the atmospheric dynamics and chemistry model to 2.5º and 4.0º latitudinal bands for the nitrous oxide module and methane module, respectively, rather than 0.5º latitudinal bands used by TEM.

For TEM in the IGSM1, monthly zonal estimates of surface air temperature, precipitation, cloudiness and atmospheric carbon dioxide concentrations from the atmospheric dynamics and chemistry model have been used (**Figure 6**a). For NEM, daily zonal estimates of surface air temperatures, ground temperatures averaged over the top 10 cm of the soil profile, precipitation and the residual between precipitation and evapotranspiration from the atmospheric dynamics and chemistry model have been used (**Figures 7**a, **8**a). As indicated before, these climate inputs have been used as drivers for the internal water balance and soil thermal modules in TEM and NEM that may not have been consistent with each other nor with the GISS land module used in the atmospheric dynamics and chemistry sub-model of the IGSM1. Vörösmarty *et al.* (1989) described the water balance module used by TEM and Liu (1996) described the water balance and soil thermal modules used by NEM. After conducting TEM simulations on each of the 62,483 fine resolution (0.5º latitude x 0.5º longitude) grid cells for a particular month, TEM estimates of the net carbon dioxide fluxes between terrestrial ecosystems across the globe and the atmosphere would be aggregated to a zonal resolution of either 7.5º or 8.0º latitude and passed back as inputs to the appropriate latitudinal band used by the atmospheric dynamics and chemistry model. A similar approach has been used to aggregate the 1º latitude x 1º longitude methane fluxes and 2.5º latitude x 2.5º longitude nitrous oxide fluxes estimated by NEM.

In the IGSM2, TEM still requires estimates of air temperature, surface solar radiation, atmospheric carbon dioxide concentrations from the atmospheric dynamics and chemistry sub-model. However, TEM now uses the surface solar radiation estimates of the atmospheric dynamics and chemistry model directly rather than calculating surface solar radiation from cloudiness estimates. Precipitation inputs are no longer required by TEM (as in the IGSM1) because monthly estimates of evapotranspiration and soil moistures are now provided by CLM (Figure 6b). In addition, TEM now uses zonal estimates of atmospheric ozone concentrations from the atmospheric dynamics and chemistry model to estimate the influence of this pollutant

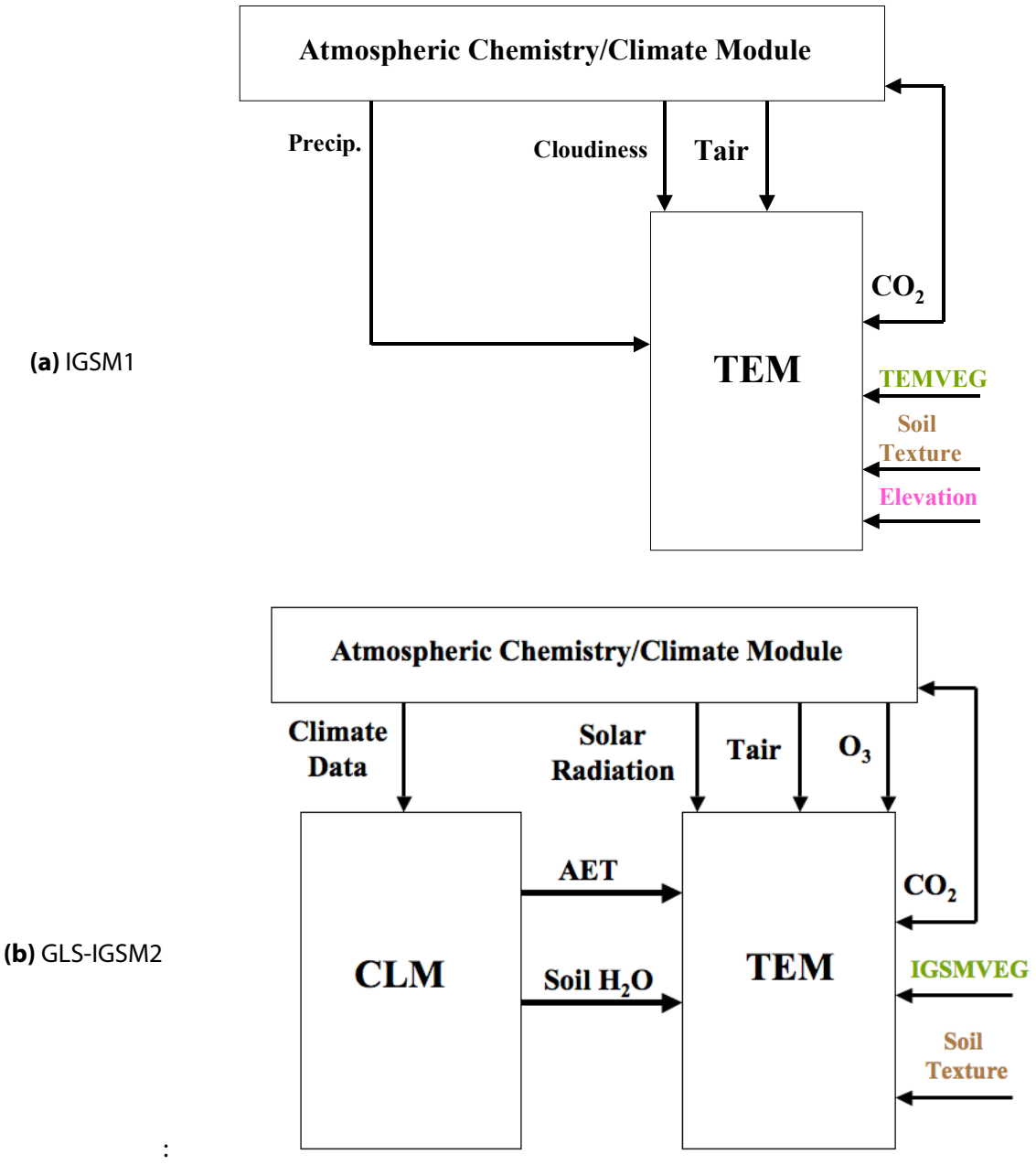

Figure 6. Sources of inputs to TEM in **(a)** the IGSM1, and **(b)** the GLS framework within the IGSM2. Inputs may be obtained either from the atmospheric dynamics and chemistry model, the Community Land Model (CLM) or spatially explicit data sets. Inputs include monthly cloudiness, solar radiation, air temperature (Tair), atmospheric carbon dioxide concentrations (CO_2), atmospheric ozone concentrations (O_3), precipitation (Precip.), actual evapotranspiration (AET), soil moisture (Soil H_2O), along with static land cover type (TEMVEG or IGSMVEG), soil texture and elevation. The TEM then provides carbon to the atmospheric dynamics and chemistry model in the form of CO_2. Land cover, soil texture and elevation inputs are provided by spatially explicit data sets.

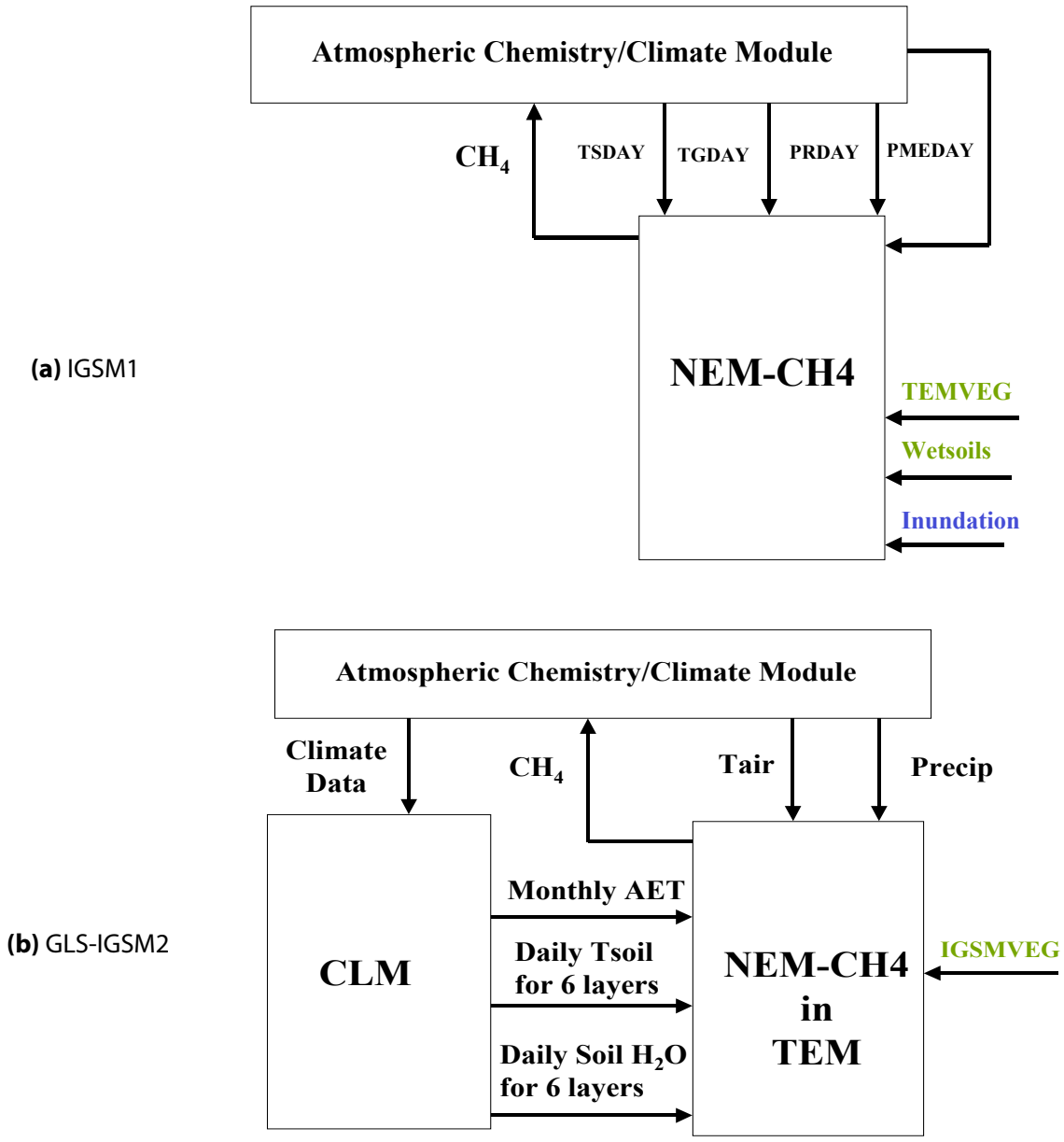

Figure 7. Sources of inputs to the methane module in NEM (NEM-CH_4) in **(a)** the IGSM1 and **(b)** the GLS framework within the IGSM2. Inputs may be obtained either from the atmospheric dynamics and chemistry model, the Community Land Model (CLM) or spatially explicit data sets. Inputs include: daily surface air temperature (TSDAY), ground temperature of the top soil-layer (TGDAY), soil temperature (Tsoil), precipitation (PRDAY), the residual between precipitation and evapotranspiration (PMEDAY) and soil moisture (Soil H_2O); monthly air temperature (Tair), precipitation (Precip.), and actual evapotranspiration (AET); and static data on land cover type (TEMVEG or IGSMVEG), wetsoils type or the relative area of inundation. The NEM-CH_4 then provides methane (CH_4) to the atmospheric dynamics and chemistry model. Land cover, wetsoils type, and relative inundataion inputs are provided by spatially explicit data sets.

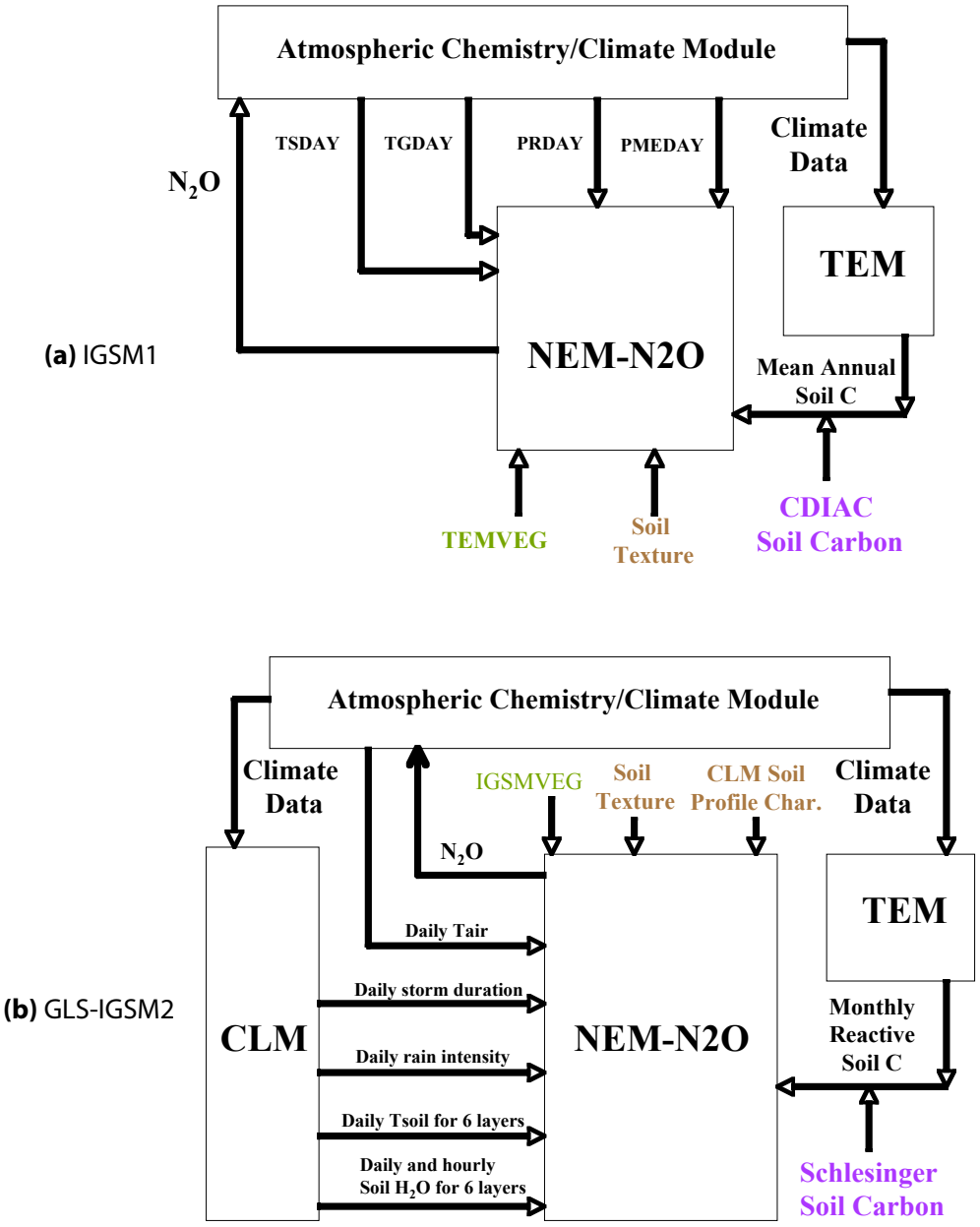

Figure 8. Sources of inputs to the nitrous oxide module in NEM (NEM-N_2O) in **(a)** the IGSM1 and **(b)** the GLS framework within the IGSM2. Inputs may be obtained either from the atmospheric dynamics and chemistry model, the Community Land Model (CLM), the Terrestrial Ecosystems Model (TEM) or spatially explicit data sets. Inputs include: hourly soil moisture (Soil H_2O); daily surface air temperature (TSDAY or daily Tair), ground temperature of the top soil-layer (TGDAY), soil temperature (Tsoil), precipitation (PRDAY), the residual between precipitation and evapotranspiration (PMEDAY), storm duration, rain intensity or soil moisture (Soil H_2O); monthly or annual soil organic carbon (Soil C); or static land cover type (TEMVEG or IGSMVEG), soil texture or soil profile hydrologic characteristics. The NEM-N_2O then provides nitrous oxide (N_2O) to the atmospheric dynamics and chemistry model. Land cover type, soil texture, soil profile characteristic and the CDIAC soil carbon inputs are provided by spatially explicit data sets. The Schlesinger soil carbon data are provided as a biome-specific look-up table.

on terrestrial carbon dynamics (Felzer *et al.*, 2004; 2005). The 4º latitudinal band output of the atmospheric dynamics and chemistry sub-model of the IGSM2 is now used directly by TEM. There is no interpolation of the climate output down to a 0.5º latitudinal band resolution or use of a baseline climate. Estimates by CLM of daily soil temperature and monthly, daily and hourly values for soil moisture variables are now also used by NEM within TEM to estimate methane (Figure 7b) and nitrous oxide (Figure 8b) fluxes.

A new procedure has also been developed that provides a statistical representation of the episodic nature and spatial distribution of land precipitation. This is required for two reasons: 1) an "episodic" provision of zonal precipitation from the IGSM's atmospheric sub-model will reflect more realistic hydrologic forcing to CLM rather than a constant precipitation rate applied at every time step within a month for every zonal band, and 2) the N_2O module of NEM requires precipitation events varying in intensity and duration along with variable dry periods between storm events to employ its decomposition, nitrification, and denitrification parameterizations (see Liu, 1996).

To enable the episodic nature of precipitation, a statistical procedure based on a Poisson-based arrival process is employed. The use of statistical packages to represent precipitation events is widely used (*e.g.*, Dunne, 2001), and has been shown to capture the broad statistical nature of precipitation events. The statistical model is based upon the procedure described by Milly (1994), who used this to study the large-scale impacts of precipitation variability on soilmoisture persistence. To employ the precipitation-event model, two parameters are required. The first is the expected value of inter-event dry period; the second is the expected value of the precipitation event's duration. Unfortunately, robust estimates of these quantities, based on long-term observational records, are elusive at the global scale or at the zonal aggregation of detail used in the IGSM. Therefore, intuitive judgments have been made as to the zonal and temporal (*i.e.* seasonal) variation of these quantities. **Figure 9** depicts the zonal/monthly variations of the expected storm duration and inter-storm periods. Generally speaking, precipitation events occur about every day at the equator as well as latitudes associated with climatological location of the Inter-Tropical Convergence Zone (ITCZ). In addition, a seasonal cycle of precipitation-event interval in mid- to high latitudes is characterized by more frequent, shorter-duration events in the summer (*i.e.* predominantly convective events every few days) and less frequent, longer duration events in the winter (*i.e.* predominantly large-scale/synoptic events every week). Precipitation events that are more associated with convective systems (*i.e.* tropical regions and mid-high latitude summer) are assigned shorter durations (one to a few hours), while precipitation events that are largely associated with large-scale dynamical systems (*i.e.* mid to high latitude synoptic weather systems) are expected to typically last on the order of half a day.

An additional provision is made within the zonal mosaic framework to account for the varying degree of precipitation amounts that are received between the ocean and land as well as across the various vegetation regimes. Using monthly observational estimates from the Global Precipitation Climatology Project Version 2 (GPCP, Adler *et al.*, 2003), the monthly precipitation rates (at 2° latitude x 2° longitude resolution) are mapped over the land/ocean

regions as given by the native and fully resolved IGSMVEG vegetation mapping (at 0.5° latitude x 0.5° longitude resolution). A monthly climatology is then constructed which prescribes the ratio of total land/ocean precipitation received as a fraction of the total zonal precipitation. This zonal, monthly climatology (**Figure 10**) is then linearly interpolated to fit the 4° zonal bands of the IGSM2, and is applied at every time-step in the IGSM2 in order to partition the simulated zonal precipitation rates over land and ocean. Recognizing that zonal land precipitation is not uniformly distributed over various land types (*e.g.,* within a latitude band, a tropical rainforest should receive much more rainfall than a desert), a further partitioning of the zonal land precipitation amongst all land cover vegetation types, across each IGSM2 latitude band is determined by conducting a similar mapping between the GPCP precipitation over land and the native vegetation distribution of GLS/IGSM2 (Fig. 4). As a result, monthly climatologies of the fraction of zonal land precipitation for each land cover type (see **Figure 11**) is further applied, at every time-step, for the given land precipitation rate of the IGSM2.

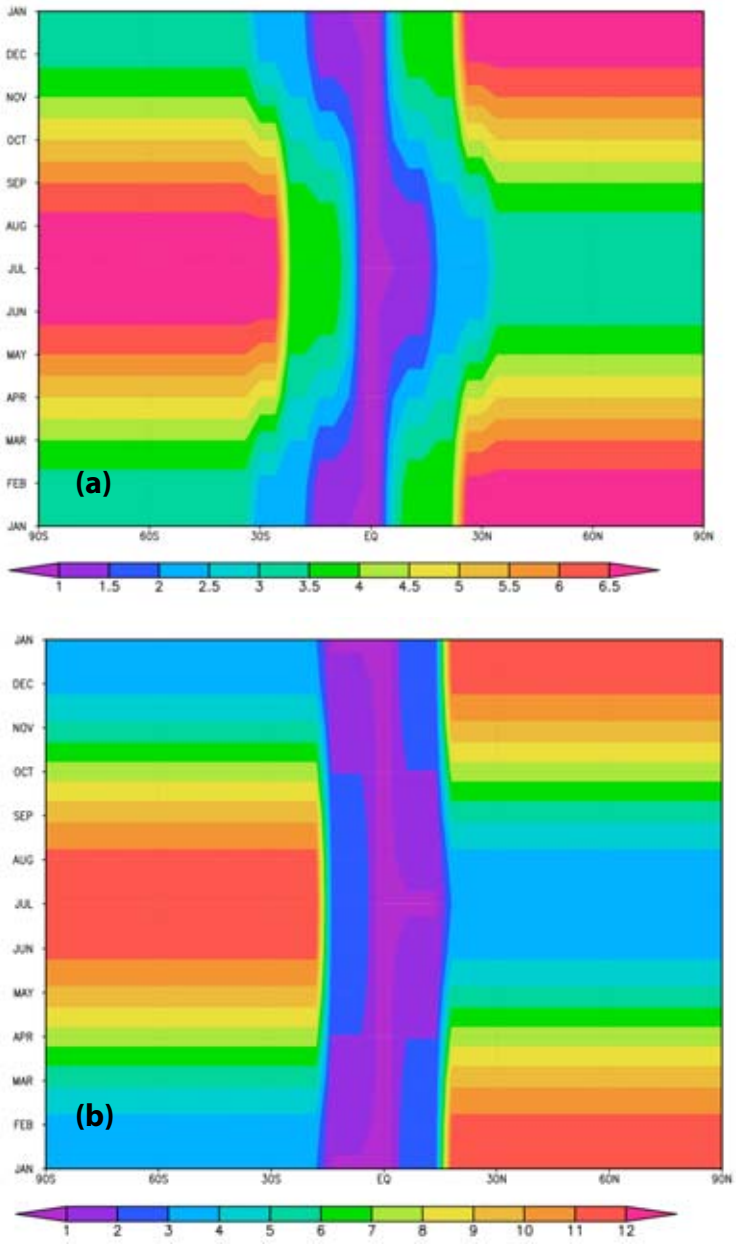

Figure 9. **(a)** Prescription of the expected inter-event period (units in days), and **(b)** the expected event duration (units in hours) for each month and latitude of the stochastic precipitation scheme of GLS.

As depicted in Fig. 2, the fluxes of energy, water, and momentum are exchanged between CLM and the atmospheric dynamics and chemistry sub-model of the IGSM2. For this implementation, the time-step of these exchanges is an hour. Upon the accumulation of all relevant monthly statistics of atmospheric forcings as well as CLM's hydrothermal profiles of wetness and temperature, TEM (with NEM) is then executed for the month. The TEM then aggregates the fluxes of carbon, methane and nitrous oxide for each zonal band, and these are passed back to the atmospheric dynamics and chemistry model.

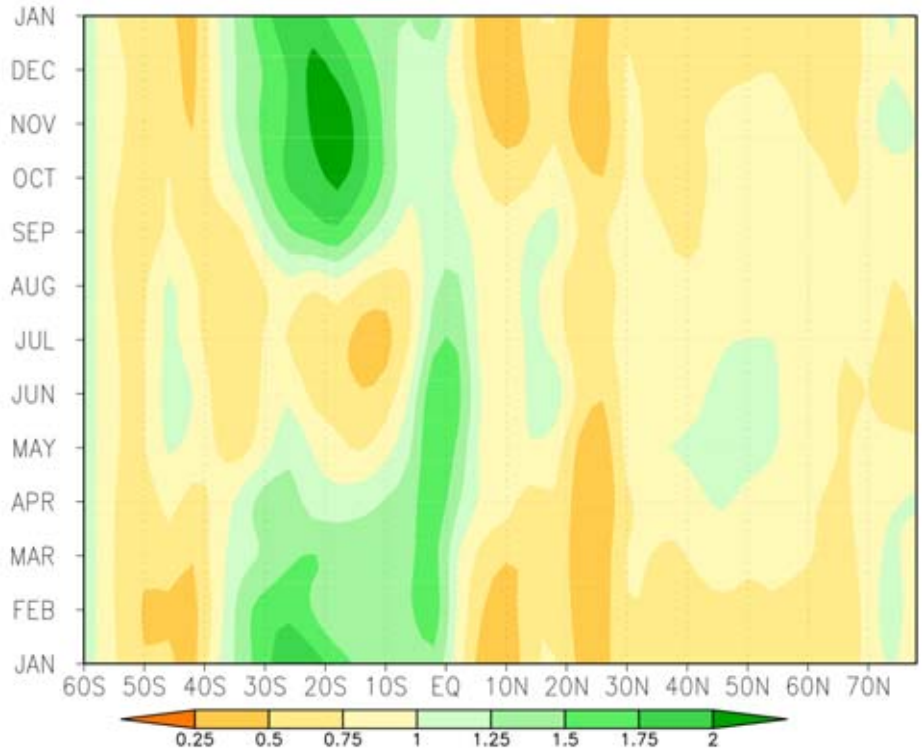

Figure 10. Ratio of zonal-land averaged precipitation to all-zonal (land plus ocean) averaged precipitation, based on the Global Precipitation Climatology Project (GPCP) monthly climatology (1979-2004) mapped against the IGSM2 land/ocean regions.

2.5 Linkages of water and energy among the land modules

The discretization of the soil profile is represented differently within CLM, NEM and TEM (**Figure 12**). The soil profile is represented in CLM as ten layers with each layer possessing a uniform temperature and moisture content. Soil temperatures and moisture contents are tracked for the top 3.436 meters of the soil profile. Similarly, the soil profile in NEM is represented with ten soil layers with each layer possessing uniform temperatures and moisture contents, but the depths of the various layers differ between the nitrous oxide module (NEM-N_2O) and the methane module (NEM-CH_4) of NEM, which are both different from the soil layers used by CLM. Soil-water storage in only the top 50 cm of the soil profile is considered by NEM for estimating nitrous oxide and methane emissions. To use the soil moisture and temperatures generated by CLM within NEM, the CLM output is interpolated to the depths used by the NEM modules.

In contrast to CLM and NEM, TEM represents the soil profile as a single layer. The depth of this layer varies with rooting depth, which varies with land cover type and soil texture, but is generally about 1 meter for grasslands and tundra, 2 meters for temperate and boreal forests and 8 meters for tropical forests. Rooting depth is also assumed to vary with soil texture within the various land cover types (Raich *et al.*, 1991; McGuire *et al.*, 1995). Within the single soil layer, soil moisture is assumed by TEM to be uniformly distributed. Soil temperatures are not used in the version of TEM incorporated into the IGSM2. To use the soil moistures generated by CLM within TEM, the amounts of soil water simulated by CLM for the top 1-meter and top 2-meters

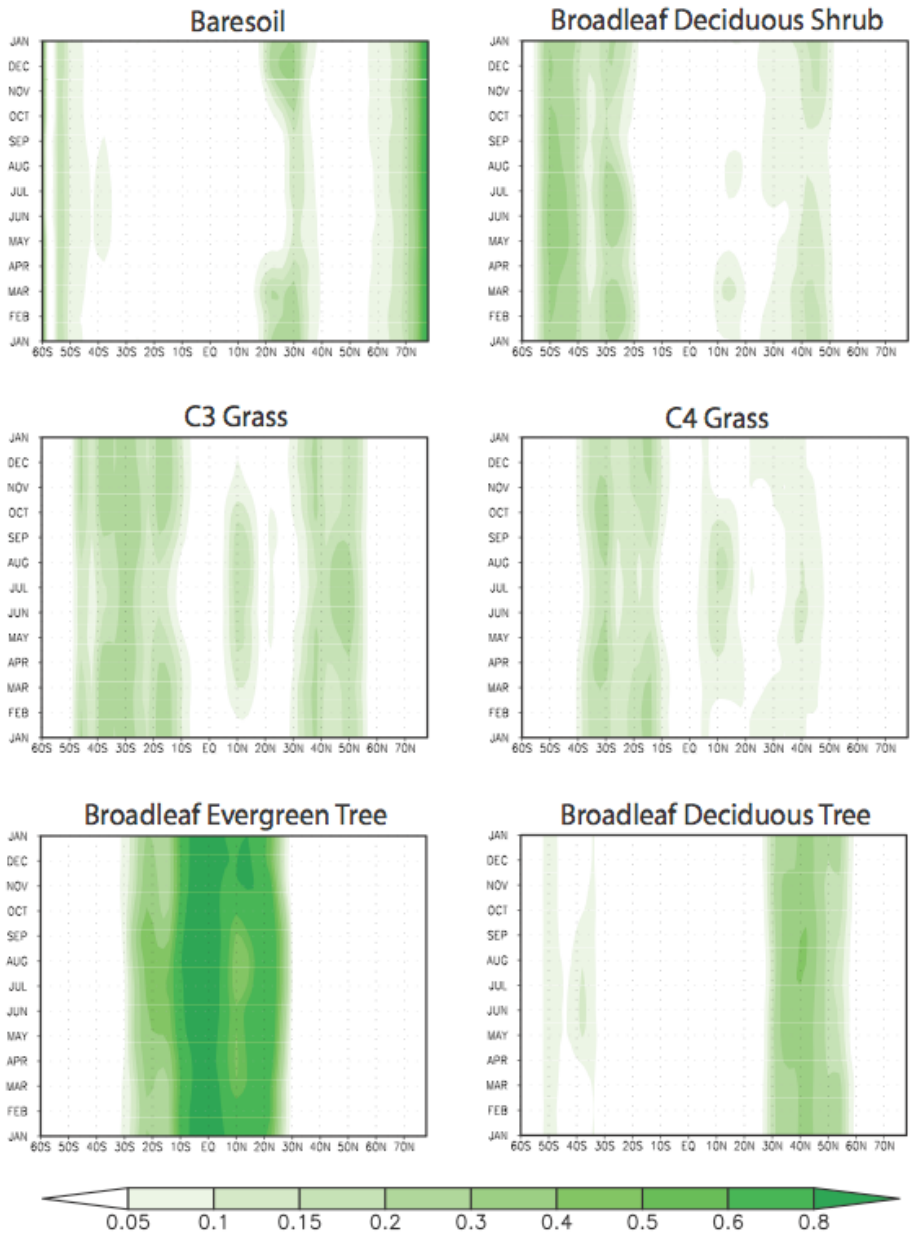

Figure 11. Zonal climatology of the fraction of zonal land precipitation that is distributed to various land cover types, as determined by mapping the GPCP climatology against the IGSM2 land distribution (see text for details). Shown are results for a subset of the various land cover types represented in the GLS land classification system.

of the soil profile are determined. If the rooting depth is less than 1 meter, the soil moisture used by TEM equals the one-meter soil moisture estimated by CLM, scaled by the rooting depth relative to a 1-meter depth. If the rooting depth is between 1 and 2 meters, then weighted-averaged soil moisture is obtained for the soil layer based on the proximity of the rooting depth to 1-meter and 2-meters depth. If the rooting depth is greater than 2 meters, then the amount of soil moisture estimated by CLM is multiplied by the ratio of the rooting depth to 2 meters to determine the soil moisture used by TEM.

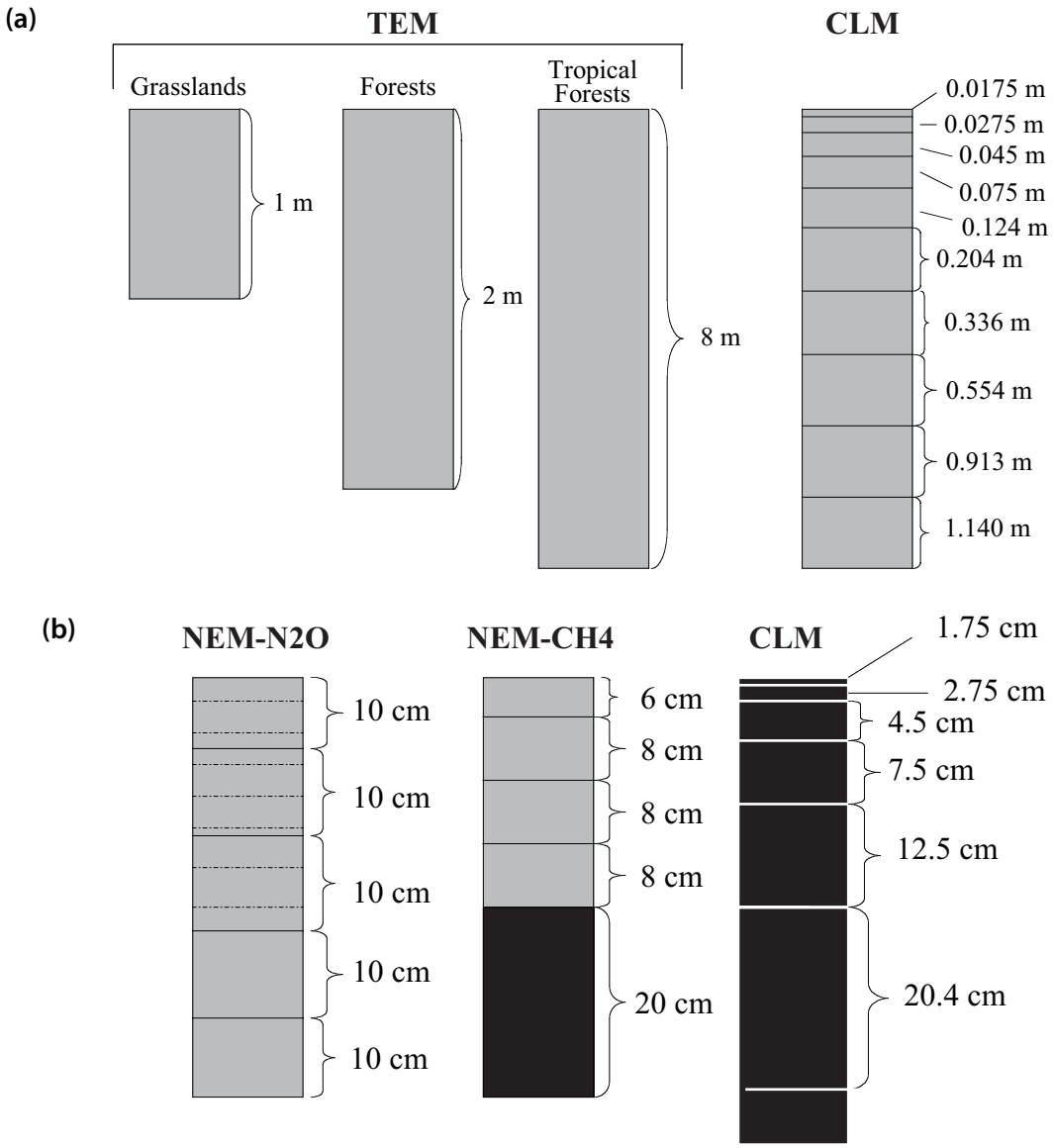

Figure 12. (a) Comparison of soil layer thicknesses among different land cover types used by TEM to that used by CLM for all land cover types. **(b)** Comparison of the top 5 soil-water storage layers between the nitrous oxide module of NEM (NEM-N_2O), the methane module of NEM (NEM-CH_4) and CLM (top 6 soil layers only). Black layers in (b) are assumed saturated for wetlands. In CLM, the whole profile of wetland soils is always assumed to be saturated. In the NEM-CH_4 module, the soil profile of boreal wetlands below 30 cm is always assumed saturated, but the upper 30 cm may or may not be saturated based on local climate conditions (see text for details). In the NEM-N_2O module, the soil moisture in the top 50 cm of the soil profile used to estimate N_2O fluxes may or may not be saturated based on local climate conditions.

Wetlands are also represented differently among the CLM, NEM and TEM. The CLM sets the entire soil profile to be continuously saturated for all wetlands. For boreal wetlands (*i.e.* IGSMVEG = 21 and IGSMVEG = 22), NEM-CH_4 normally considers only the soil profile greater than a depth of 30 cm to be continuously saturated (Fig. 12). Soil moisture above 30 cm depth is allowed to fluctuate in response to environmental conditions. For temperate and tropical

wetlands, NEM-CH_4 estimates methane fluxes from only monthly air temperatures, precipitation and evapotranspiration (Liu, 1996) so that the soil moisture content of wetlands does not influence these flux estimates other than indirectly by its effect on evapotranspiration as estimated by CLM (Fig. 7b). In NEM-N_2O, the soil moisture throughout the top 50 cm of the soil profile is normally allowed to fluctuate. In TEM, soil moisture throughout the soil profile is also assumed to fluctuate with environmental conditions, but the moisture content in soils is assumed to always be less than or equal to field capacity.

Using the prescribed saturated conditions by CLM for wetlands, NEM-CH_4 estimates much larger fluxes of methane from boreal wetlands than previous NEM estimates. By trial and error, we found that the NEM-CH_4 module within the GLS estimates about the same methane fluxes for contemporary conditions across the globe as the previous version of NEM if the water table depth for all boreal wetlands is assumed to be 9.0 cm rather than at the soil surface. Therefore, we use this assumption when developing CH_4 flux estimates with the GLS. Wetland soils are assumed saturated, however, when using the NEM-N_2O module of the GLS to estimate natural soil N_2O fluxes.

Because TEM has been developed primarily for upland ecosystems, TEM estimates that no decomposition or plant productivity occurs under saturated soil conditions. The lack of decomposition results from the implicit effects of saturated soils on limiting oxygen availability to decomposers as TEM does not simulate anaerobic decomposition. Without decomposition to regenerate inorganic nitrogen from detritus, TEM also estimates that no plant productivity occurs in saturated areas due to nitrogen limitations. Because plants really do grow and organic matter really does decompose in wetlands, we attempt to approximate the carbon and nitrogen pools and fluxes in wetlands with TEM by using parameterizations from comparable upland ecosystems along with the assumption that the soil moisture content in all wetlands is at field capacity rather than at saturation.

2.6 The linkages of carbon between TEM and NEM

In the IGSM1 (Fig. 1), TEM and NEM are two separate biogeochemical sub-models that simulate different components of carbon and nitrogen dynamics in natural terrestrial ecosystems as well as the water and energy budgets associated with these dynamics. The TEM estimates major carbon and nitrogen pools and fluxes in terrestrial ecosystems simultaneously on a monthly time-step (Fig. 3). The pools are carbon and nitrogen in vegetation biomass and soil organic matter, which include litter and standing dead, and soil inorganic nitrogen (*i.e.* ammonium plus nitrate). The fluxes include gross primary production (GPP), autotrophic respiration (R_A) of plants, heterotrophic respiration (R_H) associated with the decomposition of organic matter, litterfall and net nitrogen mineralization. Net primary production (NPP), which is an important source of food and fiber for humans and other organisms on earth, is the net uptake of atmospheric carbon dioxide by plants and is calculated as the difference between GPP and R_A. Carbon sequestration by terrestrial ecosystems is determined by net ecosystem production (NEP), which is calculated as the difference between NPP and R_H. In the IGSM, the exchanges

of carbon between terrestrial ecosystems and the atmosphere estimated by TEM are assumed to be in the form of carbon dioxide. In contrast to TEM, NEM consists of two modules that each determines a single trace gas flux: nitrous oxide by the NEM-N_2O module and methane from wetlands by the NEM-CH_4 module. The NEM-N_2O module needs estimates of total soil organic carbon to determine denitrification rates. As TEM only keeps track of soil organic carbon that is assumed to be reactive to near-term climate change (McGuire *et al.,* 1995), NEM has used the CDIAC worldwide soil organic carbon data set (Zinke *et al.,* 1986) to represent the distribution of total soil organic carbon across the globe when estimating contemporary nitrous oxide fluxes (Liu, 1996). Estimates of mean annual reactive soil organic carbon by TEM, regridded to a spatial resolution of 2.5º latitude x 2.5º longitude, are then used in the IGSM1 to determine changes in soil organic carbon for NEM (Fig. 8a) when determining future nitrous oxide fluxes in prognostic simulations (Prinn *et al.,* 1999). There has been no linkage between TEM and the NEM-CH4 module.

To facilitate future progress on simulating methane and nitrous oxide dynamics in terrestrial ecosystems, the algorithms for the two NEM modules have been incorporated into TEM within the GLS framework (*i.e.* Fig. 2). The carbon and nitrogen dynamics described by the NEM algorithms for the top 50 cm of the soil profile are still mostly separated from those described by TEM for the whole soil profile (up to 8 m depth) in the IGSM2, although TEM now provides monthly estimates of reactive soil organic carbon directly to the NEM-N_2O module each month rather than providing a mean annual estimate once a year. In addition, the relatively small loss of organic carbon from the soil as methane, estimated by the NEM-CH_4 module, is now subtracted each month from the soil organic carbon pool estimated by TEM. Although TEM simulates monthly changes in inorganic nitrogen, the NEM-N_2O module still assumes that the top 50 cm of soil contains the same constant amount of nitrogen (currently 0.5 mg NH_4-N per kg soil and 1.0 mg NO_3-N per kg soil) at the start of each year for all ecosystems. Furthermore, the potential competition for inorganic nitrogen between vegetation, nitrifiers, and denitrifiers is presently not considered in the linkages between TEM and NEM. In future model developments, we will attempt to resolve these remaining inconsistencies and better integrate the algorithms describing the carbon and nitrogen dynamics associated with fluxes of carbon dioxide, methane and nitrous oxide from terrestrial ecosystems.

The following protocol is used to link the monthly reactive soil organic carbon estimates of TEM to the NEM-N_2O module (Fig. 8b). First, TEM is run to equilibrium conditions (*i.e.* NEP = 0.0) for each land cover type within a grid cell. The resulting TEM estimate of reactive soil organic carbon is then subtracted from a mean specific estimate of total soil carbon to derive an estimate of "non-reactive" soil organic. For the remaining retrospective and/or prognostic portion of the simulation, total soil carbon is then determined for the NEM-N_2O module by adding the TEM estimate of reactive soil organic carbon, which changes month-to-month to the corresponding estimate of "non-reactive" soil organic carbon, which remains constant throughout the simulation. This total soil organic carbon is then apportioned to each 10 cm soil layer in the top 50 cm of the soil profile based on vegetation type (Figs. 2-4 in Liu, 1996).

Woody vegetation tends to have a larger proportion of total soil organic carbon in the upper layers of the soil profile while grassland tends to have a more uniform distribution of carbon throughout the soil profile. As the Zinke *et al*. (1986) soil carbon data set is based on mean biome-specific estimates that are extrapolated across the globe based on vegetation distribution, we have been able to replace the 0.5º latitude x 0.5º longitude data set with a look-up table of mean biome-specific estimates of total soil carbon (**Table 8**) based on the more updated information in Schlesinger (1997) without loss of spatial detail.

Table 8. Total soil organic carbon assumed to be stored in the top 1 meter of the soil profile in various ecosystems by the MIT IGSM (based on Schlesinger, 1997).

IGSMVEG	Description of Vegetation	Area (km^2)	Total Soil Organic Carbon ($g\ C\ m^{-2}$)
0	Bare Ground	16,942,750	0
1	Needle-leaf Evergreen Tree (NET) temperate	4,970,172	11,800
2	Needle-leaf Evergreen Tree (NET) boreal	11,381,399	14,900
3	Needle-leaf Deciduous Tree (NDT) boreal	961,615	14,900
4	Broadleaved Evergreen Tree (BET) tropical	22,634,499	10,400
5	Broadleaved Evergreen Tree (BET) temperate	3,256,313	11,800
6	Broadleaved Deciduous Tree (BDT) tropical	10,629,481	6,900
7	Broadleaved Deciduous Tree (BDT) temperate	8,298,806	11,800
8	Broadleaved Deciduous Tree (BDT) boreal	500,396	14,900
9	Broadleaved Evergreen Shrub (BES) temperate	1,488,090	6,900
10	Broadleaved Deciduous Shrub (BDS) temperate	14,634,133	5,600
11	Broadleaved Deciduous Shrub (BDS) boreal	2,403,424	21,600
12	C3 grass arctic	6,882,381	21,600
13	C3 grass	14,584,643	19,200
14	C4 grass	8,262,894	3,700
15	Crop 1	0	12,700
16	Crop 2	0	12,700
17	Wetlands (Tree tropical)	851,148	68,600
18	Wetlands (No-tree tropical)	577,466	68,600
19	Wetlands (Tree temperate)	170,464	68,600
20	Wetlands (No-tree temperate)	402,908	68,600
21	Wetlands (Tree boreal)	2,026,972	68,600
22	Wetlands (No-tree boreal)	852,242	68,600
23	Mangroves	139,041	68,600
24	Coastal salt marsh	44,368	68,600
25	Inland salt marsh	53,843	68,600
26	Floodplains (Tree tropical)	103,587	10,400
27	Floodplains (No-tree tropical)	50,417	3,700
28	Floodplains (Tree temperate)	18,703	11,800
29	Floodplains (No-tree temperate)	17,236	9,200
30	Glaciers	16,186,625	0
31	Lakes	947,146	0
32	Rice Paddies	0	12,700
33	Pastures	0	12,700
34	Urban	0	0
--	**All land cover types**	**150,273,162**	--

3. RESULTS

As described in the previous section, the representation of the earth's land surface within the IGSM has changed with the development of the GLS framework. In addition, algorithms have either been added or updated within the modules of the GLS to incorporate more recent advances in our understanding of terrestrial biophysics and biogeochemistry into the IGSM. To evaluate the consequences of these changes, we examine a pair of simulations using the IGSM2 either with the new GLS framework or with the older IGSM1 representation of the earth's land surface. In each of these simulations, the IGSM2 is run, similar to Sokolov *et al.* (2005), for a 240-year "baseline" simulation, starting with prescribed 1861-1990 greenhouse gas concentrations and followed by a standard EPPA scenario of 1991-2100 global emissions using the two-dimensional mixed layer ocean sub-model of the IGSM2 with a prescribed value of ocean heat uptake, $K_{v,}$ equal to 2.1 cm^2/s and the atmospheric dynamics and chemistry sub-model with a prescribed climate sensitivity of 2.9º K. We also compare the estimated zonal fluxes and storage terms of the land surface from these IGSM2 simulations to observational data from the latter part of the 20th century (when the most comprehensive global-scale observations are available) as well as the zonally aggregated outputs of other land/climate models run at a higher resolution to evaluate the IGSM2 results. In the analysis that follows, we first examine how estimates of key water and energy states and fluxes for contemporary climate conditions have changed using the new GLS framework. We then examine how these changes have influenced estimates of the exchange of carbon dioxide, methane and nitrous oxide between terrestrial ecosystems and the atmosphere. Finally, we examine both the historical trends in terrestrial biophysics and biogeochemistry estimated by the GLS framework and those projected for the 21st century.

3.1 Evaluation of key water and energy states and fluxes

The representation of seasonal and latitudinal patterns of land precipitation (**Figure 13**a,b) has improved in the IGSM2 (Fig. 13c) over that simulated by the IGSM1 (Fig. 13f). These improvements, which are quantified by increases in pattern correlations, ρ, and decreases in pattern RMS, ρ, have been a result of: 1) the new representation of biogeophysical processes by CLM in the GLS framework (Fig. 13d); 2) the stratification of zonal precipitation between land and oceans and among land cover types (Fig. 13e) and 3) changes in the convection parameterization of the atmospheric dynamics and chemistry model (Fig. 13c). In the IGSM1, substantial inconsistencies exist in the latitudinal and seasonal variations of land precipitation compared against two widely used global precipitation observations (the Global Precipitation Climatology Project, GPCP, of Adler *et al.*, 2003 and the CPC Merged Analysis of Precipitation, CMAP, of Xie & Arkin, 1997). Most notable is the large decrease, rather than an increase, in mid- to high-latitude summer precipitation. Further IGSM1 deficiencies include an erroneous maximum of winter precipitation at ~25-45° N, which partly overlaps the observed northern sub-tropical precipitation minimum, as well as weaker precipitation rates associated with the Inter-Tropical Convergence Zone (ITCZ) than those observed, and the timing of the northern tropical precipitation maximum is delayed by almost two months.

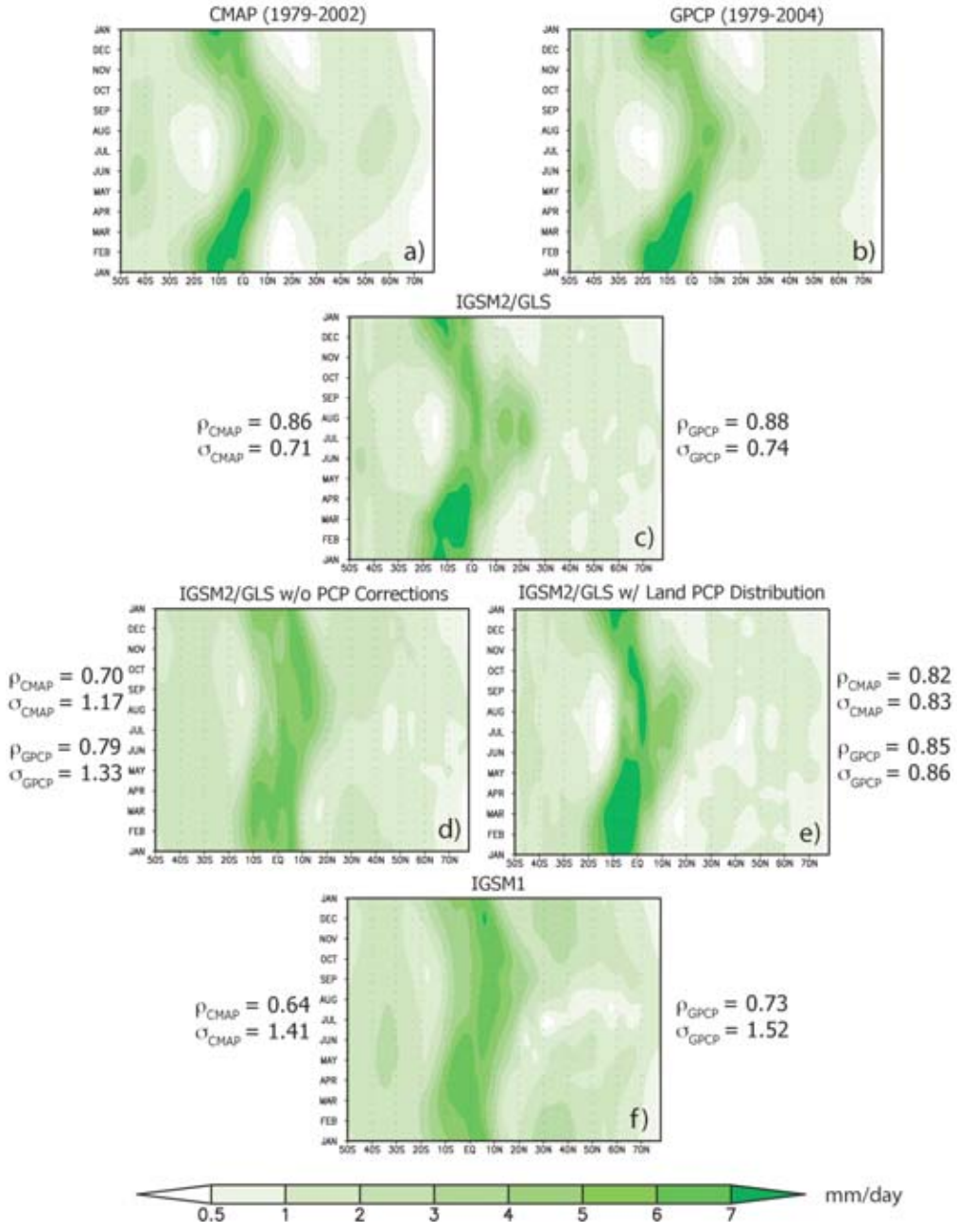

Figure 13. Monthly, zonal land-only precipitation for IGSM2/GLS simulations evaluated against two standard observational climatologies. Top panels show observed **(a)** CMAP precipitation averaged over 1979-2002 and **(b)** GPCP precipitation averaged over 1979-2004. For **(c)** the IGSM2/GLS average (1979-2004) is shown with all corrections and updates. The results from IGSM2/GLS with no land precipitation adjustments **(d)** as well as with the land precipitation distribution only (*i.e.* no precipitation parameterization updates to the atmospheric module) **(e)** are also shown (see text for details). The result for IGSM1 is given in panel **(f)**. Pattern correlations (ρ) and RMS errors (ρ) of the zonal, monthly mean annual cycles between the IGSM simulations and the GPCP, CMAP are also shown.

With the incorporation of GLS into the IGSM2, the most notable effect is to remove a large portion of the erroneous minima of summer precipitation in northern latitudes (Fig. 13d), but other deficiencies seen the IGSM1 remain. The prescribed climatological partitioning of zonal precipitation into land and ocean components, along with the further distribution of land precipitation across the various land cover types (Section 2.4) considerably enhances the simulated zonal land precipitation field (Fig. 13e). The spatiotemporal locations of the relative minima and maxima of zonal land precipitation show a much better consistency to observations. However, the IGSM2 continues to produce deficient precipitation for the northern mid-latitude summer. In contrast to IGSM1, the model now produces excessive precipitation in portions of the tropics associated with the inter-tropical convergence zone (ITCZ).

To address these remaining inconsistencies, we conducted additional testing with the IGSM2's precipitation parameterization, examining the extent to which the remaining deficiencies could be improved. The 2D (zonally averaged) atmospheric model (Sokolov & Stone, 1998), used as a climate component of the IGSM, calculates convection and large-scale condensation under the assumptions that a zonal band may be partially unstable or partially saturated, respectively. The moist convection parameterization, which was originally designed for the GISS Model I (Hansen *et al.*, 1983), requires knowledge of sub-grid scale temperature variance. Zonal temperature variance associated with transient eddies is calculated using a parameterization proposed by Branscome (see Yao & Stone, 1987). The variance associated with stationary eddies is represented by adding a fixed variance of 2 K^2 at all latitudes. For the GLS/IGSM2 implementation, we introduce a latitudinal dependence of the latter variance that follows more closely the climatological pattern (see Fig. 7.8b of Peixoto & Oort, 1996). In addition, the threshold values of relative humidity for the formation of large-scale cloud and precipitation have been modified such that a constant value for all latitudes (as used in the IGSM1) is replaced with latitudinally varying values. This modification is made to account for the dependence of the zonal variability of relative humidity on latitude. The above changes promote stronger extra-tropical precipitation rates that are clearly lacking in the IGSM1, as well as diminish the somewhat excessive tropical precipitation rates (Fig. 13e). The results of these modifications show further improvements in the zonal pattern of the annual cycle of precipitation (Fig. 13c), with lower precipitation rates over the ITCZ as well as increased summer precipitation rates over the northern midlatitudes.

In addition to improvements in the mean seasonal and latitudinal patterns of contemporary land precipitation, the representation of interannual variability in monthly land precipitation (**Figure 14**, panels **a** and **b**) has improved in the IGSM2 (Fig. 14c) over that simulated by the IGSM1 (Fig. 14f). The widespread interannual variability of land precipitation found in the extratropics in the observations is absent in the IGSM1 results. Incorporation of the GLS framework into the IGSM2 has little influence on this interannual variability (Fig. 14d), but corrections for differences in precipitation among the various land-cover types and between land and ocean result in substantial improvements in the degree and patterns of the IGSM2 simulated interannual variability of land precipitation (Figure 14e). Changes in the parameterization of convection in the atmospheric dynamics and chemistry sub-model add little benefit (Fig. 14c) to the land corrections.

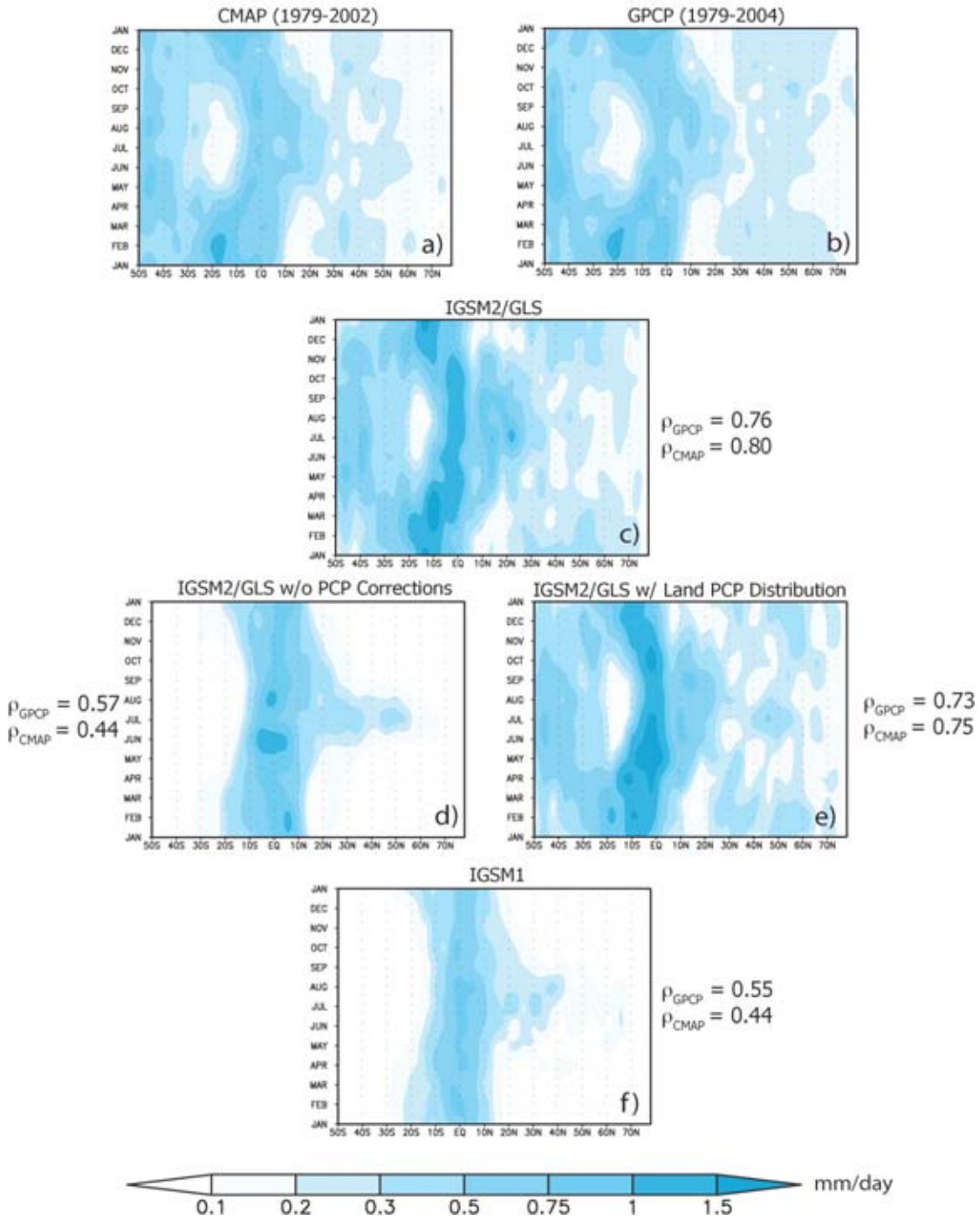

Figure 14. Inter-annual variability (given as standard deviations) of monthly zonal land-only precipitation for IGSM2/GLS simulations evaluated against two standard observational climatologies. Top panels show observed **(a)** CMAP precipitation averaged over 1979-2002 and **(b)** GPCP precipitation averaged over 1979-2004. For **(c)** the IGSM2/GLS average (1979-2004) is shown with all corrections and updates. The results from IGSM2/GLS with no land precipitation adjustments **(d)** as well as with the land distribution only (no precipitation parameterization updates to the atmospheric module) **(e)** are also shown (see text for details). The result for IGSM1 is given in panel **(f)**. Pattern correlations (ρ) of the zonal, monthly mean annual cycles between the IGSM simulations and the GPCP, CMAP are also shown.

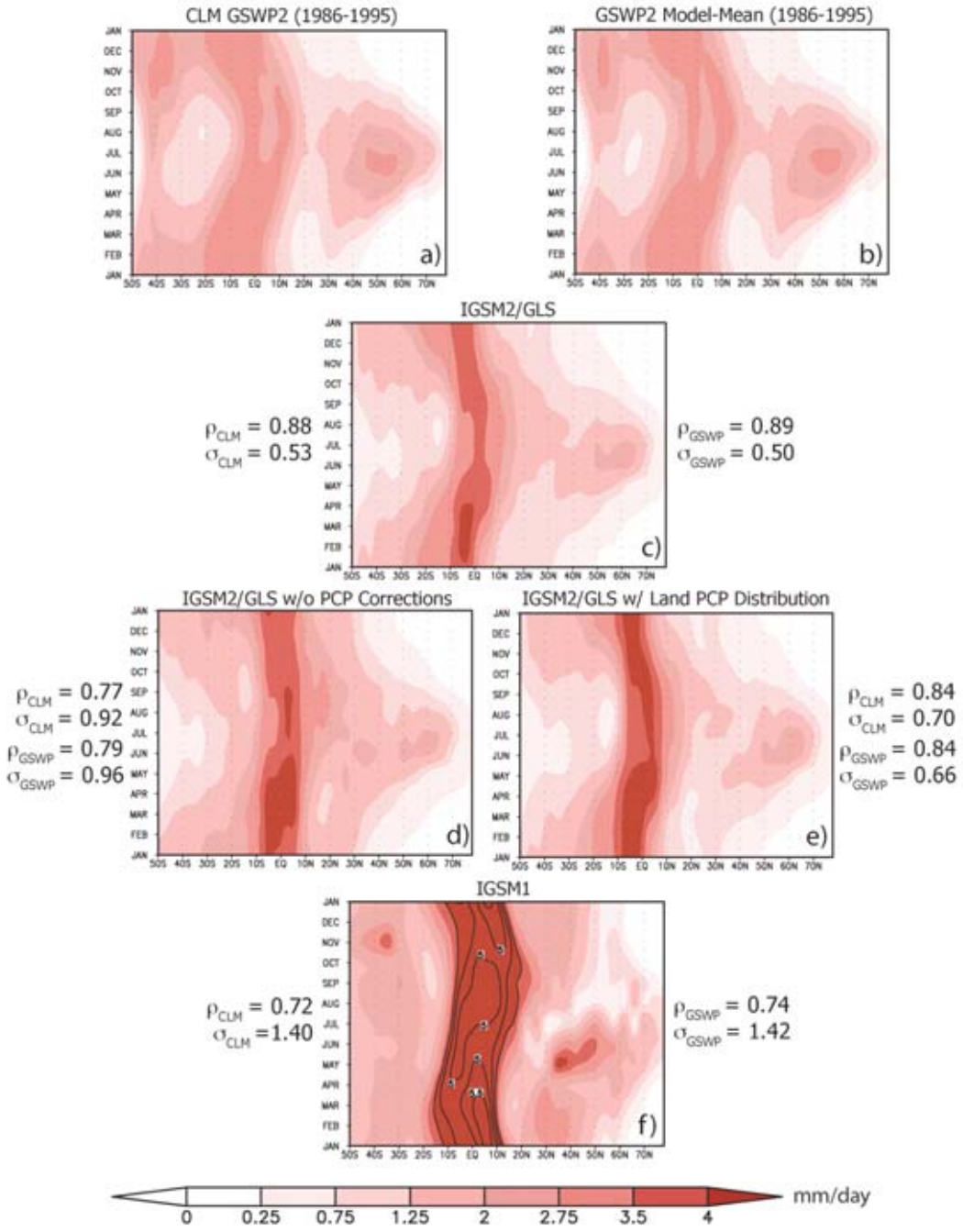

Figure 15. Zonal land evapotranspiration IGSM2/GLS simulations evaluated against state-of-the-art estimates. Panels **(a)** and **(b)** show the monthly mean annual-cycles of evapotranspiration (1986-1995) of CLM GSWP2 results and the GSWP2 model-mean of evapotranspiration for the baseline simulations (B0 runs), respectively. For **(c)** the IGSM2/GLS average (1986-1995) is shown with all corrections and updates. The results from IGSM2/GLS with no land precipitation adjustments **(d)** as well as with the land/PFT distribution only (i.e. no precipitation parameterization updates to the atmospheric module) **(e)** are also shown (see text for details). The result for the IGSM1 is given in panel **(f)**. Pattern correlations (ρ) and RMS differences (ρ) of the zonal, monthly mean annual cycles between the IGSM simulations and the Model Mean GSWP2 and CLM GSWP2 results are also shown.

The improvements to the land precipitation features in the IGSM2 result in marked improvements of evapotranspiration rates (**Figure 15**) when compared against the consensus results of "state of the art" land models (that included CLM) driven by observed atmospheric conditions from the Global Soil Wetness Project Phase 2 (GSWP2, Dirmeyer *et al.*, 2003). The deficient summertime precipitation in northern latitudes by the IGSM1 causes a drying of soil column and reduced summer evapotranspiration (Fig. 15f) not seen in the results of the GSWP2 models (Figs. 15a,b). In addition, evapotranspiration rates in tropical regions are much too high. The incorporation of the GLS framework into the IGSM2 has diminished the excessive tropical rates, as well as produced more reasonable northern midlatitude summer rates (Fig. 15d). The corrections for land versus ocean precipitation (Fig. 15d) and the use of better convection parameterizations by the atmospheric dynamics and chemistry model (Fig. 15c) has also led to further improvements in the IGSM2 estimates of seasonal evapotranspiration rates.

Given these consistencies in precipitation and evapotranspiration, the GLS also reproduces fairly well the timing of maximum and minimum soil temperature during the year as compared to the zonally-averaged 1° latitude x 1° longitude CLM result from GSWP2 (**Figure 16**). In particular, the GLS/IGSM2 shows a strong consistency in the timing of the entry and exit of the

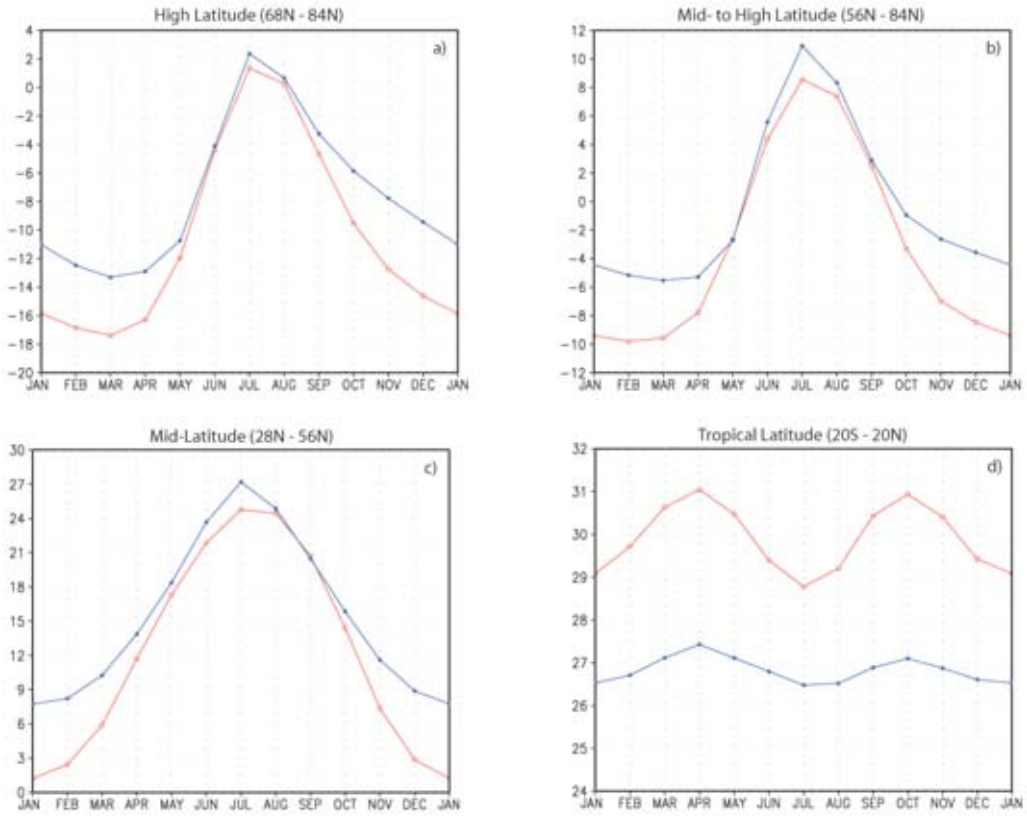

Figure 16. Mean annual cycle (1986-1995) of the thickness-weighted average soil temperature for the top 6 soil layers (to a depth of 50 cm). Blue curve (with filled circles) denotes the GLS/IGSM2 result and the red curve (with open circles) the CLM GSWP2 result (as in Fig. 15a). Panel **(a)** represents high latitude, **(b)** mid- to high latitude, **(c)** mid-latitude, and **(d)** tropical latitude regions over which the results are averaged. Units are in °C.

frozen soil season for higher latitudes (Figs. 16a,b). However, the most notable shortcomings are the warm bias in winter temperature (although consistently frozen as compared to the CLM/GSWP2 result) as well as the cold temperature bias in the tropics (Fig. 16d) and summer midlatitudes (Fig. 16c). These biases are, in part, due to the fact that the GLS is forced by zonally averaged air temperature and radiation, when there are important land/ocean differences in these quantities. These biases are more clearly seen when viewed within a single soil layer (**Figure 17**). However, the consistency of the timing of the hottest and coldest parts of the year with respect to the GSWP2 result is also evident.

During the cold season, the GLS must decide the phase of the incoming precipitation simulated by the atmospheric dynamics and chemistry model. This decision is based on a surface-air temperature criterion that if the zonal surface-air temperature provided by the atmospheric model is greater than 2.5° C, the precipitation occurs as rain, otherwise it is snowfall. Given this zonal surface-air temperature criterion, as well as the warmer soil conditions (Figures 16 and 17), it is not surprising that the extent of

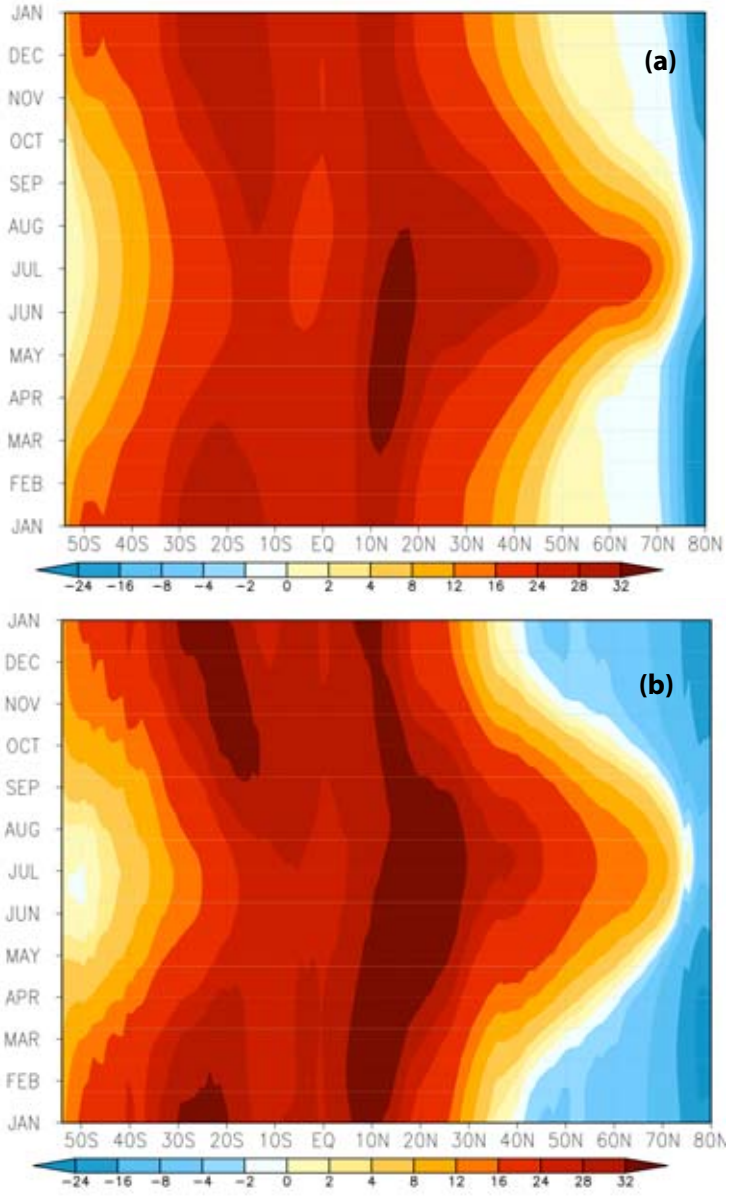

Figure 17. Latitude depiction of the mean annual cycle (1986-1995) of the 3rd soil layer temperature (depth centered at 6.75 cm with a thickness of 4.5 cm). Units are in °C. Panel **(a)** is the result based on the GLS/IGSM2 baseline simulation with soil temperature simulated by CLM. Panel **(b)** is the zonally-averaged result based on CLM's Global Soil Wetness Project Phase 2 (GSWP2) 1° latitude x 1° longitude simulation forced with observationally based atmospheric conditions.

zonal snowcover by the GLS/IGSM2 is less than what is observed (**Figure 18**). The most notable deficiencies are located in the latitude regions that show more ephemeral and fractional coverage. Nevertheless, the GLS/IGSM2 result (Fig. 18b) shows a marked improvement over the

IGSM1 land model simulation (Fig. 18c). The GLS simulates higher snowcover fractions as well as maintains the maximum extent snowcover fraction for a longer period, particularly in the northern high latitude regions, which is in better agreement with the observations. The inability of the GLS to reproduce the southernmost extent of the Northern Hemisphere snowcover seen in Figure 18 can most likely be attributed to its omission of resolving major mountainous regions in these zonal regions (*e.g.*, Himalayan Range as well the major western U.S. mountain ranges, among others), as well as the lack of the IGSM2 in providing intra-zonal variations (*i.e.* land/sea contrast) in the near-surface atmospheric conditions. Generally speaking, cold-season air temperatures over land regions are colder than over-ocean regions and conversely during summertime conditions.

To examine the significance of this land/ocean surface-air temperature issue, a monthly climatology has been constructed based on the 20th century climate model simulations of the IPCC Fourth Assessment Report (AR4) archive in a preliminary analysis. The climatology depicts the zonal and monthly surface-air temperature differences between the zonal average and the zonal averaged over land areas only.

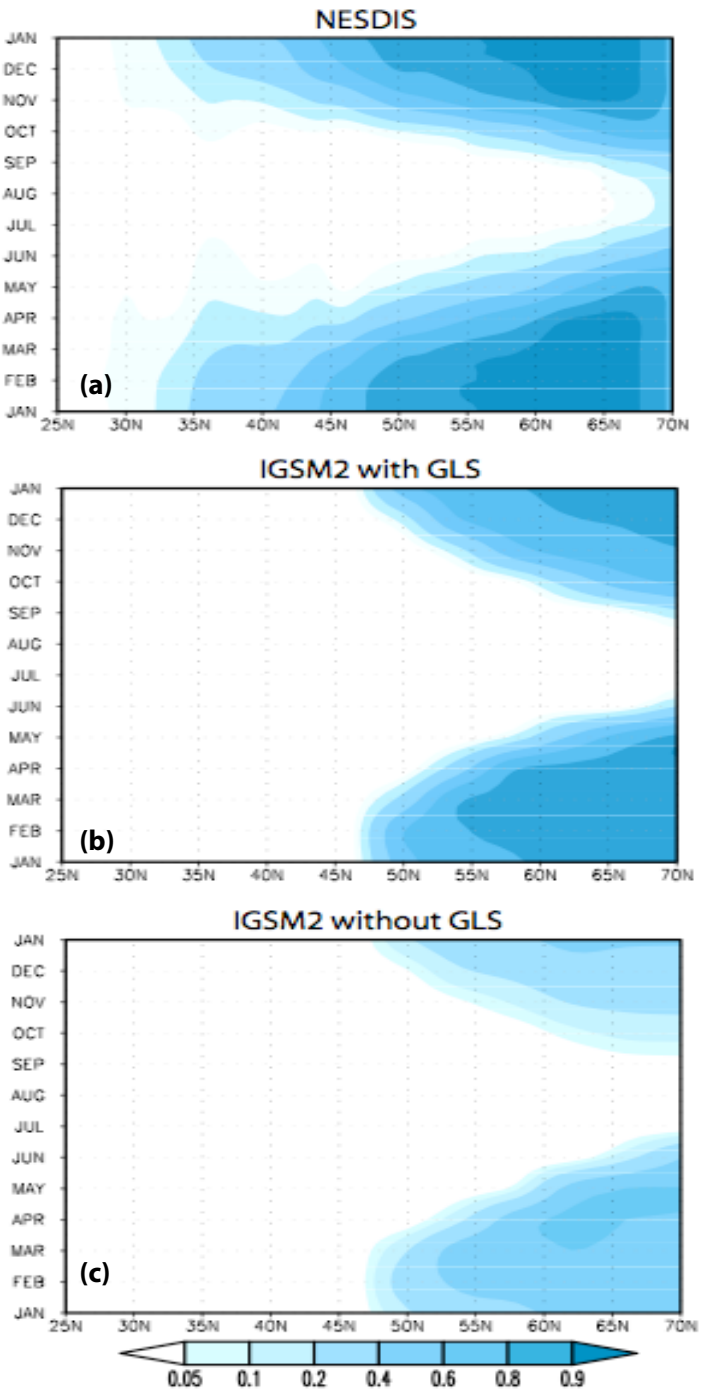

Figure 18. Zonally averaged snowcover (units in fraction of total area) for IGSM2 simulations evaluated against NESDIS observations **(a)**. Shown are mean annual cycle results for the 1972-2001 period. Panel **(c)** shows the result from IGSM2 without using the GLS (*i.e.* employing the IGSM1 land model scheme), and **(b)** displays the GLS/IGSM2 result. See text for details.

The climatology (not shown) is interpolated to the IGSM2 4° zonal grid, and this air-temperature effect is tested in GLS by re-running the baseline simulation of Sokolov *et al.* (2005). The results of this preliminary analysis (not shown) indicate that the GLS snowcover simulation is marginally improved in the seasonal extent of snowcover, although further analyses are warranted. As such, the consideration of the land/sea contrasts in surface-air temperature has not been implemented in the IGSM2, but these contrasts are the focus of ongoing analysis for potential future implementation, and also serve as a motivation for a fully three-dimensional IGSM framework to better capture the longitudinal detail in climate conditions.

3.2 Evaluation of trace-gas emissions

Similar to the biogeophysical (*i.e.* water and energy) variables evaluated in the previous section, the zonal features of TEM's simulated carbon cycling as well as methane and nitrous oxide emission in the GLS framework are judged against geographically explicit, but zonally aggregated estimates. For seasonal carbon fluxes, TEM's zonal estimates aren't substantially affected by its use of zonal mosaic land cover data in the IGSM2 rather than the 0.5º latitude x 0.5º longitude gridded data used in IGSM1, or the improvements in precipitation distribution and evapotranspiration (**Figure 19**). Generally speaking, the timing and location of the tropical carbon sink sand source regions is preserved, although the TEM/GLS estimated summertime maxima of carbon uptake, centered at 10° N (Figure 19b), is weaker than that estimated by the IGSM1 (Figure 19c) or that estimated by TEM using observed climatology (Figure 19a). Consistent among all the TEM runs is the fact that TEM produces the most prominent carbon uptake rates during the late spring through early summer at mid- to high northern latitudes. The TEM/GLS produces slight carbon emissions during mid summer between 30° and 40° N, which is consistent with the two other TEM runs considered, but the return to carbon uptake conditions for this region during late summer and early fall is not seen in the other TEM runs. One of the more desirable changes in the patterns of carbon flux by TEM/GLS, as compared to TEM in IGSM1, is the removal of the mid-summer carbon emission at northern high latitudes, which is not seen in the spatially explicit TEM simulation forced by observed atmospheric conditions. Generally speaking, most of the seasonally varying features of carbon flux from GLS/TEM show weaker magnitudes, which is not surprising given that TEM is responding to zonally averaged state and flux variables as simulated by GLS/IGSM2.

The effect of the improved hydrologic conditions has also influenced the simulation of natural soil emissions of N_2O. However, to allow the IGSM2 to estimate a similar rate of contemporary global N_2O emissions as the IGSM1, the moisture threshold for denitrification, however, has been adjusted from a value of 40% water-filled pore space in the soil (Liu, 1996) to 42.5% in the IGSM2. For the globe, TEM/NEM's average annual global emission from the GLS/IGSM2 baseline simulation is quite consistent with the most recent observationally based estimates (**Figure 20**). Moreover, the latitudinal depiction of total (*i.e.* natural and industrial) N_2O emissions from GLS and EPPA are quite consistent with the most recent estimates obtained through the inverse methods of Hirsch *et al.* (2006) and the recent Global Emissions Inventory

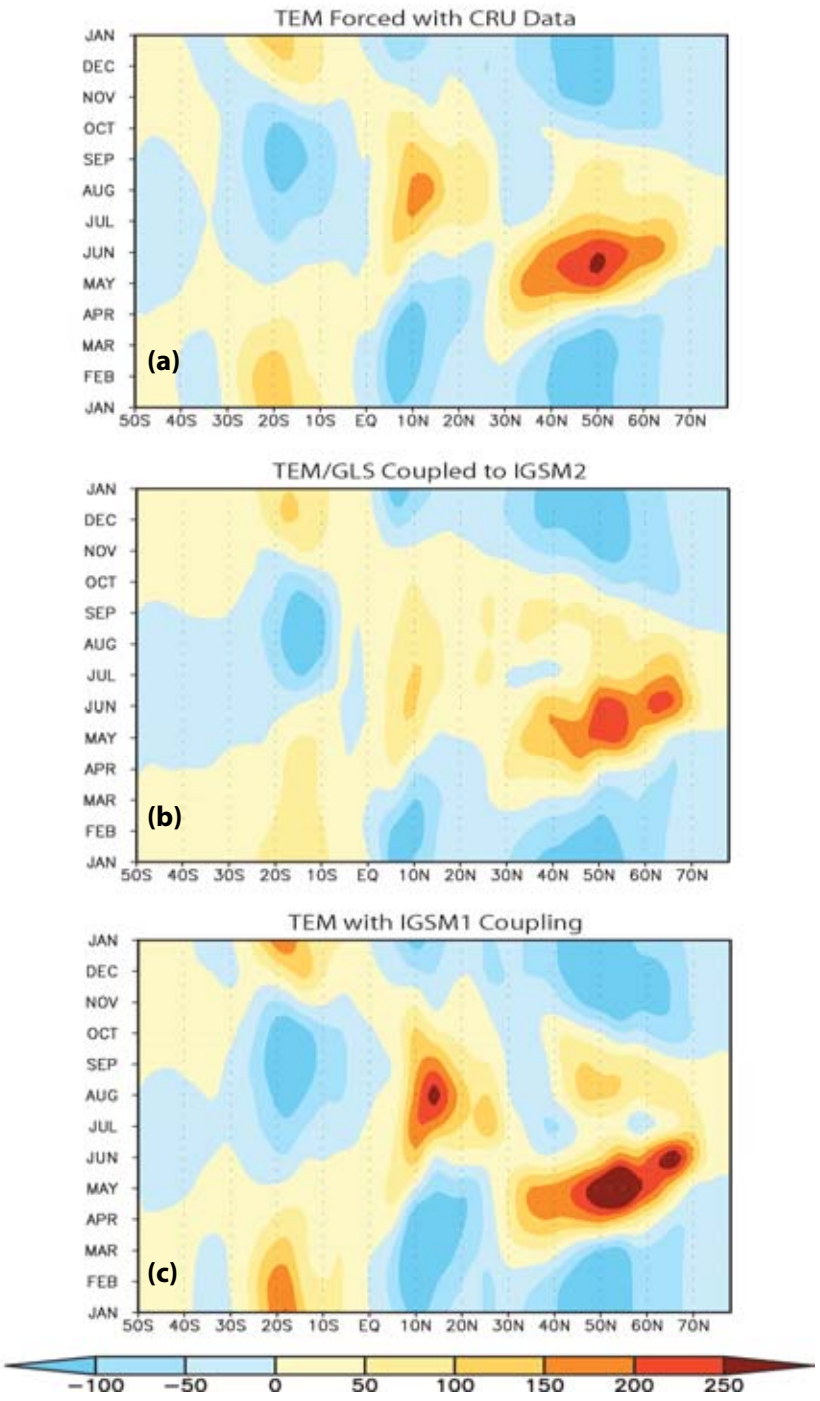

Figure 19. Mean annual cycles of zonal carbon flux (units in Tg of C/month) estimated by TEM. Panel **(a)** shows the zonally averaged result for TEM run globally at a 0.5° latitude x 0.5° resolution forced with CRU data. Panel **(b)** shows zonal TEM employed within the GLS framework and coupled to IGSM2. Panel **(c)** displays the zonally averaged 0.5° latitude x 0.5° longitude resolution results of TEM forced with transient zonal climate anomalies as done in the IGSM1 coupling framework.

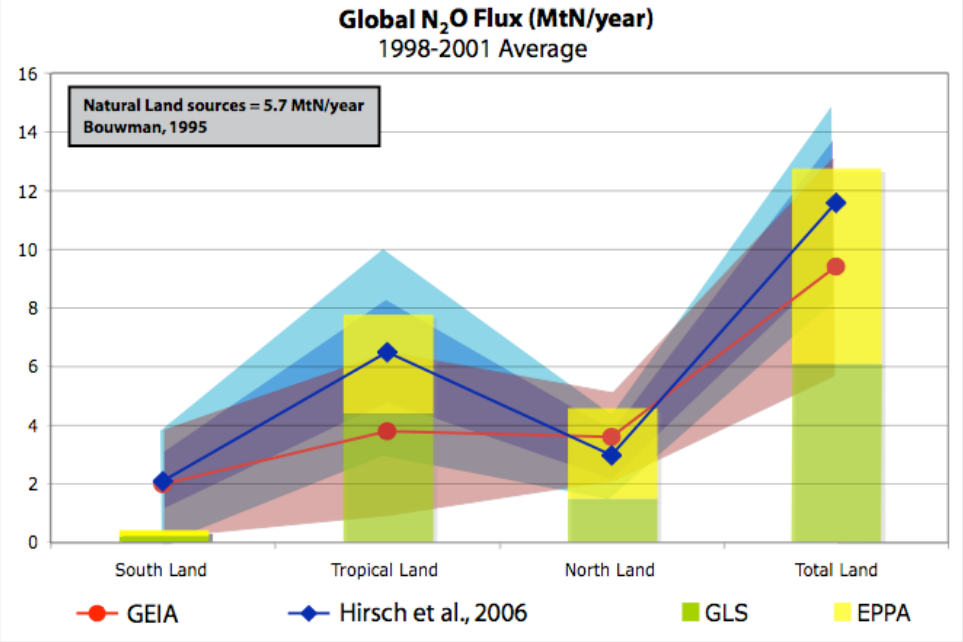

Figure 20. Estimates of N_2O emissions from the IGSM2 (denoting natural soil emissions from the GLS and anthropogenic emissions from EPPA), GEIA (Global Emissions Inventory Activity), and inverse methods (Hirsch, *et al*., 2006) for global, northern (20°N - 90°N), tropical (20°S - 20°N) and southern (90°S - 20°S) land domains. Shading denotes range of uncertainty in the GEIA (red) and Hirsch *et al.* (2006) estimates. For the Hirsch *et al.* (2006) study, the blue shading represents the 2-sigma deviation of the inverse method estimates under various assumptions (see reference for details). The annual, global estimate of natural N_2O emissions of 6.1 Mt N/year by the GLS of the IGSM2 is a little higher than the 5.7 Mt N/year estimate of Bouwman (1995).

Activity (GEIA). For TEM/GLS and the other estimates considered (Fig. 20), the tropical regions produce the highest amounts of N_2O emissions, which for the GLS are primarily attributed to emissions coming from the 10° to 20°N region during late summer (**Figure 21**b). The GLS/EPPA and the other studies estimate the lowest annual N_2O emission rates in the southern extra-tropical regions, and are within the range of uncertainty as determined from a variety of assumptions with the inverse method. This range, however, is probably not a comprehensive estimate of the total range of uncertainty in N_2O emissions in this region.

Because CH_4 emissions from boreal wetlands depend upon a constant soil moisture content in the IGSM2, improvements in the hydrologic conditions described above only influence CH_4 emission estimates from temperate and tropical wetlands. As described in Section 2.5, a prescribed constant water table depth of 9 cm is used for boreal wetlands so that the IGSM2 estimates of contemporary global CH_4 emissions that are similar to those of the IGSM1 simulations. For natural CH_4 emissions, the range of uncertainty among the current global estimates is quite large (almost a factor of 3). The global, annual CH_4 flux estimate provided by TEM/GLS is near the middle of this range (**Figure 22**a). Recent inverse methods would suggest that global emissions are more likely to be higher (Fig. 22a). With respect to the GLS/IGSM2 emission estimate, the lower global flux of CH_4 is likely a result of the relatively modest emissions from tropical and temperate wetlands, as the simulated annual emission from

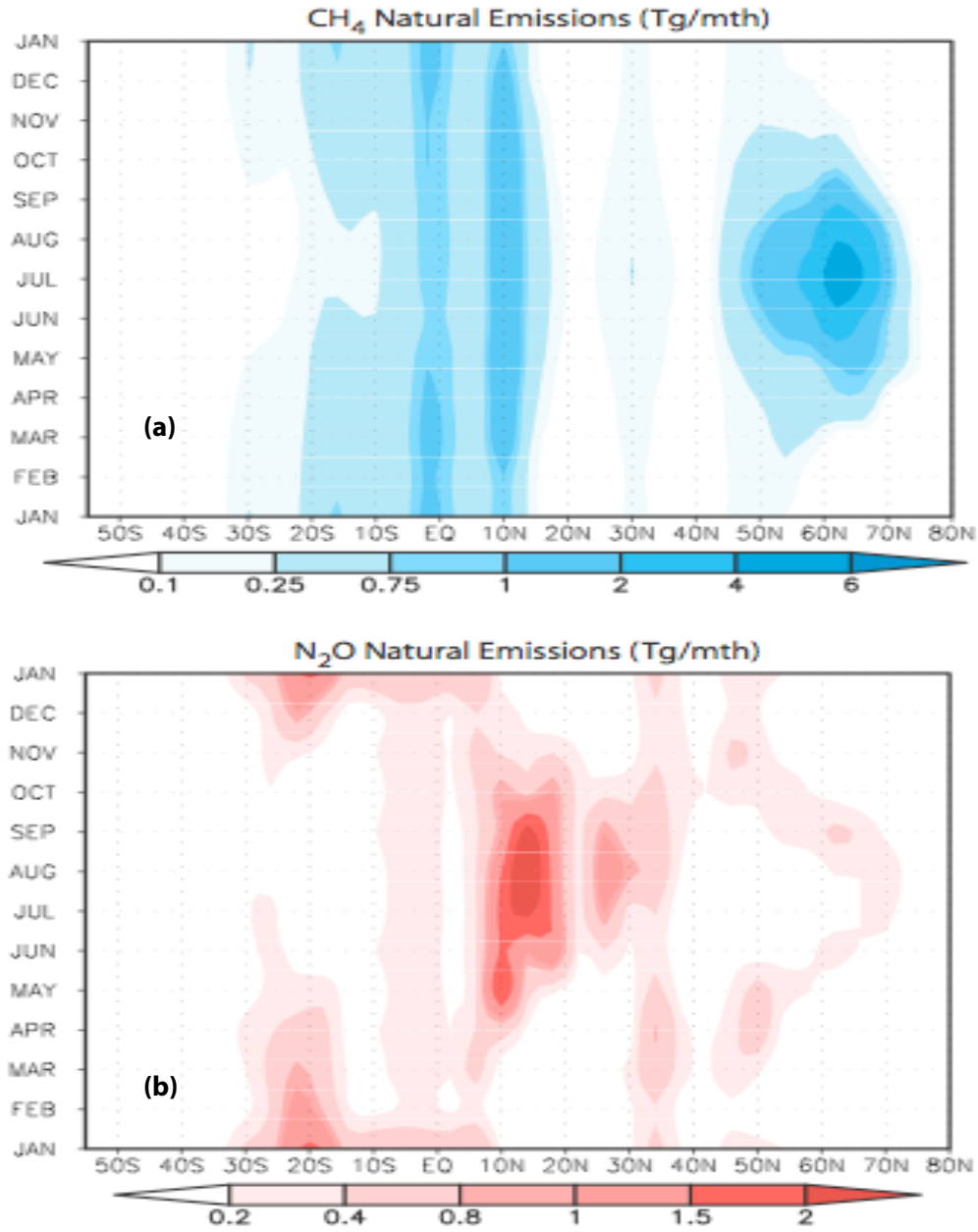

Figure 21. (a) Mean annual cycles of simulated zonal emissions of CH_4 (units in Tg CH_4/mth) and **(b)** N_2O (units of Tg N_2O/mth) from the GLS/IGSM2. Annual cycles are based on averages for the 1980-2000 baseline GLS/IGSM2 simulation period.

tundra and bog regions is more consistent with the more recent consensus of estimates (Fig. 22b). Nevertheless, the zonal features of the annual cycle of CH_4 emissions from the TEM/GLS (Fig. 21a) are characterized by a prominent maximum during the northern high latitude warm season with the highest fluxes during July. Just south of the equator, higher fluxes of methane coincide with the wetter periods of the year. On the other hand, the simulated methane fluxes about the 10° N latitude band show fairly persistent magnitudes throughout the year, with only slight decreases during January.

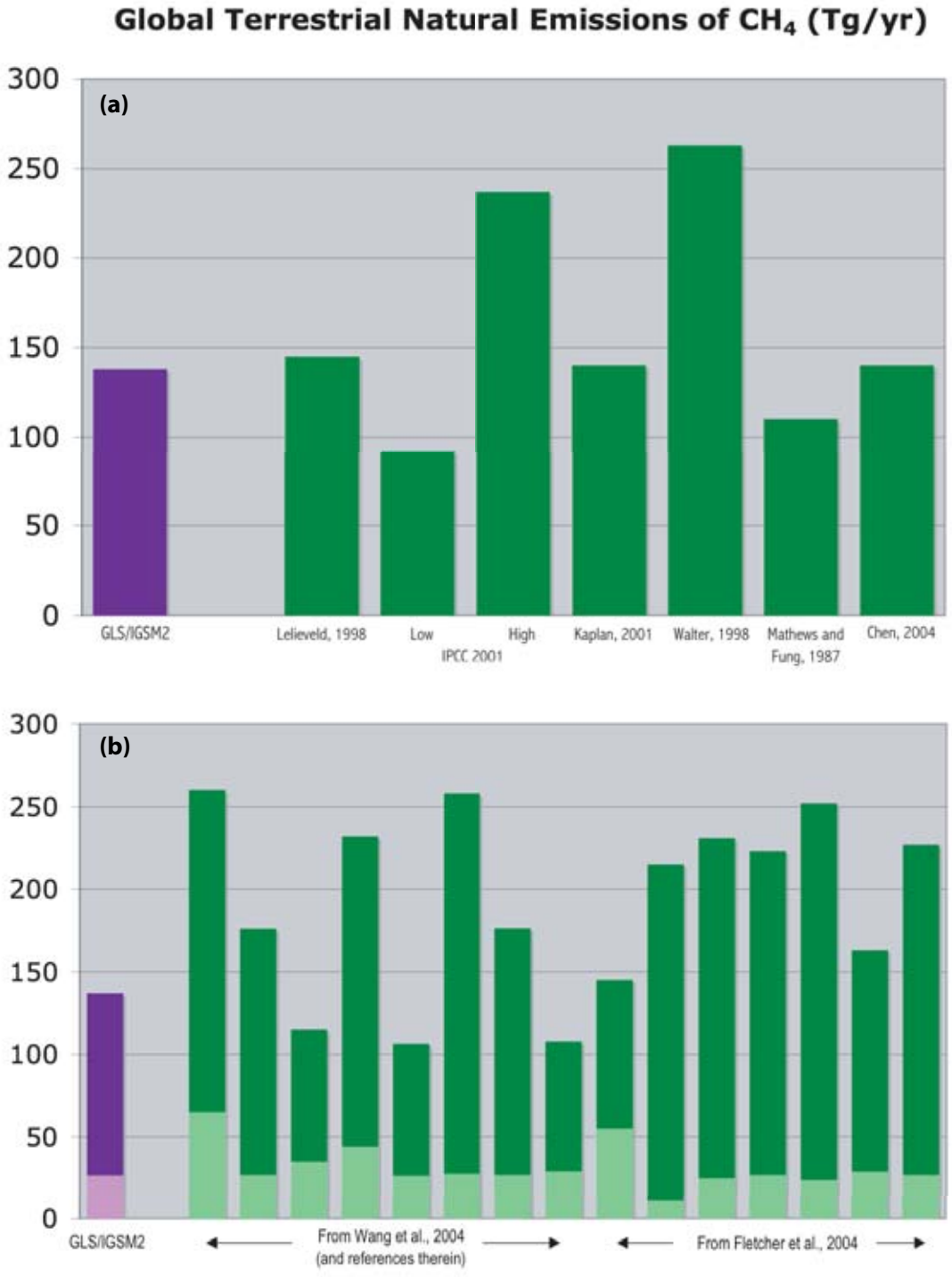

Figure 22. (a) Estimates of global terrestrial natural CH_4 emissions from the GLS/IGSM2 compared against other estimates (and references therein). In **(b)** The lighter shaded bars denote emissions from tundra/bogs while the darker shading denotes emissions from all other wetlands. For the GLS/IGSM2 estimate, the annual average value for 1991-2000 is shown. The standard deviation of the GLS/IGSM2 annual estimate during this period is ~2.7 Tg CH_4/yr.

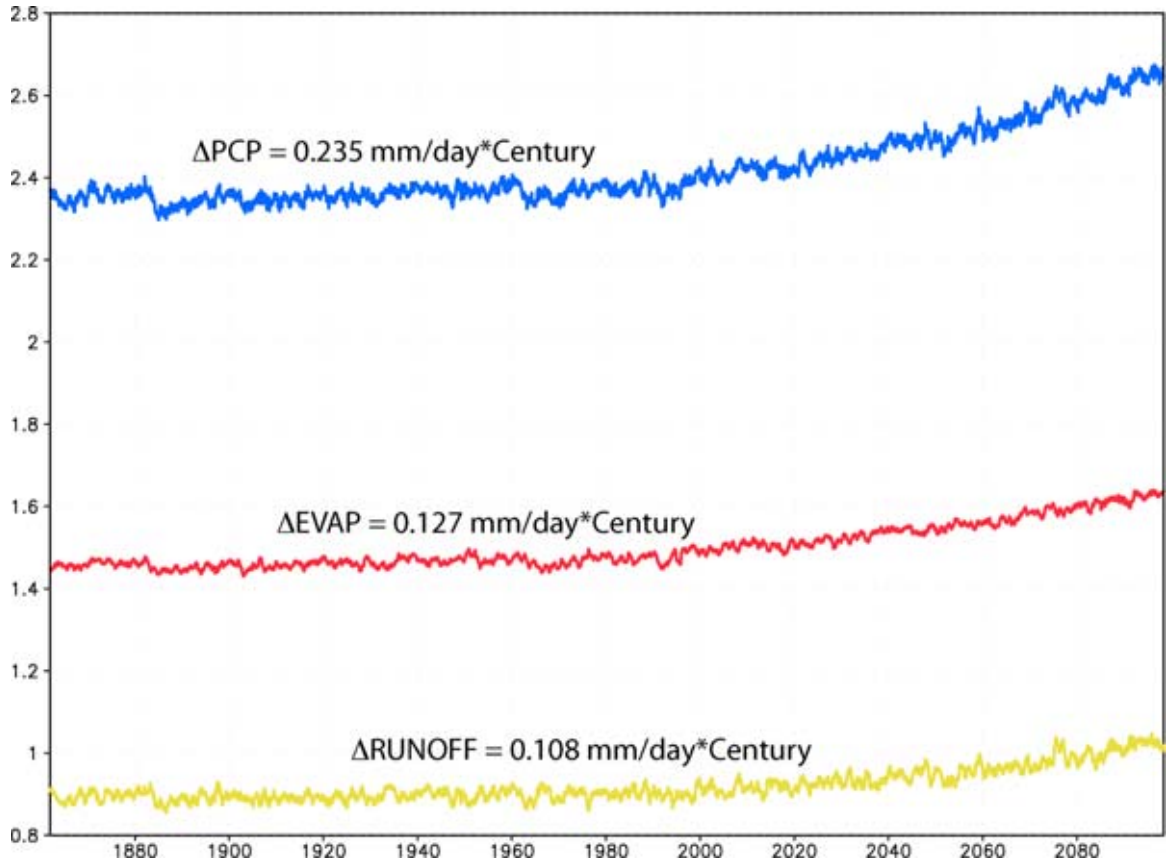

Figure 23. GLS/IGSM2 global land (area-weighted average) water flux time series: annual precipitation (blue curve), evapotranspiration (red curve), and total runoff (yellow curve) in mm/day. Also given atop each curve is the change in the 20-year mean values between the end of the 21st century (2081-2100) and the end of the 20th century (1981-2000).

3.3 Simulation of variability and trends under long-term climate changes

During the 20th century, the trends in global overland precipitation and terrestrial evaporation are small compared to those seen during the 21st century (**Figure 23**), which are on the order of 10%, 8.75%, and 12% increases in global precipitation, evaporation, and runoff respectively. In terms of partitioning, evapotranspiration receives a slightly greater portion (54%) of the global precipitation changes than global runoff (46% of the precipitation increase). The global trend of land precipitation is largely supplied by increases in the southern tropical regions (**Figure 24**), which occur throughout most of the year (*i.e*. no marked seasonality). However, notable increases in overland precipitation are also seen, primarily during the wintertime, in both northern and southern high latitudes. Notwithstanding the increases in high latitude winter precipitation (suggesting potentially increased snowfall), the GLS/IGSM2 shows a clear snow/ice albedo feedback as seen in the enhanced warming for the northern high latitude wintertime (Figure 24a). Conversely, the latitudes with the year-round, weakest warming (20°N-30°N) correspond to those with the highest fraction of bare soil (*i.e.* desert) coverage (Fig. 5). The hydrologic response (**Figure 25**) to these precipitation and temperature change patterns is quite evident. The southern subtropical changes in evapotranspiration and runoff

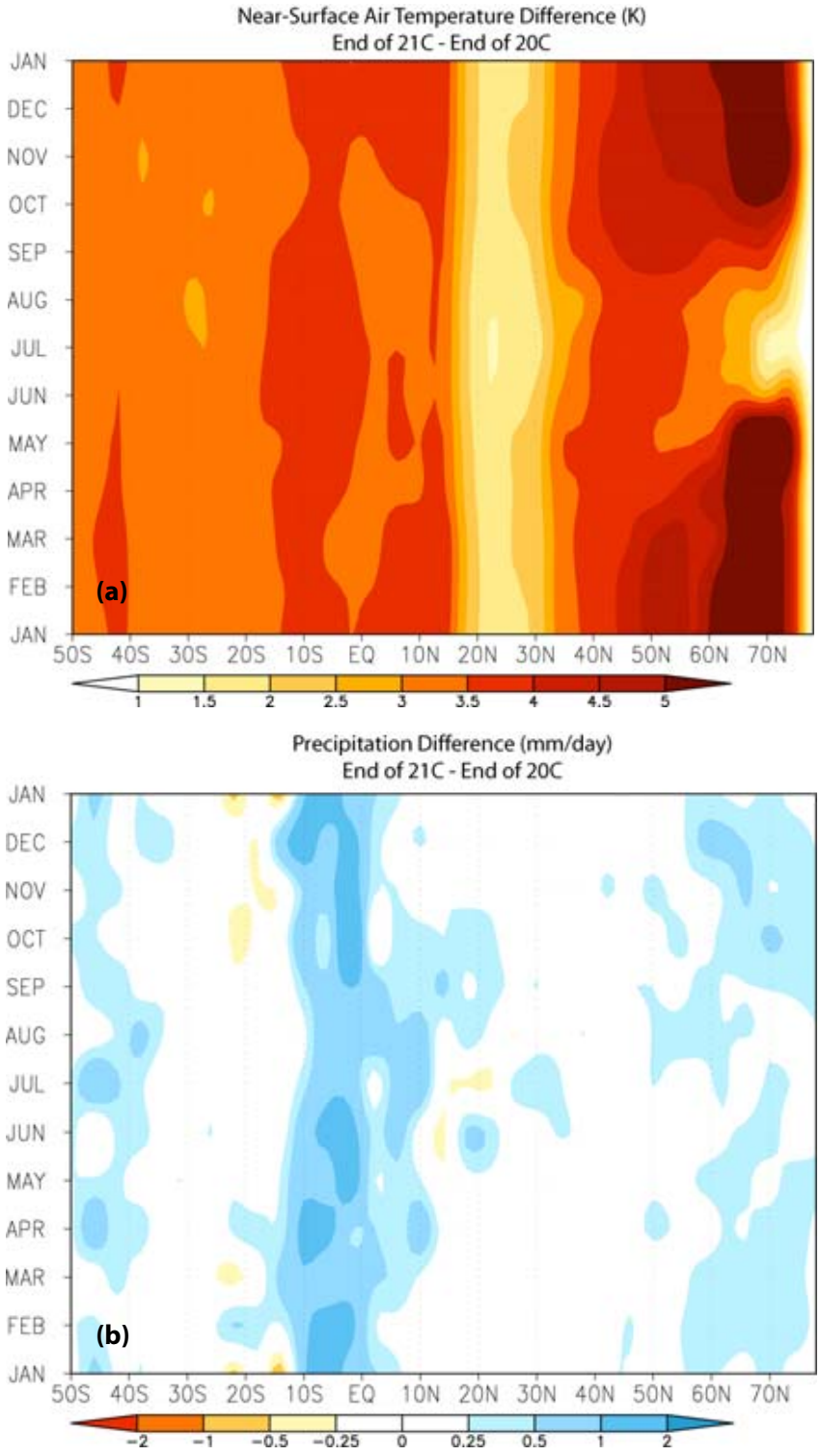

Figure 24. Latitudinal depiction of the difference in the 20-year mean annual cycles between the end of the 21st century (2081-2100) and the end of the 20th century (1981-2000), as simulated by GLS/IGSM2: **(a)** near-surface air temperature, **(b)** precipitation.

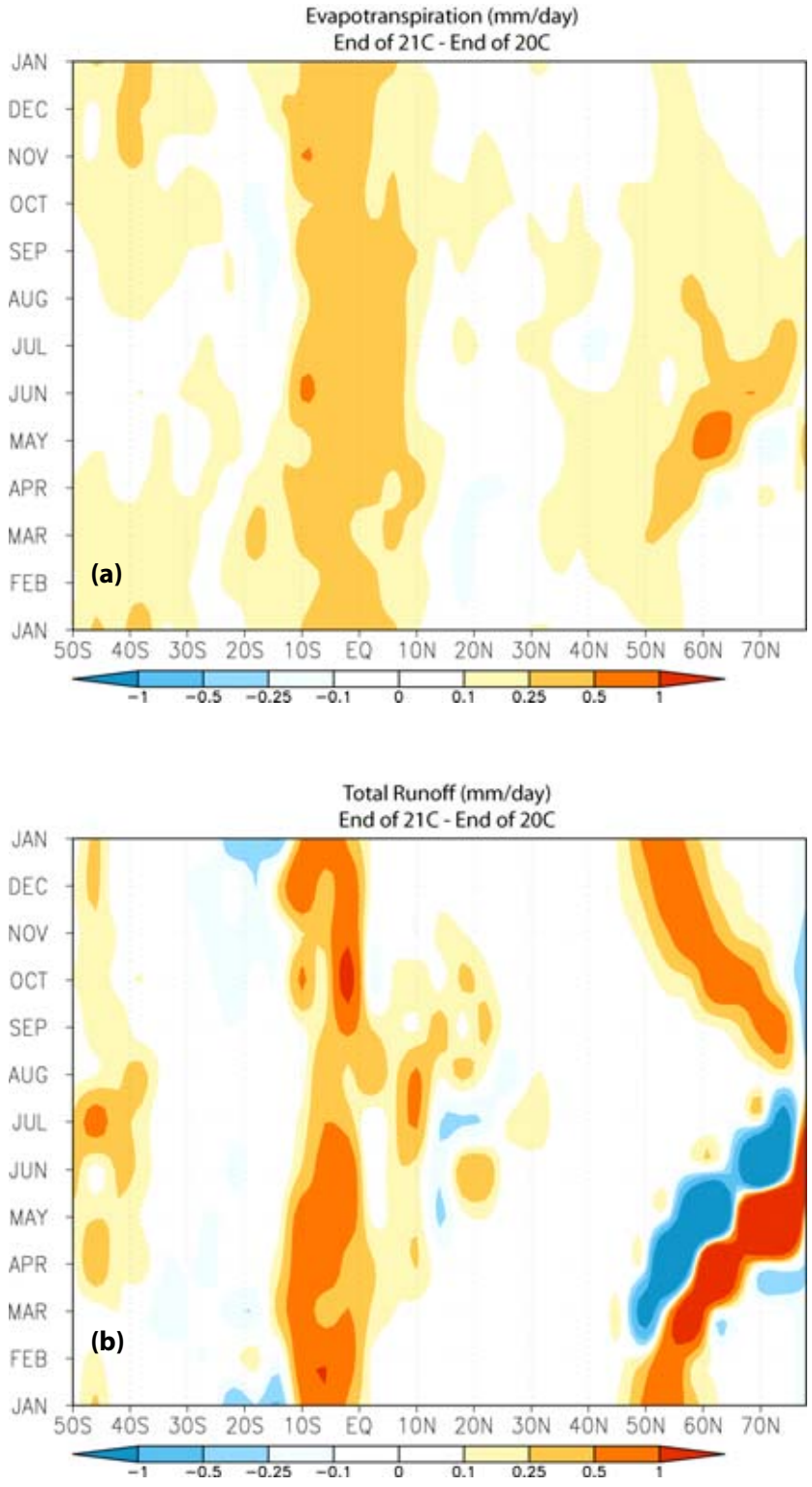

Figure 25. Latitudinal depiction of the difference in the 20-year mean annual cycles between the end of the 21st century (2081-2100) and the end of the 20th century (1981-2000): **(a)** evapotranspiration, **(b)** total runoff. Units are mm/day.

correspond closely with the precipitation and temperature changes noted above, with a greater portion of the precipitation increase partitioned into runoff than evapotranspiration. Further, in the mid- to high northern latitudes, the strong dipole pattern of large runoff increases in the early to late spring followed by strong decreases in runoff is a reflection of an earlier snowmelt and longer growing season, while the band of increased runoff stretching from the late fall through the winter months is a result of the amplified warmer conditions over the northern high latitudes (Fig. 24a) resulting in more precipitation in the form of rain than snow. The spring through summer decreases in runoff in the northern mid to high latitudes are partially offset by contemporaneous increases in evapotranspiration, which are supported by the wet conditions of the soil from the snowmelt in tandem with the higher surface-air temperatures supporting higher potential evaporation rates. The ubiquitous absence of strong evapotranspiration changes in the northern sub-tropics is consistent with the absence of large precipitation changes, the weakest air temperature warming, as well as the drier bare-soil conditions.

The trends in these hydrothermal quantities provided by CLM and the atmospheric dynamics and chemistry model have influenced the trends in natural trace-gas emissions estimated by the GLS. During the historical portion (*i.e.* prescribed atmospheric trace-gas concentrations) of the baseline GLS/IGSM2 simulation, the trends in the TEM generated fluxes of carbon, CH_4, and N_2O vary in character (**Figure 26**). The historical trends of carbon and N_2O fluxes are also accompanied by a strong degree of interannual variability in these fluxes. In contrast, the increases in CH_4 fluxes over the historical period are more distinct. The overall trend in the N_2O flux is seen as a monotonic, linear increase, which results in a ~5% increase (~3 Kt N_2O/year) in global N_2O flux during the 20th century. The trend in global CH_4 flux is more aptly described by a polynomial, and appears to closely follow variations in global temperature, as evidenced by a precipitous drop in flux in the latter years of the 19th century following the Krakatoa eruption. Over the historical period, the GLS estimates that natural CH_4 emissions increased by about 9% (~92 Kt CH_4/year) over the rates during the 1860s. For carbon uptake, TEM produces a carbon sink over the historical period with a weak, low-frequency variation (as characterized by the best least-squares fit of the annual time series). The peak during the late 19th century, coincident with the Krakatoa eruption, is one of the more prominent features. By the late 1980s, the GLS estimates that ~1.1 Gt C/year is sequestered by terrestrial ecosystems (not including the effects of land-use change). Looking at the contributions from the various land cover types, the largest variety and interannual variation between annual carbon sources and sinks are seen among the temperate land cover types, while the tropical land cover types provide the more consistent and strongest unit-area uptake of carbon during the period (**Figure 27**). As a whole, the annual unit-area carbon uptake rates in the boreal land cover types are consistently among the lowest.

During the 21st century, the trends in carbon, CH_4 and N_2O fluxes become more robust (**Figure 28**). The global CH_4 emissions increase of 53% (~77 Mt CH_4/year) follows an exponential-like path, while the trend in global N_2O emissions follows a more linear and weaker path resulting in an increase of approximately 16% (~1.6 Mt N_2O/year) by the end of the 21st century. The GLS also estimates that terrestrial carbon sequestration will continue to increase

such that ~2.7 Gt C/year will sequestered by terrestrial ecosystems at the end of the 21st century. These future trends are a little different from those reported in Sokolov *et al*. (2005) primarily as a result of the incorporation of the land versus ocean precipitation corrections into the GLS, among other minor updates to the IGSM2, since that study. On an area-weighted basis, boreal land cover types collectively provide the largest increase of carbon uptake per unit area

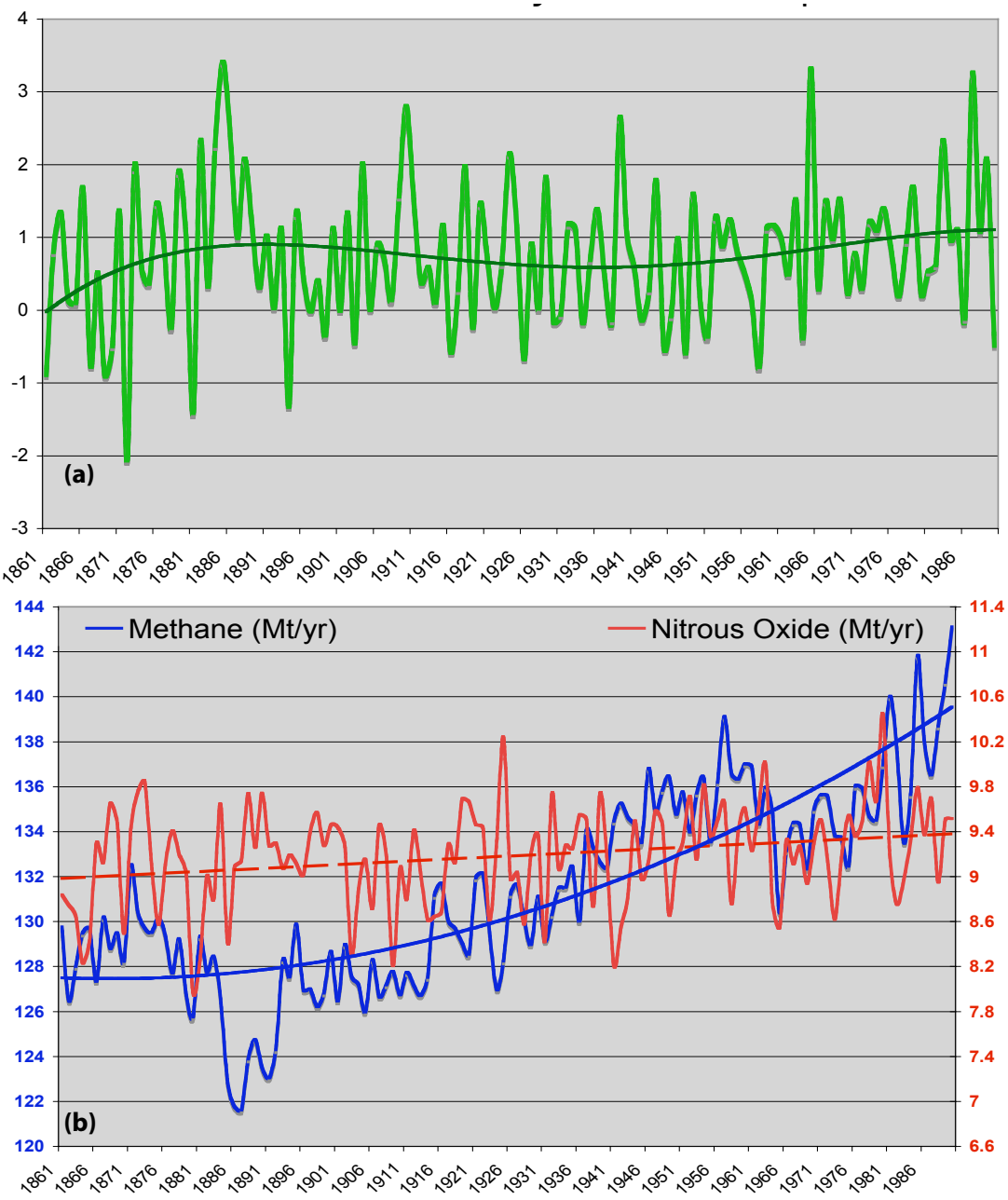

Figure 26. (a) Global emissions of methane and nitrous oxide, and **(b)** carbon uptake during the historical period (*i.e.* prescribed trace gas concentrations and climate forcings) of the baseline IGSM2/GLS simulation (see text for details). Also shown for each curve are fitted linear or polynomial trend lines.

(**Figure 29**a) and among those, broadleaf and needle-leaf deciduous as well as needle-leaf evergreen show the most robust increases (**Figure 30**). In considering the unweighted averages (Fig. 29c), the results indicate that among the various boreal land cover types, those

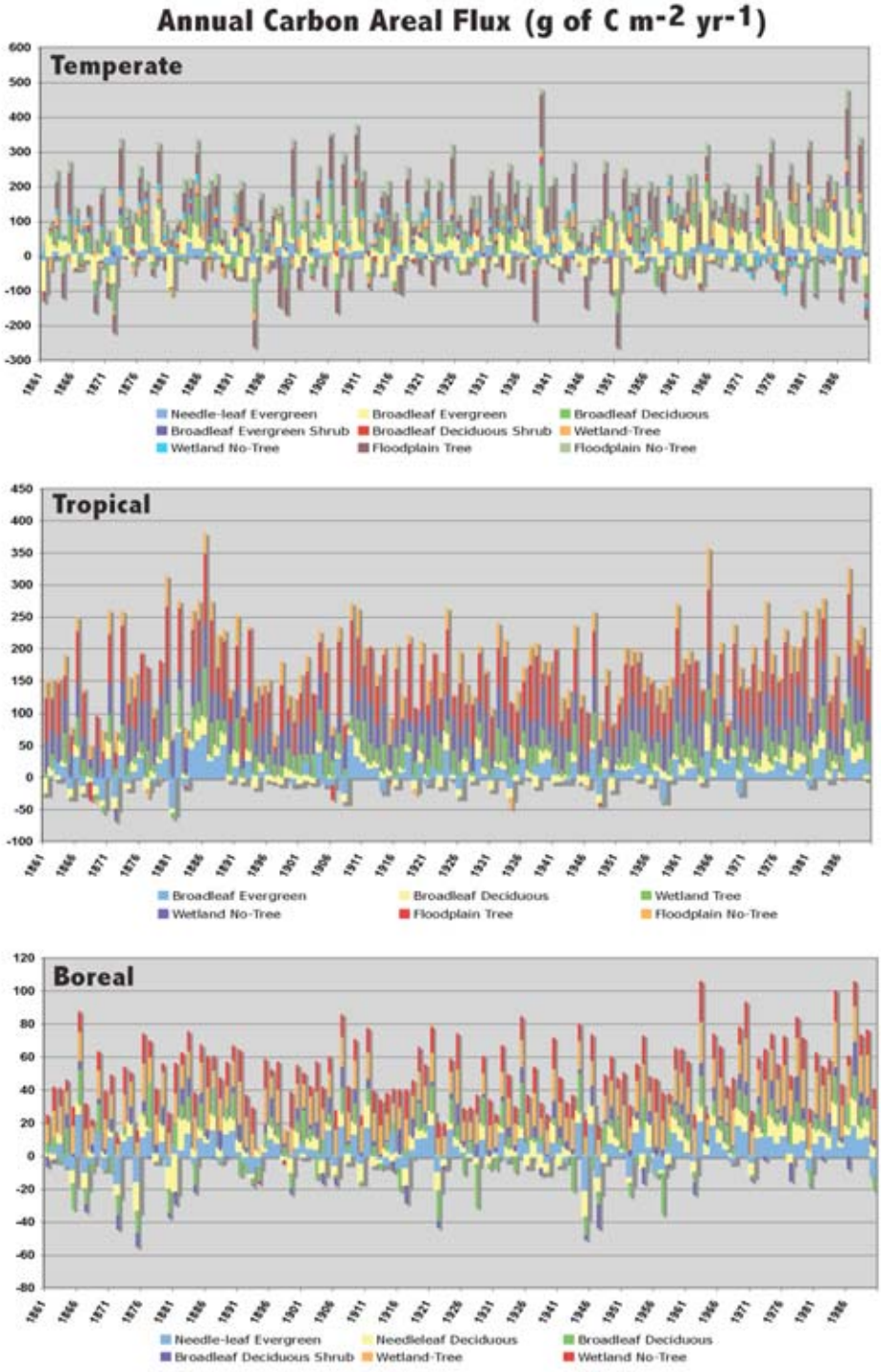

Figure 27. Distribution of historical (1861-1990) annual land-atmosphere carbon exchanges estimated by the IGSM2/GLS across **(a)** temperate, **(b)** tropical, and **(c)** boreal land cover types.

with larger/weaker increases in carbon uptake correspond with larger/smaller area coverage, which results in the relatively stronger increase for the area-weighted average. A somewhat opposite situation occurs in the tropics, as seen by the substantial, overall lower values in the unit-area carbon flux from the area-weighted averages, which is largely a result of the very

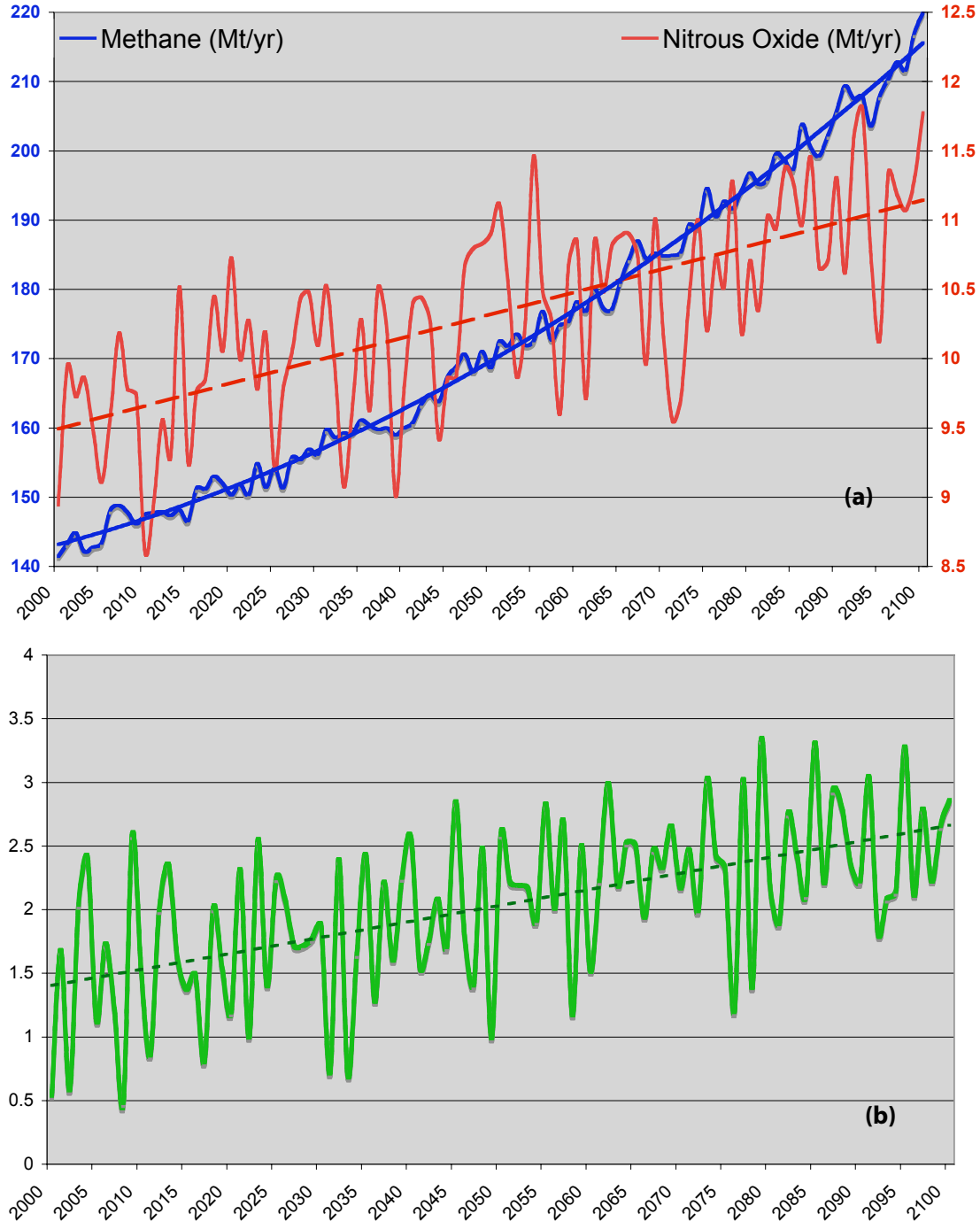

Figure 28. (a) Global emissions of methane and nitrous oxide, and **(b)** carbon uptake for the "business as usual" scenario (*i.e.* EPPA predicted emissions) of the IGSM2/GLS. Dashed lines denote the least-squares fitted trends.

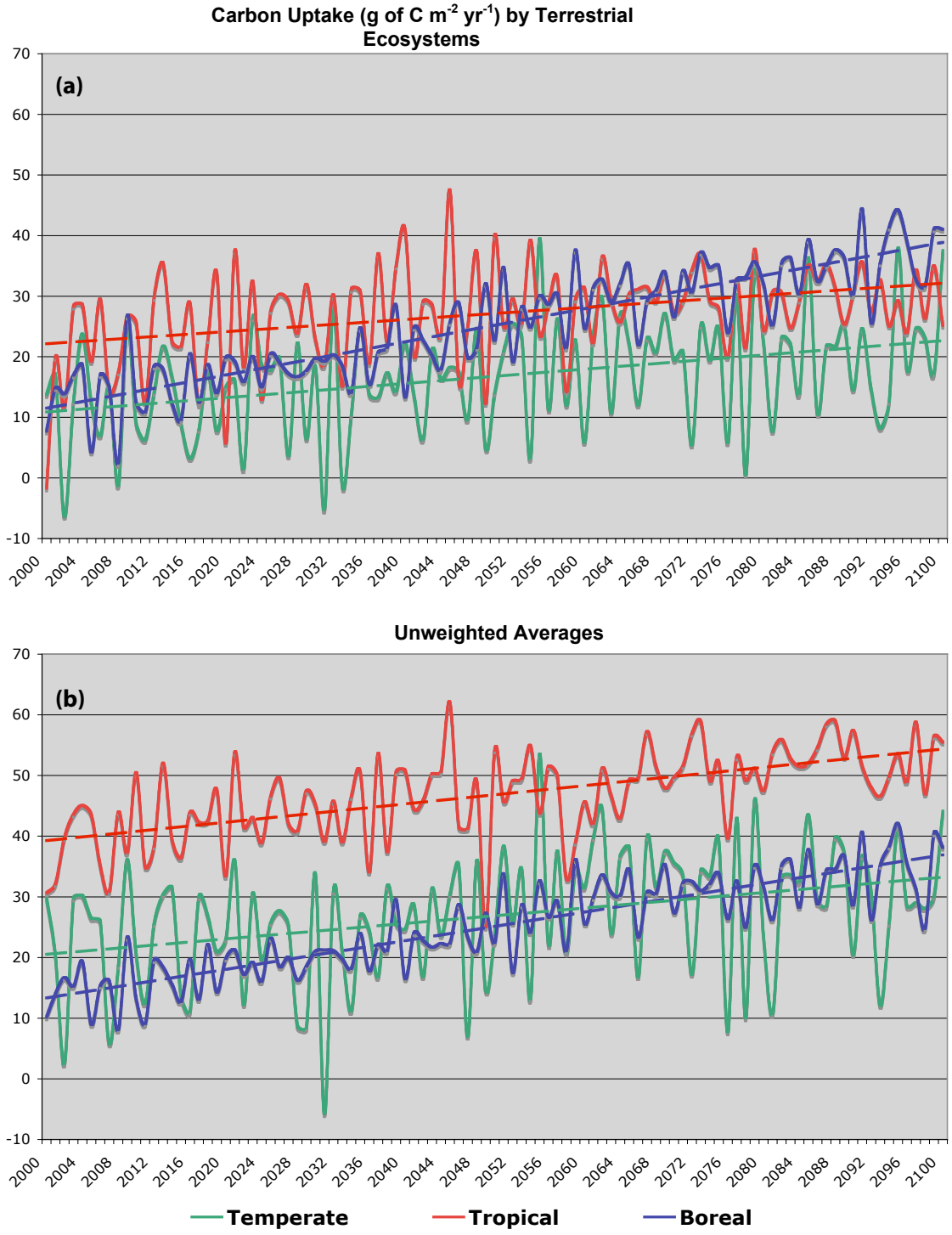

Figure 29. Projected carbon sequestration by terrestrial ecosystems. Shown are the **(a)** area-weighted and **(b)** unweighted averages of unit-area carbon uptake, which are pooled for the boreal, temperate, and tropical ecosystem land cover types. Results are based on the IGSM/GLS simulation of climate change under a "business as usual" emissions scenario of EPPA.

strong sink of carbon per unit area from the forested floodplains (Fig. 30), but coincident with its relatively small area coverage compared to other tropical land cover types (Table 8). Nevertheless, the larger increases in unit-area carbon uptake during the 21st century from the boreal ecosystems (weighted or unweighted) as compared to tropical and temperate ecosystems are consistent with the strongest warming, longer growing season, and evapotranspiration rates in

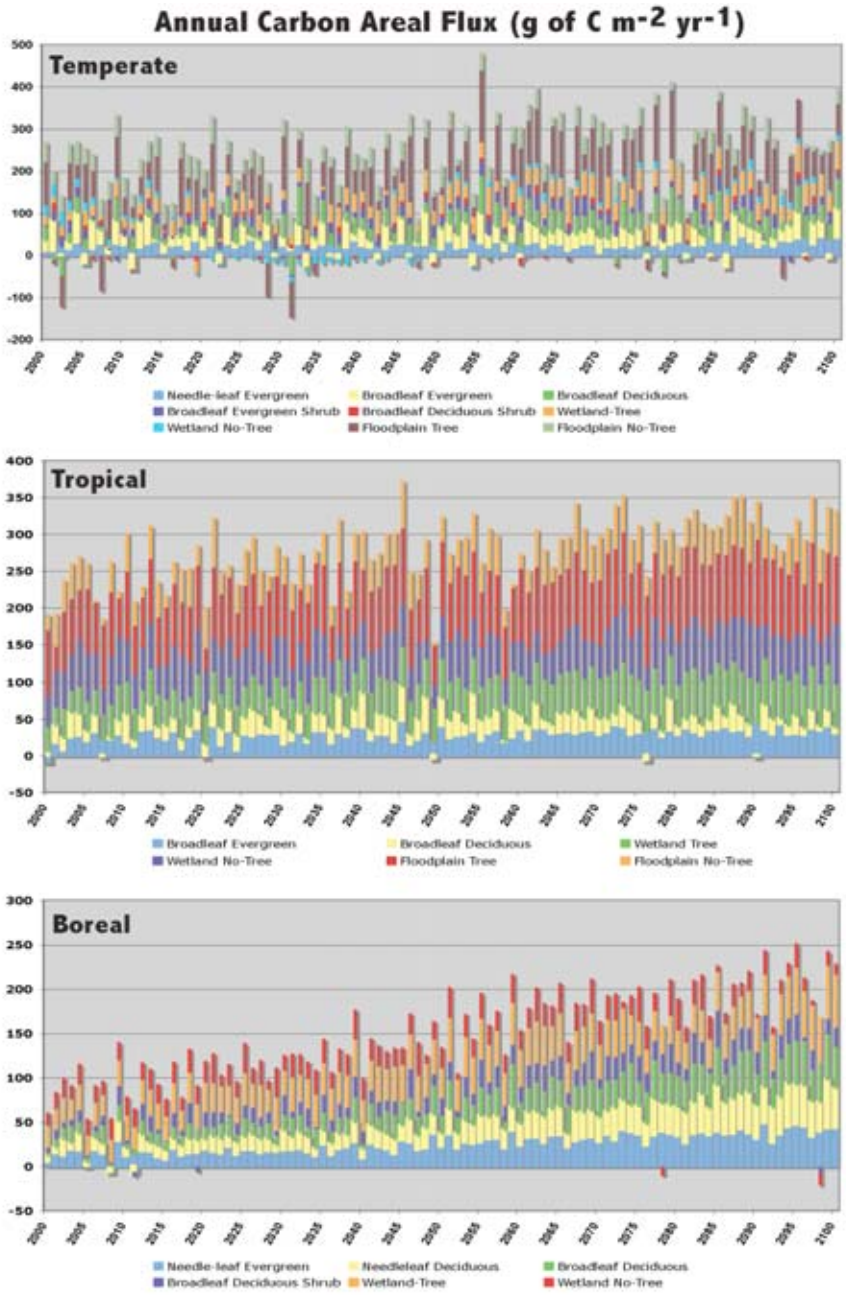

Figure 30. Distribution of projected (2000-2100) annual unit-area carbon flux (positive denotes uptake by land) as estimated by the IGSM2/GLS across land cover types. The panels show carbon exchanges from land cover types in temperate, tropical, and boreal climate regimes, respectively. Results are based on the IGSM/GLS simulation of climate change under a "business as usual" emissions scenario of EPPA.

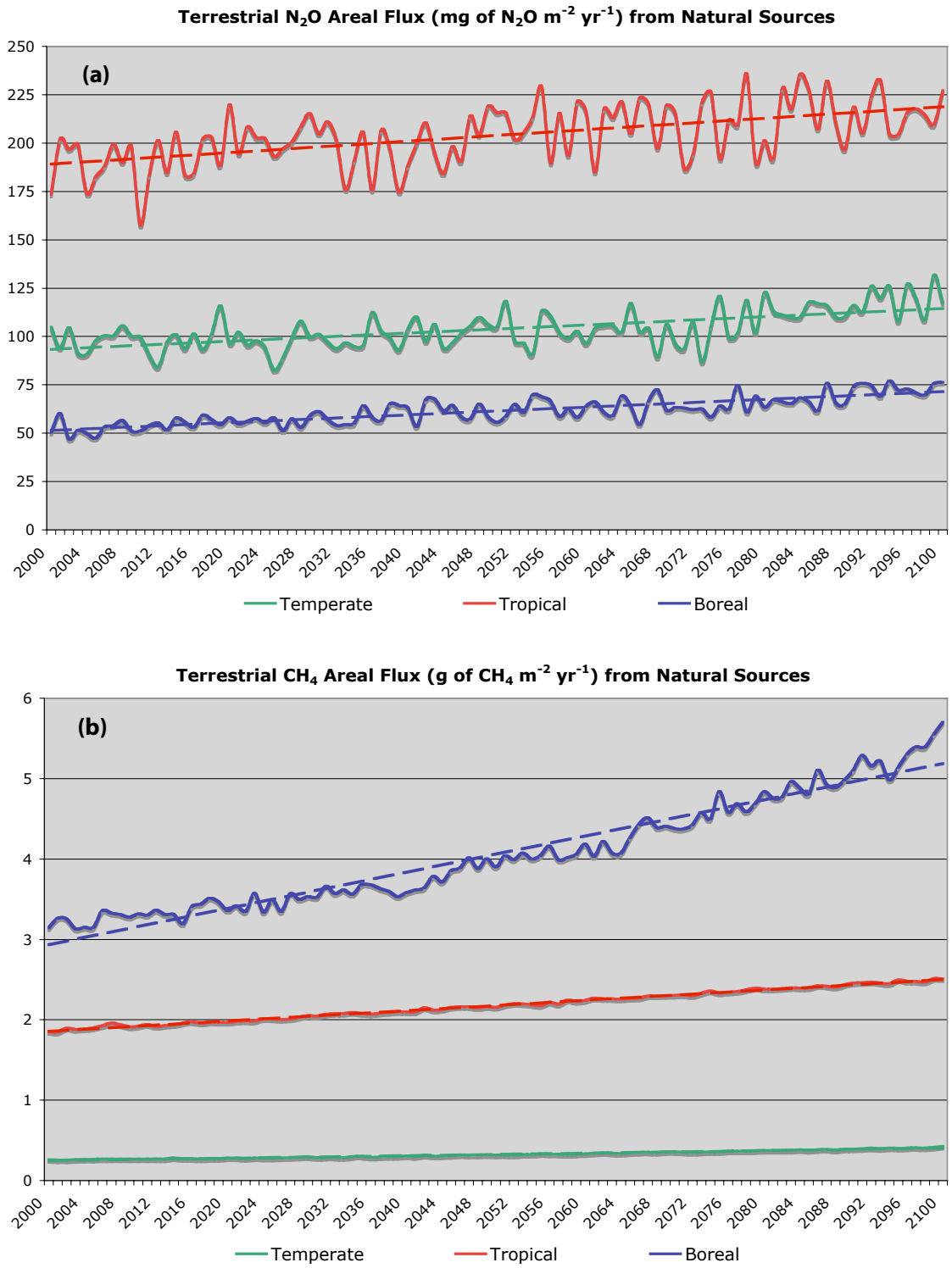

Figure 31. Projected emissions of N_2O **(a)** and CH_4 **(b)** from natural ecosystems. The results are area-weighted average fluxes and are pooled for the tropical, temperate, and boreal regimes of the TEM ecosystems. Results are based on a GLS/IGSM2 simulation of climate change under a "business as usual" emissions scenario of EPPA.

the high latitudes (Figs. 24 and 25). Similar to the 20th century, the temperate land cover types still provide the most noticeable occurrences of years in which a unit-area ecosystem acts as a carbon emitter. Collectively, the tropical land cover types produce the weakest trend in unit-area carbon uptake (Fig. 29), with the wetter ecosystems typically showing stronger unit-area uptakes and slightly larger increases than drier ones (Fig. 30).

Similar to the carbon flux results, the boreal land cover types provide by far the strongest increase in CH_4 flux per unit area (weighted average), while all land cover types contribute nearly the same increase in N_2O unit-area flux (**Figure 31**). The interannual variability in unit-area CH_4 flux is dominated by the boreal ecosystems, while for unit-area N_2O flux the tropical land cover types show the strongest magnitude. The dominant trend of CH_4 unit-area flux from the boreal land cover types is likely a result of the strong climatological emissions coming from these ecosystems (Fig. 21a) responding to the coincident enhanced warming at high latitudes (Fig. 24). The absence of any notable coincidence between the strongest climatological emissions (Fig. 21b) and enhanced trends in temperature or precipitation (Fig. 24) results in the near uniform increases in N_2O unit-area flux across the tropical, temperate, and boreal ecosystems. However, missing from this simulation is any consideration of trends in the frequency and/or intensity of precipitation events in association with global climate warming, which can substantially impact the processes that govern these emissions (*e.g.* Li *et al.*, 1992). Forthcoming analyses will address the potential impact of event-based trends in precipitation statistics under the auspice of uncertainty in global climate-change projections using the IGSM2.

4. CLOSING REMARKS

A Global Land System (GLS) model framework has been developed to represent the global terrestrial biogeophysical and biogeochemical processes in the IGSM2. In contrast to the IGSM1, in which multiple land modules were employed using different gridded representations of global land cover and soil types as well as separate and inconsistent water and energy budgets, the GLS framework employs a zonal, mosaic framework of land cover and soil types that is used by all the land modules. In addition, the GLS now ensures that all water and energy states and fluxes are balanced and consistent among all the GLS biogeophysical and biogeochemical modules. The implementation of CLM as the biogeophysical model represents a substantial advance in the IGSM's capability to represent the processes that regulate the global terrestrial water and energy budgets. Not only does CLM include more comprehensive and explicit controls on evapotranspiration, but CLM also provides a more detailed representation of the snowpack and soil-column profile, with up to 5 snow layers and 10 soil layers, as well as an explicit treatment of soil-layer frozen and liquid storages and the processes the govern them. The coupling and implementation of the GLS into the IGSM2 has also resulted in improvements in the parameterization and distribution of zonal land precipitation, which includes an observationally-based partitioning of the zonal precipitation across the various plant functional types as well as a stochastic representation of precipitation event frequency and duration.

As a result of these improvements, the GLS framework shows notable improvements in the fluxes and states of water and energy over the previous treatment of these land processes in the IGSM1. In particular, CLM's treatment of snow processes result in an improved simulation of snow cover climatology over that of the IGSM1. In addition, CLM's treatment of evapotranspiration and its controls as well as improvements in the treatment of the episodic nature and spatial distribution of precipitation across the land surfaces have resulted in substantial improvements to the evapotranspiration estimates. As such, the features of the carbon fluxes as well as key trace gas emissions of methane and nitrous oxide estimated by the TEM module in the GLS are quite comparable to estimates based on higher resolution forward-looking or inverse models constrained by observed climate forcing, as well as those estimated from TEM and NEM at finer spatial resolutions and driven by observed climatological forcings as done in the IGSM1. Given this, the GLS framework represents a key advance in the ability of the IGSM to faithfully represent terrestrial processes under a more consistent and coherent framework (than the IGSM1), and in doing so, provides a more robust treatment of the key interactions between the global terrestrial and climate systems.

While the new GLS framework has improved our ability to represent terrestrial biophysics and biogeochemistry in the IGSM, the IGSM and the GLS will continue to evolve as our scientific understanding of terrestrial dynamics continues to improve. Fortunately, the GLS framework allows improvements within any of the component modules to be easily incorporated into the IGSM and possibly even extend the capabilities of this earth system model. For example, a more explicit treatment of the aerobic/anaerobic environments that coexist in the soil column may help to improve estimates of nitrous oxide fluxes (Li *et al.*, 2000) within a future version of the TEM module of the GLS. In another example, the latest version of CLM (CLM 3.5) not only improves the representation of terrestrial biogeophysics, but has also been coupled to other terrestrial carbon models such as CLM-CN (Thornton *et al.*, 2007), among others. The replacement of the current version of CLM used in the IGSM2 (CLM 2.1) with this latest version will not only improve terrestrial biogeophysics of the IGSM, but may also allow us to test alternative formulations of terrestrial carbon dynamics (*i.e.* replace TEM with other terrestrial carbon models) within the IGSM and enhance our uncertainty assessments of global water/carbon interactions and their fate under global change scenarios.

In other cases, improvements to the IGSM may require further modifications of the linkages between the GLS and other sub-models of the IGSM. For example, an offline version of TEM has already been developed with an open nitrogen cycle that simulates the addition of nitrogen to an ecosystem by nitrogen fixation and atmospheric nitrogen deposition and the loss of nitrogen from an ecosystem by leaching of dissolved organic nitrogen and nitrate. While this new version of TEM can be readily incorporated into the GLS to improve the representation of terrestrial carbon and nitrogen dynamics over the current version of TEM in the IGSM2, which has a closed nitrogen cycle, mass balance considerations require the GLS to account for the fate of any carbon or nitrogen that is leached from upland areas to the neighboring river networks. Lateral transfer of carbon and nitrogen from the land to the oceans may be better represented with a

gridded (*i.e.* longitude and latitude) representation within the IGSM rather than a zonal representation. By design, the GLS framework has been developed so that it can readily operate in either a zonal or a gridded mode.

A better representation of the influence of human activities on terrestrial carbon dynamics within the IGSM is also desired. In the IGSM2, the GLS modules simulate only the dynamics of the original natural land cover. The influence of human activities on terrestrial carbon dynamics is determined separately with the MIT Emissions Prediction and Policy Analysis (EPPA) economic sub-model of the IGSM2 that does not consider the influence of land-use history on contemporary carbon and nitrogen dynamics of land ecosystems. To better represent the dynamics of contemporary land ecosystems, it is desirable to develop a more intimate coupling between EPPA and the GLS. Work is currently underway to extend the mosaic land cover approach used in the GLS to track parcels of land that have been disturbed at various times in the past or even in the future through the use of "disturbance cohorts". In this way, a grid cell can possess many different mosaics with unique land-use histories, and thus to a certain degree, this feature further augments the ability to consider sub-grid land-cover heterogeneity. If the EPPA model provides estimates of how the land area under different land uses change over time, the cohort approach can use this information to inform the GLS when a disturbance has occurred or when land has been abandoned to create new cohorts. The storage and fluxes of carbon within each cohort will depend on the time since disturbance and the area disturbed so that the influence of land-use history on terrestrial carbon dynamics can be taken into account. In return, the GLS can provide estimates of crop yield or timber yield back to the EPPA model for use in simulated land management decisions. If a gridded representation of the land surface is used, the GLS might also be able to provide estimates of the amount of river water available for the EPPA hydroelectric and agriculture sectors.

Thus, the GLS provides a better framework for incorporating future improvements into the IGSM in addition to providing a better representation of biogeophysical and biogeochemical processes of the land surface in the current version of the IGSM. Given this, the GLS framework represents a key advance in the fidelity of the IGSM to faithfully represent coupled terrestrial processes to the climate system, and is well poised to support more robust two-way feedbacks of natural and managed hydrologic and ecologic systems with the climate and socio-economic components of the IGSM2.

Acknowledgements

The authors wish to thank Ben Felzer for providing data for the offline TEM simulation shown in Fig. 19b. The authors also wish to thank Chris Forest and Tim Cronin for valuable discussions and comments on the manuscript.

5. REFERENCES

Adler, R. F., G. J. Huffman, A. Chang, R. Ferraro, P.-P. Xie, J. Janowiak, B. Rudolf, U. Schneider, S. Curtis, D. Bolvin, A. Gruber, J. Susskind, P. Arkin, and E. Nelkin, 2003: The Version-2 Global Precipitation Climatology Project (GPCP) monthly precipitation analysis. *J. Hydromet.,* **4**, 1147-1167.

Bonan, G. B., K. W. Oleson, M. Vertenstein, S. Lewis, X. Zeng, Y. Dai, R. E. Dickinson, and Z-L Yang, 2002: The land surface climatology of the Community Land Model coupled to the NCAR Community Climate Model. *J. Climate*, **15**, 3123-3149.

Brovkin, V., Claussen, M., Driesschaert, E., Fichefet, T., Kicklighter, D., Loutre, M.-F., Matthews, H. D., Ramankutty, N., Schaeffer, M., Sokolov, A., 2006: Biogeophysical effects of historical land cover changes simulated by six Earth system models of intermediate complexity, *Climate Dynamics*, doi: 10.1007/s00382-005-0092-6.

Chen, Y-H, 2003: Estimation of methane and carbon dioxide surface fluxes using a 3-D global atmospheric chemical transport model, Center for Global Change Science Report #73, available online at http://web.mit.edu/cgcs/www/rpts.html, 180 pp.

Claussen, M., L. A. Mysak, A. J. Weaver, M. Crucifix, T. Fichefet, M. F. Loutre, S. L. Weber, J. Alcamo, V. A. Alexeev, A. Berger, R. Calov, A. Ganopolski, H. Goosse, G. Lohmann, F. Lunkeit, I. I. Mokhov, V. Petoukhov, P. Stone, Z. Wang. 2002. Earth system models of intermediate complexity: closing the gap in the spectrum of climate system models. *Climate Dynamics,* **18**, 579-586.

Costanza, R., R. d'Arge, R. de Groot, S. Farber, M. Grasso, B. Hannon, S. Naeem, K. Limburg, J. Paruelo, R.V. O'Neill, R. Raskin, P. Sutton an dM. Van den Belt. 1997. The value of the world's ecosystem services and natural capital. *Nature*, **387**, 253-260.

Cox, P. M., R. A. Betts, C. D. Jones, S. A. Spall and I. J. Totterdell. 2000. Acceleration of global warming due to carbon-cycle feedbacks in a coupled climate model. *Nature* **408,** 184-187.

Cramer, W. P., and R. Leemans. 2001. Global 30-Year Mean Monthly Climatology, 1930-1960, V[ersion]. 2.1 (Cramer and Leemans). Data set. Available on-line [http://www.daac.ornl.gov] from Oak Ridge National Laboratory Distributed Active Archive Center, Oak Ridge, Tennessee, U.S.A.

Dai, A., W. M. Washington, G. A. Meehl, T. W. Bettge, and W. G. Strand, 2004: The ACPI climate change simulations. *Climatic Change*, **62**, 29-43.

Dai, Y., X. Zeng, R. E. Dickinson, I. Baker, G. Bonan, M. Bosilovich, S. Denning, P. Dirmeyer, P. Houser, G. Niu, K. Oleson, A. Schlosser, and Z.-L. Yang, 2003: The Common Land Model (CLM). *Bull. Amer. Meteor. Soc.*, **84**, 1013-1023.

Dickinson, R. E., K W. Oleson, G. Bonan, F. Hoffman, P. Thornton, M. Vertenstein, Z-L Yang, and X. Zeng, 2006: The Community Land Model and its climate statistics as a component of the Community Climate System Model, *J. Climate*, **19**, 2302-2324.

Dirmeyer, P. A., X. Gao and T. Oki, 2002: The Second Global Soil Wetness Project (GSWP2), International GEWEX Project Office Publication # 37, 75 pp.

Dunne, P. K., 2004: Occurrence and quantity of precipitation can be modeled simultaneously. *Int. J. Climatol.*, **24**, 1231-1239.

Felzer, B., D. Kicklighter, J. Melillo, C. Wang, Q. Zhuang and R. Prinn (*2004*) Effects of ozone on net primary production and carbon sequestration in the conterminous United States using a biogeochemistry model. *Tellus **56B,** 230-248*.

Friedlingstein, P., L. Bopp, P. Ciais, J.-L. Dufresne, L. Fairhead, H. LeTreut, P. Monfray and J. Orr. 2001. Positive feedback between future climate change and the carbon cycle. *Geophysical Research Letters* **28(8),** 1543-1546.

GLOBE Task Team and others (Hastings, David A., P. K. Dunbar, G. M. Elphingstone, M. Bootz, H. Murakami, Peter Holland, Nevin A. Bryant, Thomas L. Logan, J.-P. Muller, Gunter Schreier and John S. MacDonald), eds., 1998. The Global Land One-kilometer Base Elevation (GLOBE) Digital

Elevation Model, Version 1.0. National Oceanic and Atmospheric Administration, National Geophysical Data Center, 325 Broadway, Boulder, Colorado 80303, USA. Digital Database on the World Wide Web and CD-ROMs.

Hansen, J., G. Russell, D. Rind, P. Stone, A. Lacis, S. Lebedeff, R. Ruedy, and L. Travis, 1983: Efficient three-dimensional global models for climate studies: Models I and II. *Mon. Wea. Rev.,* **111,** 609–662.

Holland, M. M., 2003: The North Atlantic Oscillation/Arctic Oscillation in the CCSM2 and its influence on Arctic climate variability. *J. Climate*, **16**, 2767-2781.

Li, C., S. Frolking, and T. A. Frolking, 1992: A model of nitrous oxide evolution from soil driven by rainfall events: 1. Model structure and sensitivity. *J. Geophys Res.*, **97**, 9759-9776.

Li, C., J. Aber. F. Stange, K. Butterbach-Bahl and H. Papen. 2000. A process-oriented model of N2O and NO emissions from forest soils. *Journal of Geophysical Research,* **105(D4)**: 4369-4384.

Liu, Y., 1996: Modeling the Emissions of Nitrous Oxide (N2O) and Methane (CH4) from the Terrestrial Biosphere to the Atmosphere, *Joint Program Technical Report #10*, 219 pp.

Matthews, E. 1984. *Prescription of Land-Surface Boundary Conditions in GISS GCM II: A Simple Method Based on High-Resolution Vegetation Data Bases*. NASA TM-86096. National Aeronautics and Space Administration. Washington, D.C.

Matthews, E. and I. Fung. 1987. Methane emission from natural wetlands: global distribution, area, and environmental characteristics of sources. *Global Biogeochemical Cycles* **1(1),** 61-86.

McGuire, A. D., J. M. Melillo, D. W. Kicklighter and L. A. Joyce. 1995. Equilibrium responses of soil carbon to climate change: Empirical and process-based estimates. *Journal of Biogeography* **22,** 785-796.

McGuire, A. D., S. Sitch, J. S. Clein, R. Dargaville, G. Esser, J. Foley, M. Heimann, F. Joos, J. Kaplan, D. W. Kicklighter, R. A. Meier, J. M. Melillo, B. Moore III, I. C. Prentice, N. Ramankutty, T. Reichenau, A. Schloss, H. Tian, L. J. Williams and U. Wittenberg. 2001. Carbon balance of the terrestrial biosphere in the twentieth century: analyses of CO_2, climate and land-use effects with four process-based ecosystem models. *Global Biogeochemical Cycles* **15(1),** 183-206.

Melillo, J. M., A. D. McGuire, D. W. Kicklighter, B. Moore III, C. J. Vörösmarty, and A. L. Schloss. 1993. Global climate change and terrestrial net primary production. *Nature* **363,** 234-240.

Milly, P. C. D., 2001: A minimalist probabilistic description of root-zone soil water. *Water Resour. Res.*, **37**, 457-463.

New, M., M. Hulme, and P. D. Jones. 2000. Global Monthly Climatology for the Twentieth Century (New *et al.)*. Data set. Available on-line [http://www.daac.ornl.gov] from Oak Ridge National Laboratory Distributed Active Archive Center, Oak Ridge, Tennessee, U.S.A.

Peixoto J. P. and A. H. Oort, 1992: *Physics of Climate*, American Institute of Physics, New York, New York, 520 pp.

Prather, M., D. Ehhalt, F. Dentener, R. Derwent, E. Dlugokencky, E. Holland, I. Isaksen, J. Katima, V. Kirchhoff, P. Matson, P. Midgley, and M. Wang. 2001. Atmospheric chemistry and greenhouse gases, In: *Climate Change 2001*: *The Scientific Basis,* Contribution of Working Group I to the Third Assessment Report of the Intergovernmental Panel on Climate Change [Eds. J. T. Houghton, Y. Ding, D. J. Groggs, M. Noguer, P. J. van der Linden, X. Dai, K.Maskell, and C. A. Johnson (eds.)], pp. 239-287, Cambridge University Press, Cambridge, United Kingdom and New York, NY, USA.

Prinn, R., H. Jacoby, A. Sokolov, C. Wang, X. Xiao, Z. Yang, R. Eckhaus, P. Stone, D. Ellerman, J. Melillo, J. Fitzmaurice, D. Kicklighter, G. Holian, and Y. Liu. 1999. Integrated global system model for climate policy assessment: feedbacks and sensitivity studies. *Climatic Change* **41**, 469-546.

Raich, J. W., E. B. Rastetter, J. M. Melillo, D. W. Kicklighter, P. A. Steudler, B. J. Peterson, A. L. Grace, B. Moore III and C. J. Vörösmarty. 1991. Potential net primary productivity in South America: application of a global model. *Ecological Applications* **1,** 399-429.

Ridgwell, A. J., S. J. Marshall, and K. Gregson, 1999. Consumption of atmospheric methane by soils: a process-based model, *Global Biogeochemical Cycles,* **13(1)**, 59-70.

Rodell, M., P. R. Houser, U. Jambor, J. Gottschalck, K. Mitchell, C.-J. Meng, K. Arsenault, B. Cosgrove, J. Radakovich, M. Bosilovich, J. K. Entin, J. P. Walker, D. Lohmann, and D. Toll, 2004: The Global Land Data Assimilation System, *Bull. Amer. Meteor. Soc.*, **85 (3)**, 381-394.

Schlesinger, W. H. 1997. Biogeochemistry. An Analysis of Global Change. Second Edition. Academic Press, San Diego, California. 588p.

Sokolov, A. P., and P. H. Stone, 1998: A flexible climate model for use in integrated assessments. *Climate Dyn.,* **14,** 291–303.

Sokolov, A.P., C.A. Schlosser, S. Dutkiewicz, S. Paltsev, D.W. Kicklighter, H.D. Jacoby, R.G. Prinn, C.E. Forest, J. Reilly, C. Wang, B. Felzer, M.C. Sarofim, J. Scott, P.H. Stone, J.M. Melillo, and J. Cohen, 2005: The MIT Integrated Global System Model (IGSM) Version 2: Model Description and Baseline Evaluation, *Joint Program Technical Report #124*, 40 pp.

Thompson, S. L., B. Govindasamy, A. Mirin, K. Caldeira, C. Delire, J. Milovich, M. Wickett and D. Erickson. 2004. Quantifying the effects of CO2-fertilized vegetation on future global climate and carbon dynamics. *Geophysical Research Letters* **31,** L23211, doi: 10.1029/2004GL021239.

Thornton, P. E., J.-F. Lamarque, N. A. Rosenbloom, and N. Mahowald, 2007: Effects of terrestrial carbon-nitrogen cycle coupling on climate-carbon cycle dynamics. *Global Biogeochemical Cycles* (in review).

Xiao, X., J.M. Melillo, D.W. Kicklighter, A.D. McGuire, R.G. Prinn, C. Wang, P.H. Stone, A.P. Sokolov, 1998: Transient climate change and net ecosystem production of the terrestrial biosphere. *Global Biogeochemical Cycles*, **12**(2): 345-360; MIT JPSPGC *Reprint 1998-6*.

Xiao, X., D.W. Kicklighter, J.M. Melillo, A.D. McGuire, P.H. Stone, A.P. Sokolov, 1997: Linking a global terrestrial biogeochemical model and a 2-dimensional climate model: implications for the carbon budget. *Tellus*, **49**B: 18-37; MIT JPSPGC *Reprint 1997-3*.

Xie P., P. A. Arkin, 1997: Global precipitation: A 17-year monthly analysis based on gauge observations, satellite estimates, and numerical model outputs. *Bull. Amer. Met. Soc.*, **78**, 2539-2558.

Yao, M.-S. and P.H. Stone, 1987, Development of a two-dimensional zonally averaged statistical-dynamical model. I: The parameterization of moist convection and its role in the general circulation, *J. Atmos. Sci.*, **44**, 65-82.

Zeng, X., M. Shaikh, Y. Dai, R. E. Dickinson, and R. Myneni, 2002: Coupling of the Common Land Model to the NCAR Community Climate Model. *J. Climate*, **15**, 1832-1854.

Zhuang, Q., A.D. McGuire, J.M. Melillo, J.S. Clein, R.J. Dargaville, D.W. Kicklighter, R.B. Myneni, J. Dong, V.E. Romanovsky, J. Harden and J.E. Hobbie, 2003: Carbon cycling in extratropical terrestrial ecosystems of the Northern Hemisphere during the 20th Century: A modeling analysis of the influences of soil thermal dynamics. *Tellus*, **55**B: 751-776.

Zhuang, Q., J. M. Melillo, D. W. Kicklighter, R. G. Prinn, A. D. McGuire, P. A. Steudler, B. S. Felzer and S. Hu, 2004: Methane fluxes between terrestrial ecosystems and the atmosphere at northern high latitudes during the past century: a retrospective analysis with a process-based biogeochemistry model. *Global Biogeochemical Cycles,* **18**, GB3010, doi:10.1029/2004GB002239.

Zinke, P. J., A. G. Stangenberger, W. M. Post, W. R. Emanuel, and J. S. Olon. 1986. Worldwide organic soil carbon and nitrogen data. NDP-018, Carbon Dioxide Information Center, Oak Ridge National Laboratory, Oak Ridge, Tennessee

.

REPORT SERIES of the **MIT** *Joint Program on the Science and Policy of Global Change*

1. **Uncertainty in Climate Change Policy Analysis** *Jacoby & Prinn December 1994*
2. **Description and Validation of the MIT Version of the GISS 2D Model** *Sokolov & Stone* June 1995
3. **Responses of Primary Production and Carbon Storage to Changes in Climate and Atmospheric CO_2 Concentration** *Xiao et al.* October 1995
4. **Application of the Probabilistic Collocation Method for an Uncertainty Analysis** *Webster et al.* January 1996
5. **World Energy Consumption and CO_2 Emissions: 1950-2050** *Schmalensee et al.* April 1996
6. **The MIT Emission Prediction and Policy Analysis (EPPA) Model** *Yang et al.* May 1996 (*superseded by No. 125*)
7. **Integrated Global System Model for Climate Policy Analysis** *Prinn et al.* June 1996 (*superseded by No. 124*)
8. **Relative Roles of Changes in CO_2 and Climate to Equilibrium Responses of Net Primary Production and Carbon Storage** *Xiao et al.* June 1996
9. **CO_2 Emissions Limits:** ***Economic Adjustments and the Distribution of Burdens*** *Jacoby et al.* July 1997
10. **Modeling the Emissions of N_2O and CH_4 from the Terrestrial Biosphere to the Atmosphere** *Liu* Aug. 1996
11. **Global Warming Projections:** ***Sensitivity to Deep Ocean Mixing*** *Sokolov & Stone* September 1996
12. **Net Primary Production of Ecosystems in China and its Equilibrium Responses to Climate Changes** *Xiao et al.* November 1996
13. **Greenhouse Policy Architectures and Institutions** *Schmalensee* November 1996
14. **What Does Stabilizing Greenhouse Gas Concentrations Mean?** *Jacoby et al.* November 1996
15. **Economic Assessment of CO_2 Capture and Disposal** *Eckaus et al.* December 1996
16. **What Drives Deforestation in the Brazilian Amazon?** *Pfaff* December 1996
17. **A Flexible Climate Model For Use In Integrated Assessments** *Sokolov & Stone* March 1997
18. **Transient Climate Change and Potential Croplands of the World in the 21st Century** *Xiao et al.* May 1997
19. **Joint Implementation:** ***Lessons from Title IV's Voluntary Compliance Programs*** *Atkeson* June 1997
20. **Parameterization of Urban Subgrid Scale Processes in Global Atm. Chemistry Models** *Calbo et al.* July 1997
21. **Needed: A Realistic Strategy for Global Warming** *Jacoby, Prinn & Schmalensee* August 1997
22. **Same Science, Differing Policies;** ***The Saga of Global Climate Change*** *Skolnikoff* August 1997
23. **Uncertainty in the Oceanic Heat and Carbon Uptake and their Impact on Climate Projections** *Sokolov et al.* September 1997
24. **A Global Interactive Chemistry and Climate Model** *Wang, Prinn & Sokolov* September 1997
25. **Interactions Among Emissions, Atmospheric Chemistry & Climate Change** *Wang & Prinn* Sept. 1997
26. **Necessary Conditions for Stabilization Agreements** *Yang & Jacoby* October 1997
27. **Annex I Differentiation Proposals:** ***Implications for Welfare, Equity and Policy*** *Reiner & Jacoby* Oct. 1997
28. **Transient Climate Change and Net Ecosystem Production of the Terrestrial Biosphere** *Xiao et al.* November 1997
29. **Analysis of CO_2 Emissions from Fossil Fuel in Korea: 1961–1994** *Choi* November 1997
30. **Uncertainty in Future Carbon Emissions:** ***A Preliminary Exploration*** *Webster* November 1997
31. **Beyond Emissions Paths:** ***Rethinking the Climate Impacts of Emissions Protocols*** *Webster & Reiner* November 1997
32. **Kyoto's Unfinished Business** *Jacoby et al.* June 1998
33. **Economic Development and the Structure of the Demand for Commercial Energy** *Judson et al.* April 1998
34. **Combined Effects of Anthropogenic Emissions and Resultant Climatic Changes on Atmospheric OH** *Wang & Prinn* April 1998
35. **Impact of Emissions, Chemistry, and Climate on Atmospheric Carbon Monoxide** *Wang & Prinn* April 1998
36. **Integrated Global System Model for Climate Policy Assessment:** ***Feedbacks and Sensitivity Studies*** *Prinn et al.* June 1998
37. **Quantifying the Uncertainty in Climate Predictions** *Webster & Sokolov* July 1998
38. **Sequential Climate Decisions Under Uncertainty:** ***An Integrated Framework*** *Valverde et al.* September 1998
39. **Uncertainty in Atmospheric CO_2 (Ocean Carbon Cycle Model Analysis)** *Holian* Oct. 1998 (*superseded by No. 80*)
40. **Analysis of Post-Kyoto CO_2 Emissions Trading Using Marginal Abatement Curves** *Ellerman & Decaux* Oct. 1998
41. **The Effects on Developing Countries of the Kyoto Protocol and CO_2 Emissions Trading** *Ellerman et al.* November 1998
42. **Obstacles to Global CO_2 Trading:** ***A Familiar Problem*** *Ellerman* November 1998
43. **The Uses and Misuses of Technology Development as a Component of Climate Policy** *Jacoby* November 1998
44. **Primary Aluminum Production:** ***Climate Policy, Emissions and Costs*** *Harnisch et al.* December 1998
45. **Multi-Gas Assessment of the Kyoto Protocol** *Reilly et al.* January 1999
46. **From Science to Policy:** ***The Science-Related Politics of Climate Change Policy in the U.S.*** *Skolnikoff* January 1999
47. **Constraining Uncertainties in Climate Models Using Climate Change Detection Techniques** *Forest et al.* April 1999
48. **Adjusting to Policy Expectations in Climate Change Modeling** *Shackley et al.* May 1999
49. **Toward a Useful Architecture for Climate Change Negotiations** *Jacoby et al.* May 1999
50. **A Study of the Effects of Natural Fertility, Weather and Productive Inputs in Chinese Agriculture** *Eckaus & Tso* July 1999
51. **Japanese Nuclear Power and the Kyoto Agreement** *Babiker, Reilly & Ellerman* August 1999

Contact the Joint Program Office to request a copy. The Report Series is distributed at no charge.

Contact the Joint Program Office to request a copy. The Report Series is distributed at no charge.

Contact the Joint Program Office to request a copy. The Report Series is distributed at no charge.